THE RELATION OF TURBULENCE TO DIFFUSION IN OPEN-CHANNEL FLOWS

by Thomas N. Keefer

TABLE OF CONTENTS

TABLE OF CONTENTS - (Continued)

...

TABLE OF CONTENTS - (Continued)

LIST OF TABLES

LIST OF FIGURES

LIST OF FIGURES - (Continued)

THE RELATION OF TURBULENCE TO DIFFUSION IN OPEN-CHANNEL FLOWS

by Thomas N. Keefer

ABSTRACT

This investigation examines the interrelation between turbulent diffusion, dispersion, and the statistical properties of turbulence in an open-channel flow. The experiments were conducted in a 3.87-foot wide flume over four boundary roughnesses. The results are from studies made of: (1) the influence of turbulence on the vertical and lateral diffusion of plumes of heated water and a neutrally-buoyant salt solution from a point source at the mid-depth of flow; (2) the velocity-concentration covariance along the axis of a salt solution plume using a single-electrode conductivity probe and hot-film sensor; (3) lateral and longitudinal surface diffusion measured by dropping polyethylene particles on the water surface; and (4) longitudinal space-time velocity correlation measurements.

The results of the study substantiate Philip's concept relating the ratio of Eulerian to estimated Lagrangian time scales and the reciprocal of the longitudinal intensity of turbulence. The relation is used to predict coefficients of longitudinal turbulent diffusion at the water surface and in the flow field. A similar concept using an integral time scale based on the longitudinal intensity of turbulence is used to predict coefficients of both surface and depth-averaged turbulent diffusion in three coordinate directions for heated water and neutrally buoyant jets of salt solution.

Longitudinal space-time velocity correlation measurements can be used to predict the Lagrangian time scale only under limited conditions. For this study the Lagrangian scale was underpredicted by 250 percent.

A model is developed for the behavior of the longitudinal velocity-concentration covariance along the axis of a plume of neutrally-buoyant salt solution. The covariance measurements are accurate to ±20 percent. The boussinesq model of scalar transport is verified with an accuracy of ±25 percent by comparing diffusion coefficients from (1) the velocity-concentration covariance measurements with (2) those obtained at the water surface using floating particles. The hot-film single-electrode conductivity probe method for measuring the covariance offers a new tool to experimenters in turbulent mass transfer.

Under the range of conditions studied, longitudinal diffusion accounts for 4 to 13 percent of the one-dimensional dispersion process. Predictions of the dispersion coefficient by formulas such as Elder's were in error by as much as 50 percent.

The exponent in the power-law equation describing the decay of scalar quantities downstream of a jet is a linear function of the shear velocity of the channel. The length of the core region of a jet is a power-law function of the jet strength with the exponent depending on boundary roughness.

PARTIAL LIST OF SYMBOLS

Symbol		Units
b	Exponent in power law equation	0
c	Concentration fluctuation about the mean	Arbitrary
$\sqrt{\overline{c^2}}$	Root-mean-square of concentration fluctuations	Arbitrary
d	Diameter of nozzle or jet	ft
g	Acceleration of gravity	ft/sec^2
i	Subscript denoting direction, x, y, or z	0
j	Subscript denoting direction, x, y, or z	0
k_i	Arbitrary constants, i = 1 or 2	0
k_3	Constant in $\overline{uc}$ prediction equation	units·ft/sec
p	Instantaneous pressure at a point	lbs/ft^2
r	Radial coordinate direction or distance	ft
s	Subscript indicating a value obtained at the water surface	0
t	Time	secs
u	Longitudinal velocity fluctuation about the mean	ft/sec
$\sqrt{\overline{u^2}}$	Root-mean-square velocity fluctuation in x direction	ft/sec
$\overline{u_i c}$	Velocity-concentration covariance in ith direction, x, y, or z	units·ft/sec
v	Vertical velocity fluctuation about the mean	ft/sec
$\sqrt{\overline{v^2}}$	Root-mean-square velocity fluctuation in y direction	ft/sec
w	Lateral velocity fluctuation about the mean	ft/sec
$\sqrt{\overline{w^2}}$	Root-mean-square velocity fluctuation in z direction	ft/sec

PARTIAL LIST OF SYMBOLS - (Continued)

Symbol		Units
x	Longitudinal coordinate or distance, also used as subscript denoting longitudinal direction	ft
x_c	Core length of jet	ft
y	Vertical coordinate or distance, also used as subscript denoting vertical direction	ft
z	Lateral coordinate or distance, also used as subscript denoting lateral direction	ft
A	Constant in power law equation	Concentration or °C
B	Constant in power law equation	0
C	Chezy discharge coefficient	ft/sec^2
C	Instantaneous concentration	Arbitrary
$\overline{\overline{C}}$	Depth average concentration	Arbitrary
$\overline{\overline{C}}'$	Deviation from depth average concentration	Arbitrary
C_{max}	Concentration on axis of jet at fixed distance	Arbitrary
D_x	Longitudinal dispersion coefficient	ft^2/sec
F_R	Froude number	0
F	Mathematical function	0
$\overline{F}_i$	Time-average body force in i direction	lbs
L_E	Eulerian length scale	ft
L_L	Lagrangian length scale	ft
Q	Volume discharge of water	ft^3/sec
R_H	Hydraulic radius	ft
$R(\tau)$	Correlation function	0
$R_L(\tau)$	Lagrangian correlation function	0
$R_E(\tau)$	Eulerian correlation function	0

Symbol		Units
$R_E(x,r,t)$	Eulerian space-time correlation function	0
$R_u(\xi,\tau)$	Eulerian space-time correlation function	0
$\mathbf{R_E}$	Reynolds number, $U_{xs}\ Y_N / \nu$	0
S	Slope of energy grade line	0
T	Total time or temperature	secs or °C
T_{A_i}	Integral time scale in ith direction based on longitudinal turbulent intensity, $i = x$, y, or z	secs
T_{E_i}	Eulerian time scale in ith direction, x, y, or z. No subscript assumes x direction.	secs
T_{L_i}	Lagrangian time scale in ith direction, x, y, or z	secs
T_{max}	Temperature differential on axis of jet at fixed distance	°C
U	Instantaneous velocity in x direction	ft/sec
$\overline{U}$	Time average local velocity in x direction	ft/sec
$\overline{\overline{U}}$	Depth average velocity	ft/sec
$\overline{\overline{U}}'$	Deviation from depth average velocity	ft/sec
$\overline{U}_s$	Time average velocity in x direction on water surface at channel centerline	ft/sec
U_{jet}	Jet discharge velocity	ft/sec
U_{max}	Velocity on axis of jet at fixed distance	ft/sec
U_{xs}	Cross-section average or free stream velocity	ft/sec
U_*	Shear velocity, $\sqrt{g\ R_H\ S}$	ft/sec
V	Instantaneous velocity in y direction	ft/sec
$\overline{V}$	Time average local velocity in y direction	ft/sec
W	Instantaneous velocity in z direction	ft/sec

Symbol		Units
$\overline{W}$	Time average local velocity in z direction	ft/sec
W	Width of flume	ft
Y_N	Uniform flow depth	ft
α	Dimensionless depth average diffusion coefficient	0
α_s	Dimensionless surface turbulent diffusion coefficient	0
γ	Specific weight of water	lbs/ft^3
ε_i	Turbulent diffusion coefficient in ith direction, x, y, or z	ft^2/sec
ε_{is}	Turbulent diffusion coefficient in ith direction at water surface	ft^2/sec
$\overline{\overline{\varepsilon}}_i$	Depth average turbulent diffusion coefficient	ft^2/sec
$\overline{\overline{\varepsilon}}'_i$	Deviation from depth average turbulent diffusion coefficient	ft^2/sec
ε_m	Molecular diffusivity	ft^2/sec
ε_M	Momentum transfer coefficient	ft^2/sec
$\theta(x,r,t)$	Probability density distribution	0
κ	Von Karman's kappa	0
μ	Dynamic viscosity of water	$lb \cdot sec/ft^2$
ν	Kinematic viscosity of water	ft^2/sec
ξ	Separation distance in space-time correlations	ft
ρ	Mass density of water	$slugs/ft^3$
σ_i	Standard deviation in ith direction	ft
σ_t	Standard deviation of time	secs
τ	Delay time	secs
τ_{max}	Time to first zero crossing of $R(\tau)$	secs

PARTIAL LIST OF SYMBOLS - (Continued)

Symbol		Units
τ_0	Boundary shear stress	lbs/ft^2
τ_{xy}	Shear stress in horizontal plane	lbs/ft^2
ω	Philip's parameter	0
Ω	Exponent in power law equation	0
$'$	Prime denotes fluctuation about depth average	0
$-$	Bar denotes time average	0
$=$	Double bar denotes depth average	0
$\sim$	Approximately	0

Chapter I

INTRODUCTION

The streams and rivers of the world have long been used as means for disposing of domestic, agricultural, and in present times, industrial wastes. As the population continues to increase the abilities of waterways to dilute and purify these discharges are being rapidly approached and in some instances exceeded.

The problem of pollutant disposal is often not so much that of quantity but rather one of distribution. Concentrated sources of pollution which overload a stream locally might easily be handled if distributed along its length. In order to determine what spacing of pollution sources can be handled by a stream, means must be found to relate the longitudinal, lateral, and vertical spread of pollutants to measurable characteristics of the flow field.

The problem is complicated somewhat by the fact that two mechanisms are involved in the dispersal process. The first, referred to as differential convection, is spreading due to differences in mean velocity of travel within a dispersant cloud. This is a large-scale effect. The second is mixing due to the turbulent velocity fluctuations. This is a generally smaller scale effect. When concentration of a dispersant is considered in a cross-section average sense and the spreading considered only in the streamwise direction, differential convection dominates. When viewed in this way, the longitudinal spreading process is referred to as "dispersion". The mixing due to turbulence is referred to as "diffusion". Some success has been achieved at predicting the one-dimensional convection-dominated dispersion process, but much work remains to be done with the three-dimensional turbulent diffusion problem.

The capacity of a waterway to disperse a substance in a given coordinate direction is usually expressed in terms of a transfer or turbulent diffusion coefficient. These coefficients are a measure of flux per unit time per unit area per unit gradient of the property being transferred. These are generally obtained from the rate of increase of the variance of the dispersant cloud downstream of the source. While direct measurement of diffusion coefficients for a particular source and flow condition is usually possible, prediction from mean flow parameters may not be. The difficulty in such predictions lies in the fact that turbulent diffusion coefficients are described most readily in a Lagrangian rather than Eulerian frame of reference. That is, the diffusion mechanism is connected to the random motion of individual particles moving with the flow field rather than to the random motion of many particles past a single point in space. Unfortunately the most readily conducted experimental measurements are in the Eulerian framework and no comprehensive theory exists to connect the two frames of reference.

Purpose

The primary purpose of this study is to develop readily useable Eulerian-Lagrangian relations which can be used to predict the turbulent diffusion coefficients in the vertical, lateral, and longitudinal coordinate directions from the statistical properties of turbulence measurements in the Eulerian framework. To meet this objective, the Eulerian-Lagrangian relation proposed by Philip (1967) is investigated. This relation may be used to predict longitudinal turbulent diffusion coefficients both at the water surface and in the flow field from properties of the longitudinal turbulent intensity. Similar relations are developed which allow the prediction of turbulent diffusion

coefficients in the lateral and vertical directions. These predictions are also based on the properties of the longitudinal turbulent intensity.

Method of investigation

Measurements of both diffusion coefficients and turbulence characteristics were made in a steady-uniform open-channel flow in a laboratory flume to determine the relation between the two. In the experiments, which are described in Chapter III, diffusion coefficients were measured for three different dispersants under a variety of source conditions over four boundary roughnesses. Lateral and vertical diffusion were studied by injecting neturally buoyant salt solution as a horizontal jet at the mid-depth of the flow. Similar experiments were conducted with heated water to determine if any difference existed between heat and mass transfer rates. The effect of buoyancy was not studied specifically. Longitudinal and lateral diffusion were measured on the water surface by releasing buoyant polyethylene particles. Diffusion of jets and particle diffusion are discussed in the literature review of Chapter II and more extensively in the analysis of Chapter V. Longitudinal diffusion within the flow field was studied by making the first known measurements of the velocity-concentration covariance along the axis of a neutrally buoyant salt solution plume. These measurements are compared to the longitudinal surface diffusion coefficient to determine the validity of the Boussinesq form of mass transfer coefficient. The covariance measurements are discussed extensively in Chapter V.

Turbulent intensity measurements were made over each boundary on the centerline of the channel and halfway between the centerline and the flume wall in order to describe the turbulence characteristics of the flow fields. Eulerian time scales obtained from statistical analysis of

the turbulence measurements were used along with Lagrangian time scales estimated using diffusion coefficients from the particle and covariance studies to substantiate Philip's (1967) Eulerian-Lagrangian relation for longitudinal diffusion. A similar form of relation for estimating lateral and vertical diffusion coefficients was developed from the salt solution and heated water jet studies. Longitudinal space-time velocity correlations were measured over two of the boundary roughnesses. Time scales obtained from these measurements were compared to Eulerian and estimated Lagrangian time scales from the other turbulence measurements to check their applicability for predicting diffusion coefficients. The analysis is presented in Chapter V.

The data from all the studies is presented in Chapter IV. The studies of diffusing jets produced a large quantity of data from which only representative samples are included. The complete data will be published in a U.S. Geological Survey open-file report. Chapter III gives a complete description of the experimental equipment, procedure, and the parameters measured.

As stated earlier, the primary purpose of this study is to develop Eulerian-Lagrangian type relations which may be used to estimate longitudinal, lateral, and vertical diffusion coefficients from the turbulence characteristics of the flow field. The nature of the data also allowed some analysis of the short-term behavior of diffusing jets. This was carried out as a secondary part of the study. It was found that the exponent in the power law equation which describes the decay of scalar quantities downstream of a jet is linearly related to the shear velocity of the channel. This is in contrast to the turbulent diffusion coefficients which could not be predicted from mean flow parameters such as

the shear velocity. It is also shown that the core length of a jet, that is, the distance from the end of the nozzle to the point where the axis temperature or concentration is no longer equal on the average to the injected value, can be predicted from a power law equation.

In addition to the secondary analysis of the jet data, measurements were made of the longitudinal dispersion coefficient over each boundary. These measurements were used to check some classical dispersion formulas and to better define the relation between longitudinal dispersion (spread by differential convection) and turbulent diffusion (spread by velocity fluctuations). The secondary analysis of jets and dispersion is presented in Chapters II and V.

Chapter II

BACKGROUND AND REVIEW OF PREVIOUS WORK

The Eulerian diffusion equation

The governing differential equation for the diffusion of an incompressible dispersant is readily derived from the principle of conservation of mass applied to a stationary control volume. The general equation is

$$\frac{\partial C}{\partial t} + U\frac{\partial C}{\partial x} + V\frac{\partial C}{\partial y} + W\frac{\partial C}{\partial z} = \varepsilon_m\left[\frac{\partial^2 C}{\partial x^2} + \frac{\partial^2 C}{\partial y^2} + \frac{\partial^2 C}{\partial z^2}\right] \tag{1}$$

where C is instantaneous concentration, t is time, U, V, and W are the velocities in the x, y, and z directions, and ε_m is the molecular diffusivity. With appropriate initial and boundary conditions, equation 1 gives an exact description of the diffusion process in laminar flow.

In turbulent flow, the presence of instantaneous fluctuations in concentration and velocity make application of equation 1 impractical. To transform the equation to a more useable form, the concentration and velocities are replaced by a mean value and a fluctuating component. After application of Reynolds' rules of averaging, equation 1 then becomes

$$\frac{\partial \overline{C}}{\partial t} + \overline{U}\frac{\partial \overline{C}}{\partial x} + \overline{V}\frac{\partial \overline{C}}{\partial y} + \overline{W}\frac{\partial \overline{C}}{\partial z} = -\frac{\partial \overline{uc}}{\partial x} - \frac{\partial \overline{vc}}{\partial y} - \frac{\partial \overline{wc}}{\partial z}$$

$$+ \varepsilon_m\left[\frac{\partial^2 \overline{C}}{\partial x^2} + \frac{\partial^2 \overline{C}}{\partial y^2} + \frac{\partial^2 \overline{C}}{\partial z^2}\right] \tag{2}$$

where overbars indicate time averaging over a period long enough for $\overline{c}$, $\overline{u}$, $\overline{v}$, and $\overline{w}$ to approach zero, but not so long as to damp the variation of $\overline{C}$, $\overline{U}$, $\overline{V}$, and $\overline{W}$ with t. The covariance terms, $\overline{u_i c}$, arise from

transport of dispersant by the turbulent velocity fluctuations u, v, and w. Because no direct information has been available about these covariance terms, further simplification has been made by introducing an analogy between the transport of mass and momentum. Written in tensor notation the diffusion equation is

$$\frac{\partial \overline{C}}{\partial t} + \overline{U}_i \frac{\partial \overline{C}}{\partial x_i} = - \frac{\partial}{\partial x_i} \overline{u_i c} + \varepsilon_m \frac{\partial^2 \overline{C}}{\partial x_i \partial x_i} \quad . \tag{3}$$

The momentum equation for turbulent flow is

$$\rho \frac{\partial \overline{U}_i}{\partial t} + \rho \overline{U}_j \frac{\partial \overline{U}_i}{\partial x_j} = - \rho \frac{\partial}{\partial x_j} \overline{u_i u_j} + \rho \nu \frac{\partial^2 \overline{U}_i}{\partial x_i \partial x_i} + \overline{F}_i - \frac{\partial \overline{\rho}}{\partial x_i} \quad . \tag{4}$$

With the exception of the body force term, $\overline{F}_i$, and the pressure gradient terms, $\partial\overline{\rho}/\partial x_i$, the two equations are of the same form. Boussinesq, in 1877 (Hinze, 1959) introduced the concept of a turbulent or eddy viscosity, ε_M, relating the turbulent shear stresses and the velocity gradients as follows:

$$\rho \overline{u_i u_j} = - \rho \varepsilon_M \left[\frac{\partial \overline{U}_i}{\partial x_j} + \frac{\partial \overline{U}_j}{\partial x_i} \right] \quad . \tag{5}$$

An analogous concept is usually used to relate turbulent mass flux and concentration gradients as follows:

$$\overline{u_i c} = - \varepsilon_{ij} \frac{\partial \overline{C}}{\partial x_j} \quad . \tag{6}$$

When this Boussinesq form of transfer coefficient is introduced into the diffusion equation and molecular diffusion is neglected it becomes

$$\frac{\partial \overline{C}}{\partial t} + \overline{U}\frac{\partial \overline{C}}{\partial x} + \overline{V}\frac{\partial \overline{C}}{\partial y} + \overline{W}\frac{\partial \overline{C}}{\partial z} = \frac{\partial}{\partial x}\left[\varepsilon_{xx}\frac{\partial \overline{C}}{\partial x} + \varepsilon_{xy}\frac{\partial \overline{C}}{\partial y} + \varepsilon_{xz}\frac{\partial \overline{C}}{\partial z}\right]$$

$$+ \frac{\partial}{\partial y}\left[\varepsilon_{yx}\frac{\partial \overline{C}}{\partial x} + \varepsilon_{yy}\frac{\partial \overline{C}}{\partial y} + \varepsilon_{yz}\frac{\partial \overline{C}}{\partial z}\right]$$

$$+ \frac{\partial}{\partial z}\left[\varepsilon_{zx}\frac{\partial \overline{C}}{\partial x} + \varepsilon_{zy}\frac{\partial \overline{C}}{\partial y} + \varepsilon_{zz}\frac{\partial \overline{C}}{\partial z}\right] . \qquad (7)$$

Equation 7 is still far too complex for general solution. Considerable further simplification can be achieved by assuming that the principal axis of the diffusion coefficient tensor, ε_{ij}, coincides with the axis of the flow field. This reduces the off-diagonal diffusion coefficients ($i \neq j$) to zero and equation 7 becomes

$$\frac{\partial \overline{C}}{\partial t} + \overline{U}\frac{\partial \overline{C}}{\partial x} + \overline{V}\frac{\partial \overline{C}}{\partial y} + \overline{W}\frac{\partial \overline{C}}{\partial z}$$

$$= \frac{\partial}{\partial x}\left[\varepsilon_x \frac{\partial \overline{C}}{\partial x}\right] + \frac{\partial}{\partial y}\left[\varepsilon_y \frac{\partial \overline{C}}{\partial y}\right] + \frac{\partial}{\partial z}\left[\varepsilon_z \frac{\partial \overline{C}}{\partial z}\right] \qquad (8)$$

after dropping the now unnecessary double subscript on ε. This assumption makes possible the direct evaluation of the turbulent transfer coefficients from measurements of the velocity-concentration covariances and the relation

$$\varepsilon_i = \frac{\overline{u_i c}}{\partial \overline{C}/\partial x_i} . \qquad (9)$$

In practice this has seldom been done because of the difficulty of measuring the covariance terms. In this study a technique is developed for measuring the longitudinal covariance term, $\overline{uc}$, from which ε_x may be evaluated.

A more common technique for evaluating the transfer coefficients, ε_i, is from the rate of increase of the variance of diffusing clouds.

In the following two sections a review is presented of work on vertical, lateral, and longitudinal mass transfer using such methods.

Lateral diffusion

Prych (1970) presents an excellent review of available data on lateral and vertical diffusion. His review is paraphrased here.

Data from experiments with floating particles are often used to obtain values of ε_{zs}, the lateral diffusion coefficient at the free surface. Experiments of this type were first made by Orlob (1959), later by other investigators, and also in the present study. A summary of the experimental data from these investigations is given in table 1. Values of ε_{zs} for the present study were calculated by the formula

$$\varepsilon_{zs} = \frac{\overline{U_s}}{2} \frac{d\,\sigma_z^2}{dx} \quad , \tag{10}$$

where σ_z^2 is the variance of the lateral distribution of particles after traveling a fixed distance. The dimensionless diffusion coefficient α_s is defined by

$$\alpha_s = \frac{\varepsilon_{zs}}{Y_N U_*} \quad , \tag{11}$$

where Y_N is the normal flow depth and U_* is the shear velocity. The average value of α_s from each of the studies listed in table 1 ranges from 0.086 to 0.241.

Because of vertical mixing, observations of lateral mixing of solutes yield only a depth-averaged value of the lateral turbulent diffusion coefficient, ε_z. This coefficient is usually calculated using the formula

Table 1. *Summary of data on lateral diffusion of floating particles*[1]

Reference	Run number	Channel	Floating particles	Depth Y_N (ft)	Shear velocity U_* (ft/sec)	Average velocity U_{zs} (ft/sec)	Surface velocity U_s (ft/sec)	Diffusion coefficient ϵ_{zs} (ft^2/sec)	$\alpha_s = \frac{\epsilon_{zs}}{Y_N U_*}$
Orlob (1959)		Laboratory flume 4 ft wide, expanded metal screen roughness on bottom	Polyethylene discs 0.01 ft diameter, 0.005 ft thick, specific gravity = 0.975	0.0532 to .420					0.172
Sayre and Chamberlain (1964)		Laboratory flume 7.83 ft wide, sand dunes on bottom	Polyethylene discs 0.01 ft diameter, 0.005 ft thick, specific gravity = 0.960	0.57	0.115	1.63	2.04	0.0161	0.241
Sayre and Chang (1968)	LA-P-1	Laboratory flume 7.83 ft wide, roughness blocks 3/4-inch high, 5/8-inch wide, 3 inches long on bottom	Polyethylene discs 0.01 ft diameter, 0.005 ft thick, specific gravity = 0.960	0.486	0.125	0.770	1.10	0.0143	0.236
	LA-P-2			.803	.161	1.13	1.49	.0251	.196
	LA-P-3			1.217	.198	1.56	2.16	.0636	.264
Engelund (1969)	A	Laboratory flume 7.5 ft wide, 0.075 ft diameter, sand roughness on bottom	Plastic ball 0.0295 ft diameter, specific gravity = 0.288	0.179	0.118	0.984	1.25	0.0043	0.204
	B	Laboratory flume 7.5 ft wide, 0.0033 ft diameter, sand roughness on bottom	Plastic ball about 0.0115 ft diameter, specific gravity = 0.288	.567	0.052	1.010	1.13	0.0069	0.234
Prych (1970)		Laboratory flume 3.61 ft wide, smooth bottom or expanded metal screen roughness on bottom	Polyethylene particles about 0.0115 ft diameter, specific gravity = 0.95	0.128 to .364					0.204 (average)
This study		Laboratory flume 3.87 ft wide							
	S1	Smooth bottom	Polyethylene particles 0.0078 ft diameter, specific gravity = 0.986	0.915	0.0616	1.036	1.172	0.00388	0.086
	S2	Smooth bottom		.528	.0415	.852	.934	.00360	.164
	R1	1½-inch rocks on bottom		.892	.0850	.956	1.188	.01074	.142
	R2	1½-inch rocks on bottom		.469	.0694	.721	.815	.00668	.205
	RB1	1½-inch rocks and cobbles on bottom		.945	.0938	.875	1.190	.01110	.125
	RB2	1½-inch rocks and cobbles on bottom		.528	.0996	.780	.930	.01240	.236

[1]Adapted from Prych (1970).

$$\varepsilon_z = \frac{\overline{U}_{xs}}{2} \frac{d\,\sigma_z^2}{dx} \tag{12}$$

where σ_z^2 is the variance of the lateral distribution of concentration, $\overline{C}$, and $\overline{U}_{xs}$ is the cross section average velocity.

Values of ε_z and the dimensionless coefficient

$$\alpha = \frac{\varepsilon_z}{Y_N U_*} \tag{13}$$

from a number of investigations are given in table 2. These data can be divided into two groups, one from experiments in straight channels (Elder, 1959; Sayre and Chang, 1968; Sullivan, 1968; Glover, 1964; Fischer, 1967; Prych, 1970) and the other from experiments in curved channels (Glover, 1964; Yotsukura and others, 1970; Fischer, 1969). Except for Glover's data, which were from experiments in which the tracer was not neutrally buoyant, the data from straight channels yield values of α between 0.092 and 0.250. [One should observe that the often quoted value published by Elder (1959) has been corrected in table 2 as suggested by Prych (1970). All values from curved channels are greater than 0.5.]

Vertical diffusion

An estimate of the vertical diffusion coefficient for mass in a wide open-channel flow, ε_y, can be obtained from Reynolds' analogy between the transport of mass and momentum (that is, by assuming that ε for mass and momentum are equal in the y direction) by expressing τ_{xy}, the apparent shear stress on a horizontal plane, as

$$\tau_{xy} = \varepsilon_y \rho \frac{d\overline{U}}{dy} \tag{14}$$

Table 2. *Summary of lateral diffusion of solutes*[2]

Reference	Run number	Channel	Tracer	Concentration determined by	Depth y_N (ft)	Shear velocity U_* (ft/sec)	Average velocity U_{av} (ft/sec)	Diffusion coefficient ϵ_z (ft^2/sec)	$a = \frac{\epsilon_z}{y_N U_*}$
Elder (1959)		Laboratory flume 1.16 ft wide, smooth bottom	Potassium permanganate dye	Analysis of photographs with microdensitometer	0.049				0.164
Sayre and Chang (1968)	LA-D-1	Laboratory flume 7.83 ft wide, roughness blocks 3/4-inch high, 5/8-inch wide, 3 inches long on bottom	Fluorescent dyes	Continuous sampling fluorometer	0.485	0.125	0.770	0.0103	0.170
	LA-D-2				.804	.160	1.130	.0217	.179
	LA-D-3				1.215	.198	1.215	.0397	.160
Sullivan (1968)		Laboratory flume 2.5 ft wide, smooth bottom	Gentian violet dye	Analysis of photographs with microdensitometer	0.334	0.027	0.502	0.000967	0.107
					.293	.032	.607	.00104	.110
					.240	.039	.752	.00127	.133
Glover (1964)		Laboratory flumes 8 ft and 4 ft wide, rough and smooth bottoms	Sodium chloride	Measurement of fluid conductivity	0.481			0.0360	0.36
					.452			.0089	.22
		Columbia River near Richland, Wash., 1000 ft wide	Radionuclides in cooling water	Radiation counting of samples	.944			.0077	.14
					~10		~4.4	2.00	.72
Fischer (1967)	6/21	Atrisco Feeder Canal near Bernalillo, N. Mex., approximately 57.5 ft wide, 1 ft high sand dunes on bottom	Rhodamine WT dye	Analysis of samples with fluorometer	2.24	0.206	2.08	0.110	0.24
	6/23				2.18	.201	2.06	.110	.25
Yotsukura, Fischer, and Sayre (1970)		Missouri River near Blair, Neb., approximately 730 ft wide	Rhodamine B dye	Analysis of samples with fluorometer	~8.85	0.242	~5.75	1.29	0.6
Fischer (1969)	2	Curved laboratory channel, 2.5 ft wide, smooth bottom	Rhodamine WT dye	Analysis of samples with fluorometer	0.099	0.0872	1.040	0.0121	1.4
	3				.173	.0557	.885	.0230	2.4
	4				.122	.0698	.879	.0114	1.3
	5				.067	.0449	.624	.00210	.70
	6				.072	.0551	.646	.00202	.51
Prych (1970)		Laboratory flume 3.61 ft wide, smooth and rough bottoms	Sodium chloride	Measurement of fluid conductivity	0.129 to .692				0.135 (Average)
This study		Laboratory flume 3.87 ft wide	Sodium chloride	Single electrode conductivity probe					
	S1	Smooth bottom			0.915	0.0616	1.036	0.00411	0.092
	TR1	3/4-inch rock bottom			.933	.0803	.849	.00731	.097
	RB1	1½-inch rock and cobble bottom			.945	.0938	.875	.0119	.134

[2] Adapted from Prych (1970).

where ρ is the fluid density, and ε_y is the eddy viscosity. Using the Prandtl-von Karman logarithmic velocity distribution,

$$\frac{\overline{U} - \overline{\overline{U}}}{U_*} = \frac{1}{\kappa}\left(1n\ \frac{y}{Y_N} + 1\right) \quad , \tag{15}$$

where $\overline{U}$ is the local mean velocity and $\overline{\overline{U}}$ is the depth-averaged velocity, and a linear distribution of shear stress,

$$\tau_{xy} = \rho\ U_*^2\left(1 - \frac{y}{Y_N}\right) \quad , \tag{16}$$

equation 14 yields

$$\varepsilon_y = \kappa\ U_*\ y\left(1 - \frac{y}{Y_N}\right) \quad . \tag{17}$$

This expression for ε_y is zero at $y = 0$ and $y = Y_N$, and is symmetric about $y = Y_N/2$. The depth-averaged value is given by

$$\varepsilon_y = \frac{\kappa}{6}\ Y_N\ U_* \quad . \tag{18}$$

Vanoni (1946) observed the vertical distributions of suspended sediment in an open-channel flow and used the data to calculate ε_y for sediment. He found that the distribution of ε_y was similar to that given by equation 17. Jobson and Sayre (1970) introduced dye at the surface of an open-channel flow and observed the vertical concentration as a function of distance downstream. They used the data to calculate ε_y and also found that equation 17 was valid. Similar experiments with fine sediment gave nearly the same results.

Longitudinal diffusion

Because the longitudinal spreading process is governed primarily by variations in mean velocity (dispersion) with turbulence playing a

second order role, little is known about longitudinal diffusion. Existing experimental data are primarily for transport at the water surface, that is, ε_{xs}. Measurements of ε_{xs} were made by Sayre and Chang (1968), Engelund (1969), and also in the present study. In these studies floating particles were released at a point on the water surface and the distribution in time for particles to travel a fixed distance or the longitudinal distribution after a fixed time was observed. Longitudinal turbulent diffusion coefficients were then calculated from relations similar to equations 10 and 12. When normalized with the product of normal depth and shear velocity, $Y_N U_*$, Sayre and Chang's data gave values for the dimensionless diffusion coefficient from 0.470 to 1.06. Engelund's data gave values from 0.031 to 0.048. Values of $\varepsilon_{xs} / Y_N U_*$ for the present study ranged from 0.205 for the smoothest boundary to 0.535 for the roughest boundary. The longitudinal turbulent diffusion coefficient is sometimes estimated as the mean value of the vertical diffusion coefficient. This is usually computed as $(\kappa/6) Y_N U_*$ (equation 18). Kappa is often taken to be 0.4, thus $\kappa/6 = 0.067$ indicating this to be an estimate which may be up to one order of magnitude low.

Longitudinal dispersion

Another type of mixing which is of interest in open channels is the longitudinal spread of slugs of dispersant. This type of problem might arise from a short term overflow of sewage into a river or other situations where the dispersant is introduced into a stream for a short period of time. At some distance from the point of injection the dispersant becomes distributed throughout the depth and breadth of the flow and spreading is confined to the longitudinal direction. Such spreading

is dominated by variation of the mean velocity across the channel and is referred to as dispersion. The following section discusses this type of process.

Dispersion is often described by a two-dimensional depth-averaged form of the diffusion equation. The coordinate system used is one where x is along the axis of flow, y is normal upward from the channel bottom, and z is the lateral direction. If secondary circulation is neglected, $\overline{V} = \overline{W} = 0$. For steady uniform flow in an infinitely wide channel, $\frac{\partial \varepsilon_x}{\partial x} = \frac{\partial \varepsilon_z}{\partial z} = 0$. Equation 8 now becomes

$$\frac{\partial \overline{C}}{\partial t} + \overline{U}\frac{\partial \overline{C}}{\partial x} = \varepsilon_x \frac{\partial^2 \overline{C}}{\partial x^2} + \frac{\partial}{\partial y}\varepsilon_y \frac{\partial \overline{C}}{\partial y} + \varepsilon_z \frac{\partial^2 \overline{C}}{\partial z^2} \quad . \tag{19}$$

To obtain the two-dimensional form vertical mixing is assumed complete and the velocity, concentration, and the diffusion coefficients are replaced by depth-averaged values. Denoting these depth-average values by a double overbar and the deviation from the depth-average value by a prime, equation 19 transforms to

$$\frac{\partial \overline{\overline{C}}}{\partial t} + \overline{\overline{U}}\frac{\partial \overline{\overline{C}}}{\partial x} + \frac{\partial}{\partial x}(\overline{\overline{U'C'}}) = \overline{\overline{\varepsilon}}_x \frac{\partial^2 \overline{\overline{C}}}{\partial x^2} + \overline{\overline{\varepsilon}}'_x \frac{\partial^2 \overline{\overline{C}}'}{\partial x}$$

$$+ \overline{\overline{\varepsilon}}_z \frac{\partial^2 \overline{\overline{C}}}{\partial z^2} + \overline{\overline{\varepsilon}}'_z \frac{\partial^2 \overline{\overline{C}}'}{\partial z^2} \quad . \tag{20}$$

The covariance terms in equation 20 now represent convection by velocity deviations from the depth-averaged value rather than turbulence as in equation 3. Elder (1959) showed that for two-dimensional flows in which $\partial \overline{\overline{C}}/\partial z = 0$, one can write for large dispersion times

$$\overline{\overline{U'C'}} = -D_x \frac{\partial \overline{\overline{C}}}{\partial x} \quad . \tag{21}$$

D_x is the longitudinal dispersion coefficient. Using the Prandtl-von Karman logarithmic velocity distribution to obtain $\overline{U}'$ and the Reynolds' analogy to obtain ε_y, Elder obtained

$$D_x = \frac{0.404}{\kappa^3} Y_N U_* \quad , \tag{22}$$

where κ is von Karman's constant. For $\kappa = 0.41$, $D_x = 5.86\ Y_N\ U_*$. Elder confirmed his result for a wide shallow channel over a smooth boundary.

Dispersion coefficients found in natural streams often exceed the value predicted by equation 19 by factors of 10 and higher. To account for this discrepancy Fischer (1966) adapted Taylor's (1954) theory of convective dispersion in axisymmetric pipe flow. He concluded that transverse mixing combined with lateral variations in velocity are the dominant mechanisms of dispersion in natural channels. Prediction of dispersion by Fischer's methods requires that the geometry, the transverse velocity distribution, and the lateral mixing coefficient $\overline{\overline{\varepsilon}}_z$ be known for a typical cross section.

Eulerian-Lagrangian time scale relations and diffusion

On the basis of experimental evidence that the probability distribution of diffusing particles was Gaussian, Batchelor (1949) concluded that concentration (weight per unit volume) satisfies equation 7 when the diffusion coefficient tensor is given by

$$\varepsilon_{ij} = \frac{1}{2} \frac{d\ \overline{\sigma^2_{ij}}}{dt} \quad , \tag{23}$$

and $\overline{\sigma^2_{ij}}$ is equal to $\overline{x_i x_j}$, the variance of the path length of an emsemble of single particles initially positioned at the origin at some time t after release. This is also equivalent to the covariance of a cloud of

particles initially positioned at the origin, a time t after release. The term $\overline{\sigma_{ij}^2}$ is related to the Lagrangian velocity correlations, $R_{L_{ij}}(\tau)$, by the theorem of Taylor (1954):

$$\overline{\sigma_{ij}^2} = 2\left(\overline{u_i^2} \cdot \overline{u_j^2}\right)^{\frac{1}{2}} \int_0^t \int_0^{t^*} \left[R_{L_{ij}}(\tau) + R_{L_{ji}}(\tau)\right] d\tau \, dt^* \tag{24}$$

where

$$R_{L_{ij}}(\tau) = \frac{\overline{u_i(\tau) \cdot u_j(0)}}{\left(\overline{u_i^2} \cdot \overline{u_j^2}\right)^{\frac{1}{2}}} \quad . \tag{25}$$

Here u_i and u_j are fluctuating velocity components.

Batchelor has shown that the time rate of change of the covariance matrix of the displacement, $\partial(\overline{x_i x_j})/\partial t$, can be written as

$$\frac{\partial(\overline{x_i x_j})}{\partial t} = \left(\overline{u_i^2} \cdot \overline{u_j^2}\right)^{\frac{1}{2}} \int_0^t \left[R_{L_{ij}}(\tau) + R_{L_{ji}}(\tau)\right] d\tau \quad . \tag{26}$$

By taking the time of integration, t, large enough, the integral in equation 26 will approach a constant, since as t becomes large, $R_{L_{ij}}(\tau)$ and $R_{L_{ji}}(\tau)$ approach zero. By defining the Lagrangian integral time scale as

$$T_{L_{ij}} = \lim_{t \to \infty} \int_0^t R_{L_{ij}}(\tau) \, d\tau \tag{27}$$

equation 26 becomes

$$\frac{\partial(\overline{x_i x_j})}{\partial t} = \left(u_i^2 \cdot u_j^2\right)^{\frac{1}{2}} \left[T_{L_{ij}} + T_{L_{ji}}\right] \quad . \tag{28}$$

When the principal axis of the correlation tensors $R_{L_{ij}}(\tau)$ and $R_{L_{ji}}(\tau)$ coincide with the axis of the flow field, $T_{L_{ij}}$ and $T_{L_{ji}} = 0$ for $i \neq j$. Dropping the unnecessary double subscripting equation 23 becomes

$$\varepsilon_i = \overline{u_i^2}\, T_{L_i} \quad . \tag{29}$$

Direct measurement of the Lagrangian correlation function so that ε_i could be found from equation 29 is not currently feasible, meaning that it can be done only at great expense. Measurement of the longitudinal Eulerian time scale, however, is relatively easy from the autocorrelation function of a turbulence signal. It is thus desirable to develop a relation between the Eulerian and Lagrangian correlation functions.

Working from the assumption of a homogeneous isotropic turbulence field with no mean motion, Philip (1967) assumed that the Eulerian space-time correlation function, $R_E(x,r,t)$, could be expressed as

$$R_E(x,r,t) = \exp\left[-\frac{\pi}{4}\left(\frac{x^2 + 3.138\, r^2}{L_E^2} + \frac{t^2}{T_E^2}\right)\right] \quad , \tag{30}$$

where L_E is the Eulerian integral length scale, T_E is the Eulerian integral time scale, x is the longitudinal coordinate direction and r is the radial coordinate direction. The functional form of equation 30 was determined by physical reasoning and mathematical convenience. After transforming to a space with mean motion he was able to express the relation between Eulerian and Lagrangian time scales as

$$\frac{T_L}{T_E} = \left(1 + \frac{\omega^2}{\overline{u^2}}\right)^{\frac{1}{2}} F(\omega) \quad , \tag{31}$$

where $\overline{u^2}$ is the mean square of the velocity fluctuations and $\omega = (\sqrt{\overline{u^2}}\ T_E)/L_E$. The function $F(\omega)$ is an equation which was solved by numerical techniques for various values of the parameter ω. The present study tends to confirm the general form of Philip's relation.

Baldwin and Mickelsen (1963) investigated the possible relation between Lagrangian and space-time Eulerian measurements. Space-time correlations are generated by measuring one of the turbulence components u_i at two points in the flow field separated by a distance ξ. By delaying one u_i signal with respect to the other by a time τ it is possible to map this function in the ξ,τ plane. The function $R(\xi,\tau)$, evaluated along $\xi = \overline{U}_i\tau$, should be approximately equal to the Lagrangian single particle correlation if two assumptions are satisfied. First, the Lagrangian derivative is assumed to be

$$\frac{Dv}{Dt} \simeq \frac{\partial v}{\partial t} + \overline{U}\,\frac{\partial v}{\partial x} \quad ,$$

and second, the interchange of particle averaging and space-time averaging is assumed to be the same as the assumption that the mean-square Lagrangian and Eulerian turbulent velocity fluctuations are equal.

Using these assumptions, Baldwin and Mickelsen used the space-time correlations to predict the variance of diffusing matter. This was done by rewriting equation 24 as

$$\overline{\sigma_i^2} = 2\left(\overline{u_i^2}\right) \int_0^t \int_0^{t'} \left[R_u(\xi,\tau)\Big|_{\xi=\overline{U}\tau} d\tau \right] dt' \quad . \tag{32}$$

This equation overpredicted their experimental results by factors of 1.5 to 3.3.

Diffusion of turbulent jets

As mentioned in the introduction, the data for obtaining diffusion coefficients were obtained at some distance from the point of dispersant injection. This was done to insure that dispersant particles were spreading under the influence of the ambient turbulence in the flow and not due to momentum induced by the injector jet. The data also allowed some observations on the short term behavior of the jet itself. This section is a very short review of an extensively studied subject to give the reader background for the analysis of Chapter V.

The classic "engineering" (oriented toward practical application) approach to jet diffusion into quiescent fluid was developed by Albertson and others (1948). Under the assumptions of hydrostatic pressure distribution, dynamic similarity of velocity profiles, and normal distribution of the longitudinal velocity within the jet, a complete description of the flow field was found containing only one experimental constant. The equation for the decrease in centerline velocity, U_{max}, was given by

$$\frac{U_{max}}{U_{jet}} \frac{x}{d} = 6.2 \quad , \tag{33}$$

where U_{jet} is the jet discharge velocity and d is the jet diameter. The velocity distributions were approximated by error curves as

$$\text{Log}_{10} \frac{\overline{U}}{U_{jet}} \frac{x}{d} = 0.79 - 33 \frac{r^2}{x^2} \quad , \tag{34}$$

where $\overline{U}$ is the longitudinal velocity and r is the radial coordinate.

The "engineering" approach to jet diffusion into secondary streams was taken by Forstall and Shapiro (1950). The equation given for the decrease in centerline velocity was given as

$$\frac{U_{max}}{U_{jet} - U_{xs}} = \frac{x_c}{x} \quad \text{for} \quad x > x_c \quad , \tag{35}$$

where U_{xs} is the mean velocity of the stream into which the jet is injected, and x_c is the distance from the nozzle to the end of the core of the jet. x_c is given by

$$\frac{x_c}{d} = 4 + 12 \frac{U_{xs}}{U_{jet}} \quad . \tag{36}$$

The velocity distributions were approximated by cosine curves as

$$\frac{\overline{U} - U_{xs}}{U_{max} - U_{xs}} = \frac{1}{2}\left(1 + \cos \frac{r}{2r_{mv}}\right) \quad , \tag{37}$$

where r_{mv} is the radial coordinate where $\overline{U} = (U_{xs} + U_{max})/2$. $\overline{U}$ is the local mean velocity at any point in the jet. Forstall and Shapiro (1950) give an excellent list of references and a table showing previous work on jet diffusion. Hinze (1959) and Townsend (1956) present the analytic approach to the problem. This paper will take the "engineering" approach to show the effect of ambient turbulence on the decay of a jet in a shear flow.

Chapter III

EXPERIMENTAL EQUIPMENT AND PROCEDURE

The objectives of the experiments were to: (1) measure the statistical properties of concentration and temperature profiles from which vertical and lateral diffusion coefficients within the flow field could be determined; (2) measure the longitudinal velocity-concentration covariance to determine the longitudinal turbulent diffusion coefficient within the flow field; (3) measure the distribution of floating particles in order to determine the lateral and longitudinal turbulent diffusion coefficients at the water surface; (4) determine the longitudinal dispersion coefficient using fluorescent dye techniques; and (5) define the turbulence characteristics of the flow field in terms of the longitudinal turbulence intensity (including space-time velocity correlations) and its statistical properties. The longitudinal turbulence parameters are readily measured and offer the most hope of relating turbulence to real-world diffusion and dispersion problems. With this in mind, diffusion, dispersion, and turbulence measurements were made in a laboratory flume over four boundary conditions representing a wide range of roughness. These experiments are described in three sections. The first describes the experimental equipment. The second describes the various experimental parameters which were measured. The third describes the experimental procedure.

Experimental equipment

Flume.--All the experiments were conducted in a flume 3.87 feet wide, 2 feet deep, and 120 feet long. The interior of the plywood

flume was surfaced with a fiberglass finish, except for a section of the left sidewall 24 feet long which was made of transparent plexiglass. The slope of the plywood channel could be adjusted from 0 to 1.5 percent by 12 sets of screw jacks which supported the flume. To avoid heat and salt solution buildup within the flume, flow was not recirculated. Water was withdrawn from Horsetooth Reservoir near the Colorado State University hydraulics laboratory which provided a near-infinite supply of water at a constant temperature and 200 feet of head. Flow was throttled to desired discharges by a 36-inch ball valve and two 12-inch globe valves. Discharge was measured by means of an orifice in the supply line. The water was passed through the flume and discharged into a small stream leading to an irrigation reservoir.

The flume was equipped with an instrument carriage which rested on rails mounted on the flume. The carriage was capable of traveling the entire length of the flume. The carriage was equipped with a traversing mechanism for moving sensing elements throughout the depth and breadth of the flow field. The flume and carriage are illustrated in figure 1.

Roughness.--Four boundary roughnesses were used in this study. The first was a hydraulically smooth surface provided by the fiberglass finish on the plywood. The second was a hydraulically rough surface obtained by covering the flume bed with a layer of 3/4-inch diameter crushed rock as shown in figure 2. The third was a rough surface obtained by covering the flume bed with a layer of 1½-inch diameter crushed rock as shown in figure 3. The fourth was a rough surface obtained by scattering at random 3- to 6-inch diameter cobbles on top of the 1½-inch crushed rock as shown in figure 4.

Dispersant injection.--Hot water and salt solution were injected into the flow field parallel to the direction of flow through curved nozzles extending through the water surface at the channel centerline. Three sizes of nozzles were used. Their inside diameters were 0.468 cm, 1.049 cm, and 1.882 cm. All three nozzles were constructed of flexible copper tubing. The large nozzle and the support system are illustrated in figure 5.

Flow of hot water and salt solution were regulated by means of commercially available pressure regulators in the respective supply lines. An air-water manometer attached to the outlet side of whichever regulator was being used was read to determine the discharge of the nozzle. The manometer was calibrated by first submerging the nozzle in a container to the depth of flow to be run in the flume. The weight of water spilled from the container per unit time was then determined at a wide range of manometer readings.

Hot-water system.--Hot water was supplied by a Payne 168-85 pb gas-fired water heater. This heater was capable of supplying continuous output of 168 gallons per hour at 100°F above stream temperature. No hot water shortage was encountered at any time during the study. The system is shown in figure 6.

The injection temperature of the hot water was controlled by a Powers FOTOPANEL Model 440-2000 thermostatic mixing valve. The valve operates by mixing hot and cold water to maintain some preset temperature. Originally designed for use in photochemical work, the mixing valve is capable of maintaining ± 0.1°F output temperature. The system is shown in figure 7. Only at extremely low flow rates with the small nozzle was any instability of temperature encountered.

Salt system.--Salt solution was mixed and stored in a specially constructed 500-gallon pressure tank as shown in figure 8. A one-half horsepower stirring motor inside the tank kept the solution constantly mixed. Water at the mean flow temperature was circulated through a cooling radiator to maintain the solution in the tank at the same temperature as the flow. Pressure to force the solution from the tank was supplied by a large air compressor. The capacity of the tank allowed approximately 3 hours of steady running at maximum flow rate from the large nozzle.

The salt solution was composed of water, methyl alcohol, and salt. The alcohol content was varied to maintain the mixture at neutral buoyancy. A typical mixture consisted of 10.4 pounds of salt, 6.16 gallons of alcohol, and 493 gallons of water.

Plane source injector for dispersion.--In order to simulate a uniformly distributed plane source of dispersant, a tilting trough was mounted 5 feet above the bed of the flume. The capacity of the trough was approximately 1 gallon. When rotated quickly the trough produced a nearly vertical sheet of dispersant which impacted on the water surface with sufficient momentum to penetrate through the depth of flow.

The dispersant used in this study was Rhodamine WT dye. It was detected by a commercially available fluorometer. Water was siphoned from the flume and through a flow-through door of the instrument. This allowed measurement of concentration versus time profiles. The output of the fluorometer was recorded on a strip-chart recorder.

Particle diffusion.--Particle diffusion measurements were made by dropping small polyethylene particles (3/32-inch diameter; specific gravity, 0.986) onto the water surface through a funnel located at the centerline of the flume. The particles were dropped at the same longitudinal station where the jets were injected into the flow. The particles were collected from the water surface at a particular station in a compartmented trap. The trap consisted of one hundred 1-centimeter wide by 10-centimeter high by 10-centimeter long screen wire compartments suspended from a support perpendicular to the direction of flow so as to just skim the water surface. The particles were timed over the distance to the trap using a stop watch.

Conductivity probe.--All temperature and concentration measurements were made with a single-electrode conductivity probe. The probe used was patterned after those of Keeler (1964). Such probes operate on the theory that when an extremely large and an extremely small electrode are immersed in an electrolyte solution, the resistance between the two will be governed by the volume elements adjacent to the small electrode. This theory is documented by Gibson and Schwarz (1963). A cross section of the probe used in this study is illustrated in figure 9. The final probe configuration is a combination of theory and trial-and-error. The platinum wire size was selected using the mathematical model of Gibson and Schwarz. The 0.002-inch diameter gave a high frequency cutoff (10 percent power loss point) of 100 Hertz. Power spectral density analysis of turbulence in water has shown practically no power beyond 50 Hertz. The probe was thus judged adequate for correlation measurements. Elaborate shielding of the probe was found necessary because of the hypersensitivity of the bridge

unit to stray capacitance changes. Original designs without shielding were sensitive to position in the flow field. The shielding corrected this except for positions within 2 inches of the rock boundaries. No problems were encountered when working over the smooth boundary. The final design is a good tool for temperature or conductivity measurements in water. The resistance measuring unit used in this study was a Tektronix 3C66 carrier amplifier originally designed to operate strain gages. This unit was used without modification. Power for the carrier amplifier was provided by a compatible Tektronix oscilloscope on which the output was displayed. A "signal-out" jack provided 3 volts of DC output for each centimeter of deflection on the scope display screen. This voltage was used to drive a strip-chart recorder through an averaging circuit while collecting data.

Probe calibration for response to concentration was accomplished as follows: First, a series of standard salt solutions were prepared ranging in concentration from 0 (distilled water) to 10,000 mg/ℓ. These solutions were stored in a constant temperature bath. The bath was cooled by water at stream flow temperature. A calibration curve of output voltage versus concentration was constructed by immersing the probe in each of the standards and recording the voltage output. The carrier amplifier unit was adjusted to give zero output in flume water.

Probe calibration for response to temperature was accomplished as follows: Water at the ice point was placed in an insulated container. The temperature was measured using a calibrated thermometer. The probe was then immersed and the output voltage adjusted to zero. Incremental amounts of hot water were added to the container and mixed thoroughly. After each addition the temperature and output voltage were recorded.

Probe response proved to be linear within ±1 percent to both concentration (conductivity) and temperature. This made it unnecessary to run elaborate calibrations during measurements. Simply by checking the response at one concentration or temperature, it was possible to detect probe deterioration. If probe deterioration was detected the probe tip was cleaned and recoated with platinum black to restore original sensitivity.

Turbulence system.--Turbulence measurements were made with a dual-channel constant temperature anemometer. Parabolic shaped hot-film sensors were used because of their resistance to signal drift caused by fluid-borne contaminants. These sensors are illustrated in figure 10.

Auxiliary equipment used in conjunction with the anemometer and the conductivity-probe system included: A strip-chart recorder for recording mean output voltage; a true rms meter for determining the magnitude of voltage fluctuations; and an F.M. magnetic tape recorder for recording voltage fluctuations. A schematic of the electrical hookup for both units is shown in figure 11. In addition to the anemometer system a 1/8-inch diameter pitot tube and a pressure transducer and indicator were used to measure local mean velocities.

All sensors were calibrated for response to velocity at several overheat ratios as described by McQuivey (1967). This allowed compensation for changes in sensor output due to changes in mean temperature or due to contamination build-up on the sensor.

The following two sections will describe the experimental variables and parameters and the data collection procedure, respectively.

Description of experimental variables and parameters

The following kinds of data were taken in the investigation. The measurements, which are described in detail later, fall into three general areas as follows:

Basic hydraulic parameters

Water-surface slope

Water discharge

Water temperature

Average depth of flow

Relative depth

Mean velocity

Velocity profiles

Shear velocity

Shear stress at the bed

Kinematic viscosity

Reynolds number

Froude number

Chezy discharge coefficient

Turbulence characteristics

Longitudinal turbulence intensity

Relative turbulence intensity

Autocorrelation function and Eulerian integral time scale

Macroscale of turbulence

Space-time correlations

Diffusion and dispersion

Temperature and concentration profiles

Velocity-concentration covariance

Jet strength

Jet Froude number

Depth average diffusion coefficients

Surface diffusion coefficients

Dispersion coefficient

Variances A and B

Basic hydraulic parameters

Water-surface slope.--The water surface and bed slopes were determined by using an engineer's level and a point gage mounted on the carriage. Water surface and bed elevations were measured at 12-foot intervals along each side of the flume. This was repeated several times. The mean water-surface slope for each run was determined by averaging the corresponding slopes of the least square lines through the measured elevations.

Water discharge.--The water discharge in the flume was determined in the supply pipe line with a calibrated orifice meter connected to a water-mercury manometer. Several readings were recorded to obtain a good average.

Water temperature.--The water temperatures were measured to the nearest one-tenth of a degree centigrade with a mercury thermometer. The temperature reported was based on an average of about 10 readings obtained during data collection. The temperature did not vary more than 0.5 degree centigrade during a measurement series.

Average depth of flow.--The depth of flow over the smooth boundary was just the depth from the water surface to the bed. For flow over the rock roughnesses the depth is not defined so easily. The average depths reported over the rock roughnesses were determined by extrapolating velocity profiles to zero. For flow over the 3/4-inch rock the depth was taken from the water surface to 1/4 inch below the average tops of the rocks. For flow over the 6-inch cobbles the depth was taken from the water surface to 1/2 inch below the average tops of the 1½-inch rocks.

Relative depth.--The relative depth is the depth above the channel bottom as defined above divided by the total depth at the vertical of interest.

Mean velocity.--The mean velocity reported was determined from the observed values of discharge, Q, average depth, Y_N, and the width, W , by use of the continuity equation,

$$U_{xs} = \frac{Q}{Y_N \cdot W} \quad . \tag{38}$$

Velocity profiles.--Profiles of the local mean velocity were obtained with a pitot tube, a pressure transducer, and a transducer indicator. For each boundary condition a series of profiles were taken down the centerline of the channel to determine if flow was fully developed at the test section. Detailed information on the distribution of local mean velocity was needed for reduction of the turbulence data, which is described in the following sections.

Shear velocity.--Shear velocity is defined as $\sqrt{g\ R_H\ S}$ or $\sqrt{\tau_0/\rho}$, where g is the gravitational constant, R_H is the hydraulic

radius, and S is the water-surface or energy slope. The hydraulic radius definition was used in the present study.

Shear stress at bed.--The shear stress or tractive force at the bed is a parameter commonly used as a measure of the intensity of forces related to resistance to flow and transport of sediment particles. It is computed by the formula

$$\tau_0 = \gamma R_H S \quad , \tag{39}$$

where S is the water-surface or energy slope, and γ is the specific weight of water.

Kinematic viscosity.--The kinematic viscosity of the water was determined from the temperature of the water and appropriate standard tables.

Reynolds number.--The Reynolds number is a ratio of the viscous forces to the total inertial forces in the channel. It is defined as

$$R_E = \frac{U_{xs} Y_N}{\nu} \quad . \tag{40}$$

It is commonly used as a measure of the effect of viscosity on the flow pattern.

Froude number.--The effect of gravity on flow pattern is commonly related to the Froude number, which is the ratio of gravity forces to the total inertial force. As commonly used and reported here,

$$F_R = \frac{U_{xs}}{\sqrt{g Y_N}} \quad . \tag{41}$$

Chezy discharge coefficient.--The Chezy coefficient, C, is a common parameter used to express the resistance to flow. The coefficient is usually non-dimensionalized by dividing by the gravitational constant, g. The values reported here are computed from the formula

$$\frac{C}{\sqrt{g}} = \frac{U_{xs}}{\sqrt{g\ Y_N\ S}} \quad , \tag{42}$$

where S is the slope of the energy grade line.

Turbulence characteristics

Longitudinal turbulence intensity.--The longitudinal turbulence intensity is defined as the root-mean-square value of the deviations of the longitudinal velocity from its local mean value. That is, $u = \sqrt{\overline{u^2}}$. The turbulence intensity was determined as follows.

The first step was to convert analog F.M. tape recordings of the hot-film sensor output into digital form. Sign waves of known frequency and amplitude were digitized along with the data to serve as references in converting from digitizer units to voltages. As shown in figure 11, the analog signals were fed into an F.M. multiplexer which allowed simultaneous digital conversion of two channels of data. When digitizing a single signal the sample rate was 2000 samples per second. When digitizing two signals, such as the space-time correlation data, the sample was doubled to 4000 per second. This gave 2000 samples per second of each signal. When sampling two signals the multiplexer was operated in simultaneous mode whereby both signals were sampled at the same time to avoid time offsets in correlation measurements.

The second step was the statistical analysis of the digital tapes. This was done by the computer facilities at Colorado State

University. Data from each recorded point were analyzed to determine the mean, standard deviation, variance, trend line, and autocorrelation function.

The final step in determining the magnitude of the velocity fluctuations was to convert the root-mean-square values (variances) into velocity units from arbitrary digitizer units. This was done by first multiplying each variance by a conversion factor equal to the ratio of the root-mean-square of a known size wave to its root-mean-square as indicated by the computer. Multiple overheat ratio calibration curve techniques developed by McQuivey (1967) were then applied to find the root-mean-square velocity fluctuations.

Relative turbulence intensity.--Because the magnitudes of the longitudinal velocity fluctuations are not very meaningful by themselves they are often non-dimensionalized by dividing by the local mean velocity, the cross-section average velocity, or the shear velocity. These ratios, particularly the first two, give an indication of the relative strengths of the turbulent diffusive transport and the mean convective transport at any point in the flow. In equation form the three expressions for relative intensity are

$$\frac{\sqrt{\overline{u^2}}}{\overline{U}}\ , \qquad \frac{\sqrt{\overline{u^2}}}{U_{xs}}\ , \qquad \text{and} \qquad \frac{\sqrt{\overline{u^2}}}{U_*}\ . \tag{43}$$

Autocorrelation function and the Eulerian integral time scale.--The Eulerian integral time scale is defined as the area under the autocorrelation curve

$$\int_0^\infty R_E(\tau)\ d\tau = T_E\ , \tag{44}$$

where $R_E(\tau)$ is the autocorrelation function defined as

$$\frac{\overline{u(t) \cdot u(t-\tau)}}{\sqrt{\overline{u^2}}\ \sqrt{\overline{u^2}}} = R_E(\tau) \tag{45}$$

where t is time and τ is the delay time. The computation procedure is performed on a digitally-converted two-channel simultaneous recording of the output of the hot-film anemometer. The two channels are first correlated with one another at zero delay time giving $R_E(0) = 1.0$. One channel is then delayed an incremental time τ and the signals are again correlated. This procedure is repeated until $R_E(\tau) = 0$. This procedure and the integration to determine T_E were performed by the computer on multiplexed digital data from each point where the intensity was measured. The time scale, T_E, provides a measure of the eddy size associated with the flow.

Macroscale of turbulence.--To get an indication of a mean eddy size in the direction of the flow, the macroscale of turbulence is defined as

$$L_E = \overline{U}\ T_E \tag{46}$$

where $\overline{U}$ is the local mean velocity and T_E is the Eulerian integral time scale as defined above. This scale is a reasonable approximation of mean eddy size as long as the velocity is uniform; that is, $dx \cong \overline{U}\ dt$.

Space-time correlation.--Space-time correlations are performed by placing two hot-films at desired space locations and correlating their outputs after delaying the signal from one film with respect to the other. A typical application, as done in this study, is to place one film in a fixed position upstream. A second film is placed downstream and spaced at several distances along the flow. The spacing

distance is large compared to the dimensions of the probes, that is, several feet compared to several inches. This hopefully allows the small-scale turbulence generated by the upstream probe support time to decay before reaching the downstream film. At each location downstream from the first film a two-channel tape recording (one channel for each film) is made. This tape is converted to digital form and analyzed by computer, as described under "Longitudinal turbulent intensity". The analysis is quite similar to autocorrelation except two signals are used instead of one, and a family of curves is generated. At a fixed probe spacing, ξ_1, beginning with zero delay time, τ, the upstream signal is correlated with the downstream signal. This is repeated for longer and longer delay times until $R_u(\xi,\tau)$ approaches zero, giving a single correlation curve. (If $\xi_1 = 0$, this is the autocorrelation curve.) Next the procedure is repeated for a second probe spacing, ξ_2, and so on to ξ_n. The result is a set of correlation curves which can be drawn isometrically. The point of maximum correlation on each ξ_n curve is a measure of the rate at which turbulence is convected downstream by the flow. A curve drawn through the n peaks would hopefully approximate the Lagrangian correlation function. The computational formula for the correlation functions is

$$R_u(\xi,\tau) = \frac{\overline{u_\xi(t)\ u_0(t-\tau)}}{\sqrt{\overline{u_\xi^2}}\ \sqrt{\overline{u_0^2}}}, \qquad (47)$$

where u_0 is the longitudinal turbulent velocity component at the upstream probe position and u_ξ is the longitudinal turbulent velocity component at the downstream probe position.

Diffusion and dispersion

Temperature and concentration profiles.--The determination of the distribution of concentration and temperature in diffusing plumes under various ambient turbulence conditions and varying injection conditions was one of the prime experimental objectives. A minimum of five sets (vertical and horizontal) of profiles through the diffusing plume were collected for each nozzle discharge. The rate of increase of the variance of these profiles provide data for computing the vertical and lateral turbulent diffusion coefficients.

Velocity-concentration covariance.--The longitudinal velocity-concentration covariance, $\overline{uc}$, can be related directly to the longitudinal diffusion coefficient and the mean concentration gradient by means of a Boussinesq-type transfer coefficient as described in Chapter II. The measurements were made by placing a parabolic hot-film sensor and single-electrode conductivity probe in a special holder which held them within 1/16 inch of each other. Power spectral density measurements from a previous study (written communication, McQuivey and Keefer, 1971) indicated that this spacing was less than the microscale of turbulence and should thus give accurate correlations. The effect of the hot-film on the conductivity probe was checked by recording the mean and root-mean-square of the concentration signal with and without the hot-film being turned on. Visual observation of the recording showed no significant interaction. An inverse procedure was used to check the effect of the conductivity probe on the hot-film.

The assembly was mounted on the traversing mechanism of the carriage. Simultaneous recording was made of the output from both sensors. This record was digitized and operated on for the

cross-correlation coefficient, R, and the root-mean-square of both signals $\sqrt{\overline{u^2}}$ and $\sqrt{\overline{c^2}}$, which were converted to the covariance by the formula

$$\overline{uc} = R \sqrt{\overline{u^2}} \sqrt{\overline{c^2}} \quad . \tag{48}$$

Jet strength.--The jet strength of the nozzle is defined as

$$\text{Jet strength} = \frac{U_{\text{jet}}}{U_{xs}} \tag{49}$$

where U_{jet} is the mean velocity of the nozzle and U_{xs} is the mean velocity of the flow field.

Depth-average diffusion coefficients.--The rate of increase of the variance of the concentration and temperature profiles downstream of the hot water and neutrally-buoyant salt solution jets were used to obtain depth and width averaged values of the vertical and lateral turbulent transfer coefficients ε_y and ε_z. To obtain ε_y and ε_z the strip-chart recordings of voltage versus position were first converted to digital punch card form. A computer program was then written which analyzed each profile for mean, standard deviation, and two types of variance called A and B. Formula B accounted for reflection of diffusing material off the boundaries of the channel. Both computations are explained in a later section. The program fit least squares lines through the two sets of variances and solved for ε_y and ε_z from the equation

$$\varepsilon_i = \frac{U_{xs}}{2} \frac{d\,\overline{\sigma_i^2}}{dx} \quad . \tag{50}$$

Surface diffusion coefficients.--Surface diffusion coefficients in the x and z directions were determined from the floating particle data. An electronic desk calculator was used to compute the variance of the travel times and the variance of the lateral concentration distributions as indicated by the compartmented trap. ε_{xs} and ε_{zs} were then computed from the formulas

$$\varepsilon_{xs} = \frac{\overline{U}_s^3}{2} \frac{d\,\overline{\sigma_t^2}}{dx} \tag{51}$$

and

$$\varepsilon_{zs} = \frac{\overline{U}_s}{2} \frac{d\,\overline{\sigma_z^2}}{dx} \quad . \tag{52}$$

Because of the non-uniformity of the surface velocity across the width of the channel a small portion of the spread of the particles was due to dispersion. The data from the velocity profiles indicated that the error may have approached 7 percent for the 6-inch cobble boundary.

Longitudinal dispersion coefficient.--The one-dimensional longitudinal dispersion coefficient, D_x, is a measure of a stream's ability to spread slugs of pollutants once vertical and lateral mixing are complete.

Two sets of concentration versus time profiles were taken at each of six 10-foot intervals downstream of the plane source generated by the tilting trough described in the equipment section. A fluorometer and strip-chart recorder were used to obtain the profiles.

The first step in the reduction of the dispersion data was to convert the analog concentration (voltage) versus time curves to digital punch card form. A minimum of 40 points were digitized on each curve.

The second step in the reduction was a statistical analysis of the digitized data. The mean, standard deviation, and variance were determined for all the curves.

The final step was the calculation of dispersion coefficients from the relationship

$$D_x = \frac{U_{xs}^3}{2} \frac{d\,\sigma_t^2}{dx} \quad . \tag{53}$$

This was done by fitting a least squares line through σ_t^2 versus x plots to determine $d\,\sigma_t^2/dx$. All computations were done by computer.

Variance A and Variance B.--As mentioned previously the variance of each experimental temperature, concentration, or dye distribution was determined by two methods. The first, referred to as Variance A, was simply the standard statistical definition

$$\sigma_x^2 = \sum_{j=1}^{k} \frac{C_j(x_j - \bar{x})^2}{N} \tag{54}$$

where $\bar{x}$ is the mean value of the x_j values,

$$N = \sum_{j=1}^{k} C_j \quad ,$$

and C_j is the concentration of dispersant at $x = x_j$. Similar formulas hold for the variance in the y and z directions. For the variance of temperature distributions C_j is replaced by T_j, the mean difference between the ambient stream temperature and the temperature at point x_j in the dispersing plume.

The second calculation, referred to as Variance B, was designed to account for reflection of the plume from the sidewalls, water surface, or bed. Based on the idea that the temperature or

concentration distribution of a dispersing plume approaches normality at large distances from a source the variance may be said to be

$$\sigma_i^2 = \frac{1}{2\pi[C_{max} \text{ or } T_{max}]^2} \tag{55}$$

where C_{max} and T_{max} are the peak values in a given concentration or temperature profile. This formula is easily derived from the formula for a normal probability distribution. When the value for Variance B exceeded that of Variance A it was assumed that reflection was taking place and the B value was used in subsequent calculations. Except at large distances from the source (8-10 feet) the difference between the two variances seldom exceeded a few percent.

The experimental sequence and procedure for collecting the data are described in the following section.

Procedure

The first step in a series of measurements over a given roughness was to establish uniform flow. An attempt was made to keep the cross-section average velocity equal to 1 foot per second. The flow depth was approximately 1 foot in each case. Uniform flow was determined by plotting graphs of the water surface and the bed elevations and adjusting the flume until the two were parallel.

The next five steps in a measurement series were not always performed in a set order. The amount of time available on a given day determined the procedure used.

The turbulence data sequence usually began with a series of velocity profiles. One profile was taken halfway between the centerline and the wall at longitudinal station 75 where the injector nozzles

were located. A profile was then taken at the centerline at the same station. These were followed by four more profiles at the centerline at 5-foot intervals downstream.

Next the longitudinal turbulence intensity measurements were made. Vertical profiles of approximately 20 points were taken on centerline and halfway between the centerline and the wall at longitudinal station 75. Data taken at each point in a profile included a simultaneous strip-chart recording of the mean anemometer output voltage and the rms meter output, a 3-minute F.M. tape recording of the AC component of the anemometer output, and the location of the probe with respect to the water surface.

Following this the longitudinal space-time velocity data were taken. For these measurements two hot-film probes were operated simultaneously. One probe was placed at a fixed position on the centerline of the flume and the other was moved downstream on the centerline from point to point. The data included seven stations at 2-foot intervals (that is, two through 14-foot total spacing) at each of three elevations below the water surface.

The dispersion data sequence consisted of collecting 12 concentration versus time records at stations downstream of an instantaneous plane-source injection of dispersant. A siphon nozzle was placed at mid-depth on the centerline at the desired station. The nozzle was hooked to the flow-through door on the fluorometer. The full scale output of the fluorometer was adjusted to give full scale deflection of the chart recorder. With the chart recorder running at an appropriate speed (trial and error), 1 gallon of dispersant was injected into the flume. This procedure was repeated at stations 10, 20, 30, 40, 50, and

60 feet below the injection point. After reaching station 60 all stations were repeated in reverse order.

The hot-water diffusion sequence began with stabilizing the system temperature. Two to 3 hours before measurements were begun the water heater was turned on and flow at injection temperature was initiated through the injection system. This insured that the 75 feet of plumbing between the heater and the injection point would be at equilibrium temperature when data were being taken.

After the system stabilized, the injection temperature was measured. This was done by running the heated water from the nozzle being used into an insulated container for 3 to 5 minutes. The temperature of the water in the container was then measured. It was found that for an indicated temperature of 75°F on the thermostatic mixing valve a temperature of 74.6°F was produced at the injection point. This temperature was maintained for all runs. This gave a temperature difference of approximately 30°F between flowing and injected water.

After measuring the injection temperature the conductivity probe was checked for maximum response. The insulated container was filled with water at injection temperature and the output voltage of the carrier amplifier was recorded. This full deflection was an easily made check on whether the conductivity probe was operating properly.

After the probe was checked for full scale response it was mounted on the traversing mechanism. The nozzle discharge was adjusted to the desired value and data taking commenced. First, a vertical temperature profile at the centerline was taken at a desired distance downstream of the nozzle. This located the peak temperature with respect to the water surface. Temperature profiles were generated by having one man

traverse the probe in steps, calling out the location at each step, while a second man marked the location on a strip-chart recording of the carrier amplifier output voltage. Vertical profiles were followed by horizontal profiles located at the depth of peak temperature in the vertical. Data were taken at intervals downstream until the response limit of the probe was reached or when vertical mixing became complete. This process was repeated for four jet strengths (discharges) for each of the three nozzles.

The salt solution diffusion sequence began with mixing a 500-gallon tank of dispersant. After the solution was prepared the cooling water and the stirring motor were turned on and the temperature allowed to stabilize. The tank was then pressurized and data taking commenced. Full scale deflection in the injector solution was checked and a procedure identical to that for the temperature profiles was used to collect the concentration profiles. As nearly as possible the nozzle discharges used for the salt solution were the same as those used for hot water.

The velocity-concentration covariance measurements proceeded as follows. After establishing uniform flow the 1.094 cm injector nozzle was placed at mid-depth on the centerline of the flume. The 500-gallon tank was filled with dispersant and pressurized. Discharge from the nozzle was adjusted to approximately twice stream velocity. There was no special reason for this figure other than convenience in tracking the plume on a single carrier amplifier scale over about 20 feet of distance. The conductivity probe and hot-film sensor were then checked for response and mounted on the traversing mechanism.

The next step was to locate the axes of the diffusing plume. This was done by taking a series of vertical and horizontal concentration profiles at stations downstream of the nozzle. Once the path of maximum average concentration was defined, a longitudinal concentration profile was traced out along this path.

The final step in the measurements was the simultaneous recording of the concentration and velocity signals on an F.M. tape recorder. Twelve points were recorded along the plume axis from 2 to 20 feet below the injection point. In addition to the tape recordings a strip-chart record was made of the mean and root-mean-square of both signals. Three minutes of data were recorded at each point. This sequence was done only over the smooth, 1½-inch rock, and 6-inch cobble boundaries.

The final data sequence was collecting data on the diffusion of particles at the water surface. Two hundred particles were dropped and timed over five distances. After completing a particle experiment over the flow depth used in the heat-salt solution experiments (approximately 1 foot), the depth was cut in half, uniform flow reestablished, and a second set of data collected. A set of dispersion measurements were also made for the one-half depth flows. The particle sequence was completed only over the smooth, 1½-inch rock, and 6-inch cobble boundaries.

This completes the presentation of the experimental variables and parameters and the procedure. The next chapter presents the data from all the studies.

Chapter IV

PRESENTATION OF DATA

This chapter presents the results of the various studies. The presentation is divided into three parts. First the basic hydraulic data for all four flow conditions are presented. Next the turbulence data, including the space-time correlations, are presented. Finally, the diffusion-dispersion data are presented. The diffusion-dispersion section includes dye-dispersion data, particle-diffusion data, velocity-concentration covariance data, and jet-diffusion data for both heat and salt solution. Analytic considerations are given in Chapter V and are dealt with only briefly in this chapter.

Basic hydraulic data

The basic hydraulic parameters for the four boundary conditions are shown in table 3. The 14 columns present respectively: (1) the boundary condition; (2) the run designation; (3) the uniform flow depth, Y_N; (4) the slope of the energy grade line, S; (5) the volume discharge of water, Q; (6) the cross-section average velocity, U_{xs}; (7) the water surface velocity at the channel centerline, $\overline{U}_s$; (8) the shear velocity, U_*; (9) the boundary shear stress, τ_0; (10) the kinematic viscosity, ν; (11) the mean flow temperature; (12) the Reynolds number, R_E; (13) the Froude number, F_R; and (14) the Chezy discharge coefficient, $C/\sqrt{g}$. Columns (9) through (14) are completed only for runs S1, TR1, and RB1 where large quantities of data were taken. These were the only runs where both temperature and concentration profiles were collected for the study of diffusing jets.

Table 3. *Basic hydraulic parameters*

Boundary condition	Run designation	Normal depth Y_N (ft)	Slope $S \times 10^3$	Volume discharge Q (ft^3/sec)	Cross-section average velocity U_{xs} (ft/sec)	Surface velocity $\overline{U}_s$ (ft/sec)	Shear velocity U_* (ft/sec)	Boundary shear stress τ_0 (lbs/ft^2)	Kinematic viscosity $\nu \times 10^5$ (ft^2/sec)	Temperature (°C)	Reynolds number $R_E \times 10^{-4}$	Froude number F_R	Chezy discharge coefficient $C/\sqrt{g}$
(1)	(2)	(3)	(4)	(5)	(6)	(7)	(8)	(9)	(10)	(11)	(12)	(13)	(14)
Smooth	S1	0.915	0.119	3.672	1.036	1.172	0.0616	0.0046	1.62	5.20	5.851	0.191	16.8
	S2	.528	.143	1.643	.852	.934	.0415	------	----	----	-----	-----	----
3/4-inch rock	TR1	0.933	0.324	3.071	0.849	-----	0.0803	0.0125	1.72	2.70	4.605	0.155	10.6
1½-inch rock	R1	0.892	0.367	3.450	0.956	1.188	0.0850	------	----	----	-----	-----	----
	R2	.469	.394	1.302	.721	.815	.0694	------	----	----	-----	-----	----
6-inch cobble	RB1	0.945	0.443	3.205	0.875	1.190	0.0938	0.0170	1.73	2.65	4.779	0.159	9.3
	RB2	.528	.744	1.591	.780	.930	.0996	------	----	----	-----	-----	----

Turbulence characteristics

Relative turbulent intensity.--The variation in relative turbulence intensity with depth is illustrated in figures 12, 13, and 14. Presented in figure 12 is the variation of turbulent intensity at the centerline of the channel for runs S1, TR1, and RB1. The relative intensity increases in roughly equal steps from the smooth boundary to the 6-inch cobble boundary. The curves illustrate well the effect of the boundary on the flow field. Over the smooth boundary (S1), the intensity increases gradually from 0.015 at the water surface to 0.080 at a relative depth of 0.10. Below 0.10 the increase appears exponential. Over the 3/4-inch rock boundary (TR1) the gradual increase is from 0.04 at the water surface to 0.110 at a relative depth of 0.20. Over the 6-inch cobble boundary (RB1) the gradual increase is from 0.02 at the water surface to 0.10 at a relative depth of 0.5. Below y/Y_N = 0.5 the relative intensity increases rapidly. There is no apparent systematic variation of the turbulent intensity with Reynolds number.

Presented in figure 13 is the variation of the relative turbulent intensity with depth halfway between the centerline of the channel and the side walls for runs S1, TR1, and RB1. The variation is essentially the same both in distribution and magnitude except for the appearance of small "humps" in the curves for S1 and TR1 at y/Y_N = 0.4. These may be due to secondary circulation or sidewall effects.

Presented in figure 14 is the variation of relative turbulent intensity with depth at the centerline of the channel for the ~0.5 foot depth flows S2, R2, and RB2. The intensities at the water surface are respectively 0.030, 0.055, and 0.085. These values compare well with

0.030, 0.059, and 0.092 at y/Y_N = 0.56 (the average ratio of depths S2/S1, RB2/RB1) for the ~1.0 foot depth runs. This indicates that the boundary influence on the turbulence structure is more a function of absolute than relative depth.

Autocorrelation function.--Figures 15, 16, 17, 18, 19, and 20 present the variation of the autocorrelation function, $R(\tau)$, with depth for runs S1, TR1, and RB1 at the centerline of the channel and halfway between the centerline and the channel walls. The autocorrelation function is plotted for five or six relative depths for each run. Also shown on the figures are values of T_E, the Eulerian time scale, which are approximated by the formula

$$T_E = \int_0^{\tau_{max}} R_E(\tau)\, d\tau \quad , \tag{56}$$

where τ_{max} is the time to where $R_E(\tau)$ first crosses zero. T_E does not show any pronounced systematic variation with depth. As might be expected, the values of T_E decrease as the roughness of the boundary increases, indicative of greater mixing in the flow. The average values are 1.519, 0.873, and 0.813 seconds for runs S1, TR1, and RB1, respectively.

Other parameters.--For the benefit of others who wish to compare data, tables 4, 5, 6, and 7 contain the data plotted in previous figures 12 through 20, as well as the mean velocity profiles, the absolute turbulence intensity, $\sqrt{\overline{u^2}}$, the relative intensity measured against the shear velocity, $\sqrt{\overline{u^2}} / U_*$, and the macroscale of turbulence, L_E . The data are shown as functions of relative depth.

Space-time correlation data.--The results of the longitudinal space-time velocity correlation measurements over the smooth boundary

Table 4. *Turbulence parameters, run* S1

Centerline							Halfway between centerline and wall						
Relative depth $\frac{y}{Y_N}$	Local mean velocity $\overline{U}$ (ft/sec)	Absolute turbulence intensity $\sqrt{\overline{u^2}}$ (ft/sec)	Relative turbulence intensity $\frac{\sqrt{\overline{u^2}}}{\overline{U}}$	Relative turbulence intensity $\frac{\sqrt{\overline{u^2}}}{U_*}$	Eulerian time scale T_E (secs)	Eulerian macroscale L_E (ft)	Relative depth $\frac{y}{Y_N}$	Local mean velocity $\overline{U}$ (ft/sec)	Absolute turbulence intensity $\sqrt{\overline{u^2}}$ (ft/sec)	Relative turbulence intensity $\frac{\sqrt{\overline{u^2}}}{\overline{U}}$	Relative turbulence intensity $\frac{\sqrt{\overline{u^2}}}{U_*}$	Eulerian time scale T_E (secs)	Eulerian macroscale L_E (ft)
0.963	1.096	0.027	0.025	0.61	2.342	2.566	0.963	1.007	0.026	0.026	0.592	1.335	1.344
.908	1.090	.024	.022	.54	1.566	1.706	.908	1.012	.026	.026	.592	1.431	1.448
.854	1.091	.023	.021	.52	1.405	1.532	.854	1.042	.026	.025	.563	1.433	1.493
.799	1.102	.022	.020	.50	1.432	1.578	.799	1.077	.025	.023	.524	1.459	1.561
.744	1.110	.023	.021	.52	2.043	2.267	.744	1.105	.023	.021	.477	1.523	1.682
.690	1.110	.024	.022	.54	1.343	1.920	.690	1.110	.025	.023	.524	1.355	1.504
.635	1.108	.026	.023	.59	1.422	1.575	.635	1.107	.027	.025	.568	1.333	1.475
.580	1.095	.029	.026	.68	1.516	1.660	.580	1.094	.029	.026	.592	1.426	1.560
.526	1.077	.033	.031	.75	1.995	2.148	.526	1.075	.032	.030	.683	1.283	1.379
.471	1.055	.037	.035	.84	1.620	1.709	.471	1.046	.034	.033	.749	1.640	1.715
.416	1.001	.040	.040	.91	1.581	1.582	.416	1.001	.037	.037	.843	2.334	2.339
.362	.970	.044	.045	1.00	2.724	2.642	.362	.970	.039	.040	.910	1.351	1.310
.307	.938	.046	.049	1.04	1.504	1.410	.307	.933	.046	.049	1.045	1.504	1.410
.252	.907	.053	.059	1.21	2.407	2.326	.252	.908	.054	.061	1.228	1.412	1.282
.198	.879	.057	.065	1.30	1.353	1.628	.198	.880	.063	.072	1.436	1.821	1.602
.143	.845	.061	.072	1.38	1.575	1.565	.143	.846	.067	.079	1.522	1.492	1.269
.089	.797	.069	.087	1.57	1.543	1.265	.089	.797	.071	.089	1.612	2.133	1.700
.034	.700	.088	.125	2.00	2.064	1.444	.034	.742	.083	.119	1.886	1.324	.926
.025	.647	.099	.153	2.25	1.525	.986	.027	.671	.096	.143	2.181	1.244	.836
.017	.645	.119	.170	2.50	1.002	.616	.016	.610	.105	.172	2.386	1.241	.732
-----	-----	-----	-----	----	-----	-----	.009	.541	.123	.228	2.800	.943	.510

Table 5. *Turbulence parameters, run* TR1

Centerline							Halfway between centerline and wall						
Relative depth $\frac{y}{Y_N}$	Local mean velocity $\overline{U}$ (ft/sec)	Absolute turbulence intensity $\sqrt{\overline{u^2}}$ (ft/sec)	Relative turbulence intensity $\frac{\sqrt{\overline{u^2}}}{\overline{U}}$	Relative turbulence intensity $\frac{\sqrt{\overline{u^2}}}{U_*}$	Eulerian time scale T_E (secs)	Eulerian macroscale L_E (ft)	Relative depth $\frac{y}{Y_N}$	Local mean velocity $\overline{U}$ (ft/sec)	Absolute turbulence intensity $\sqrt{\overline{u^2}}$ (ft/sec)	Relative turbulence intensity $\frac{\sqrt{\overline{u^2}}}{\overline{U}}$	Relative turbulence intensity $\frac{\sqrt{\overline{u^2}}}{U_*}$	Eulerian time scale T_E (secs)	Eulerian macroscale L_E (ft)
0.943	1.132	0.048	0.042	0.598	0.824	0.932	0.943	0.867	0.043	0.050	0.531	1.255	1.083
.890	1.123	.051	.045	.630	1.214	1.363	.890	.870	.045	.052	.554	.835	.796
.836	1.120	.051	.046	.620	.747	.836	.836	.879	.047	.053	.581	.629	.525
.782	1.124	.054	.048	.667	.690	.775	.782	.886	.051	.058	.620	.783	.693
.729	1.126	.057	.051	.704	.716	.806	.728	.889	.054	.061	.667	.665	.591
.675	1.124	.061	.054	.754	1.349	1.516	.675	.889	.055	.062	.679	.734	.652
.622	1.120	.062	.055	.767	.647	.724	.622	.880	.058	.066	.716	.755	.664
.588	1.120	.064	.057	.781	.821	.919	.568	.865	.062	.072	.765	1.349	1.166
.514	1.101	.067	.061	.828	.769	.846	.514	.842	.065	.071	.803	.813	.686
.461	1.067	.072	.068	.888	.763	.814	.461	.829	.071	.086	.876	.498	.412
.407	1.012	.073	.072	.903	.656	.669	.407	.827	.068	.087	.840	.949	.784
.354	.954	.077	.081	1.000	1.095	1.044	.354	.838	.074	.088	.913	.766	.641
.309	.900	.088	.092	1.025	.634	.588	.300	.842	.077	.092	.951	.913	.768
.247	.847	.085	.100	1.050	.765	.647	.274	.830	.082	.099	1.012	.831	.688
.193	.785	.089	.113	1.098	.896	.546	.193	.719	.086	.119	1.061	.841	.585
.139	.695	.097	.140	1.198	1.061	.716	.139	.661	.094	.142	1.160	1.042	.688
.086	.570	.119	.209	1.470	.679	.387	.086	.567	.111	.195	1.370	.644	.365
.032	.340	.136	.400	1.679	.445	.153	.032	.334	.129	.385	1.592	.473	.157

Table 6. *Turbulence parameters, run* RB1

Centerline							Halfway between centerline and wall						
Relative depth $\frac{y}{Y_N}$	Local mean velocity $\overline{U}$ (ft/sec)	Absolute turbulence intensity $\sqrt{\overline{u^2}}$ (ft/sec)	Relative turbulence intensity $\frac{\sqrt{\overline{u^2}}}{\overline{U}}$	Relative turbulence intensity $\frac{\sqrt{\overline{u^2}}}{U_*}$	Eulerian time scale T_E (secs)	Eulerian macroscale L_E (ft)	Relative depth $\frac{y}{Y_N}$	Local mean velocity $\overline{U}$ (ft/sec)	Absolute turbulence intensity $\sqrt{\overline{u^2}}$ (ft/sec)	Relative turbulence intensity $\frac{\sqrt{\overline{u^2}}}{\overline{U}}$	Relative turbulence intensity $\frac{\sqrt{\overline{u^2}}}{U_*}$	Eulerian time scale T_E (secs)	Eulerian macroscale L_E (ft)
0.934	1.219	0.089	0.073	0.851	0.833	1.015	0.947	1.049	0.089	0.084	0.851	0.861	0.903
.885	1.210	.090	.074	.862	.942	1.139	.894	1.049	.086	.081	.823	.816	.855
.835	1.200	.091	.076	.872	.922	1.106	.841	1.065	.087	.081	.832	.737	.784
.785	1.190	.093	.078	.890	.734	.873	.783	1.095	.090	.082	.861	1.348	1.476
.736	1.172	.094	.080	.900	.692	.811	.735	1.115	.093	.083	.890	.837	.933
.686	1.155	.096	.083	.918	.742	.857	.683	1.099	.097	.083	.928	1.291	1.418
.636	1.130	.099	.088	.947	.739	.835	.598	1.072	.101	.094	.965	.913	.978
.586	1.100	.102	.093	.976	.889	.977	.545	1.071	.107	.099	1.024	.763	.817
.537	1.066	.105	.098	1.004	.610	.650	.492	1.028	.106	.103	1.013	.671	.689
.487	1.022	.107	.104	1.025	.689	.704	.439	.977	.113	.115	1.081	.693	.677
.437	1.012	.110	.109	1.053	.633	.640	.386	.914	.116	.118	1.110	.814	.743
.388	.919	.113	.123	1.031	1.080	.992	.333	.843	.121	.143	1.158	.843	.710
.338	.851	.118	.139	1.129	.801	.681	.280	.488	.129	.163	1.236	.613	.483
.288	.798	.127	.159	1.215	.676	.539	.228	.714	.134	.187	1.282	.734	.524
.239	.730	.133	.182	1.273	.614	.448	.175	.621	.141	.227	1.350	.947	.588
.189	.649	.139	.214	1.330	.854	.554	.122	.502	.156	.310	1.493	.614	.308
.139	.548	.152	.277	1.456	1.016	.556	.069	.362	.181	.500	1.731	.812	.293
.089	.410	.173	.423	1.654	.861	.353	.016	.168	.233	1.386	2.228	.737	.123
.040	.282	.197	.700	1.884	.420	.118	-----	-----	-----	-----	-----	-----	-----

Table 7. *Turbulence parameters, half depth runs*

Run designation	Relative depth $\frac{y}{Y_N}$	Local mean velocity $\overline{U}$ (ft/sec)	Absolute turbulence intensity $\sqrt{\overline{u^2}}$ (ft/sec)	Relative turbulence intensity		Eulerian time scale T_E (secs)	Eulerian macroscale L_E (ft)
				$\frac{\sqrt{\overline{u^2}}}{\overline{U}}$	$\frac{\sqrt{\overline{u^2}}}{U_*}$		
S2	0.928	0.97	0.031	0.032	0.748	1.594	1.546
	.833	.96	.034	.035	.821	1.858	1.782
	.739	.95	.036	.038	.916	1.346	1.278
	.644	.94	.039	.041	.988	1.629	1.539
	.549	.92	.044	.048	1.156	1.594	1.467
	.455	.90	.049	.054	1.300	2.099	1.885
	.360	.88	.051	.058	1.399	1.519	1.334
R2	0.900	1.16	0.067	0.058	0.788	0.873	1.012
	.676	1.09	.079	.072	.929	.944	1.029
	.452	.98	.084	.086	.988	.737	.723
	.228	.83	.103	.124	1.212	.829	.687
	.037	.51	.137	.268	1.613	.668	.342
RB2	0.960	0.94	0.098	0.104	0.984	0.981	0.921
	.866	.93	.080	.086	.884	.706	.656
	.771	.91	.086	.095	.865	.817	.744
	.676	.89	.104	.117	1.043	.722	.642
	.581	.86	.110	.128	1.105	.697	.600
	.487	.83	.124	.149	1.246	.741	.615
	.392	.77	.143	.186	1.436	.811	.624
	.297	.70	.162	.231	1.628	.871	.610
	.203	.60	.164	.274	1.647	.711	.427

(S1) are shown in figures 21, 22, and 23. The figures are for 0.15, 0.45, and 0.75 foot below the water surface, respectively. Shown on each of the figures is a time scale value obtained by planimetering the curve estimated by eye through the peaks of the correlation curves. These will be compared with the Eulerian and Lagrangian time scales in Chapter V.

The results of the longitudinal space-time velocity correlation measurements over the 3/4-inch rock boundary (TR1) are shown in figures 24, 25, and 26. The figures present data from 0.15, 0.45, and 0.75 feet below the water surface, respectively. Time scale values are also shown on these figures and will be discussed in Chapter V.

Diffusion and dispersion

The diffusion and dispersion data are presented in two groups. The first group contains the results of the dye dispersion experiments and the results of the floating particle studies. The second group contains the results of the studies of diffusing jets of heated water and salt solution.

Dispersion and particle diffusion.--The dispersion and particle diffusion data are presented together because of the similarity in the data reduction procedures. Presented in figures 27, 28, and 29 are the variances from the dispersion studies and from the lateral and longitudinal particle diffusion studies versus distance below the injection point for all four boundary conditions. These figures show the general quality of the data.

To minimize the effect of scatter, computer-fitted least squares lines were used to compute the dispersion and diffusion coefficients. The results of these computations are shown in table 8. The largest

Table 8. *Dispersion and surface diffusion coefficients*

Run designation	S1	S2	TR1	R1	R2	RB1	RB2
Longitudinal dispersion coefficient D_x (ft^2/sec)	0.226	0.186	0.521	0.274	0.169	0.877	0.797
Longitudinal surface diffusion coefficient ε_{xs} (ft^2/sec)	0.00916	0.01060	Data not taken	0.03354	0.01687	0.03089	0.02812
Lateral surface diffusion coefficient ε_{zs} (ft^2/sec)	0.00388	0.00360	Data not taken	0.01074	0.00668	0.01110	0.01240

dispersion coefficient, 0.877 ft^2/sec, was obtained for the ~1.0 ft depth 6-inch cobble boundary and the smallest, 0.169 ft^2/sec, for the ~0.5 ft depth 1½-inch rock boundary (R2). The largest longitudinal diffusion coefficient, 0.0335 ft^2/sec, was obtained for the ~1.0 ft depth flow over the 1½-inch rock boundary (R1). The smallest, 0.0092 ft^2/sec, was obtained for the ~1.0 ft depth over the smooth boundary (S1). The largest lateral diffusion coefficient, 0.0124 ft^2/sec, was obtained for the ~0.5 ft depth flow over the smooth boundary (S2).

Velocity-concentration covariance measurements.--The results of the velocity-concentration covariance studies are presented in tables 9, 10, and 11. The order of presentation is smooth boundary (S1), 1½-inch rock boundary (R1), and 6-inch cobble boundary (RB1). The data in the tables are presented in 7 columns, as follows: Column 1, the station in feet below the injector nozzle where measurements were made; Column 2, the cross-correlation coefficient, R, computed for the signals from the hot-film sensor and conductivity probe; Column 3, the absolute turbulent intensity, $\sqrt{\overline{u^2}}$; Column 4, the intensity of concentration fluctuations, $\sqrt{\overline{c^2}}$; Column 5, the velocity-concentration covariance, $\overline{uc}$; Column 6, the mean concentration gradient along the axis of the plume, $\partial\overline{C}/\partial x$; Column 7, the longitudinal turbulent diffusion coefficient, ε_x, computed from $\overline{uc}$ and $\partial\overline{C}/\partial x$ (equation 9). The longitudinal surface diffusion coefficient, ε_{xs}, from the particle experiments is shown for comparison purposes. There are no data for stations 2 through 8 for run RB1 because of an accidental oversaturation of the averaging circuit while making mean concentration gradient measurements. Although it may have been possible to extrapolate the gradient from

Table 9. *Velocity-concentration covariance data, smooth boundary*

Station (ft)	Cross correlation coefficient R	Absolute turbulent intensity $\sqrt{\overline{u^2}}$ (ft/sec)	Concentration intensity $\sqrt{\overline{c^2}}$ (units)	Velocity concentration covariance $\overline{uc}$ (ft·units/sec)	Concentration gradient $\frac{\partial \overline{C}}{\partial x}$ (units/ft)	Longitudinal diffusion coefficient ε_x (ft^2/sec)
(1)	(2)	(3)	(4)	(5)	(6)	(7)
2	0.2346	0.0347	20.77	0.1690	17.31	0.0098
3	.1691	.0416	10.25	.0722	6.25	.0116
4	.1113	.0342	10.25	.0401	3.04	.0128
5	.0808	.0294	6.65	.0158	1.74	.0091
6	.0457	.0322	6.37	.0094	1.10	.0085
8	.0397	.0231	4.98	.0046	.53	.0087
10	.0494	.0231	3.32	.0038	.30	.0126
12	.0265	.0251	2.77	.0018	.19	.0097
14	.0283	.0294	1.94	.0016	.13	.0122
16	.0241	.0267	1.66	.0011	.09	.0119
18	.0218	.0312	1.85	.0012	.07	.0171
20	.0186	.0342	1.38	.0009	.05	.0175

Surface longitudinal diffusion coefficient, ε_{xs}, in ft^2/sec = 0.00916

Table 10. *Velocity-concentration covariance data, 1½-inch rock boundary*

Station (ft)	Cross correlation coefficient R	Absolute turbulent intensity $\sqrt{\overline{u^2}}$ (ft/sec)	Concentration intensity $\sqrt{\overline{c^2}}$ (units)	Velocity concentration covariance $\overline{uc}$ (ft·units/sec)	Concentration gradient $\frac{\partial \overline{C}}{\partial x}$ (units/ft)	Longitudinal diffusion coefficient ε_x (ft^2/sec)
(1)	(2)	(3)	(4)	(5)	(6)	(7)
1	0.1705	0.0677	16.20	0.1883	16.320	0.0116
2	.1587	.0598	11.29	.1073	2.900	.0371
3	.0815	.0499	8.22	.0334	1.041	.0322
4	.1011	.0482	6.62	.0322	.721	.0447
5	.0838	.0408	5.03	.0173	.442	.0395
6	.0734	.0436	3.31	.0106	.302	.0350
8	.0619	.0460	2.33	.0067	.130	.0511
10	.0738	.0434	1.53	.0049	.103	.0475
12	.1074	.0452	.87	.0042	.122	.0345
14	.0862	.0428	.64	.0024	.065	.0362
16	.0458	.0431	.52	.0010	.031	.0325
18	.0212	.0457	.34	.0003	.008	.0413
20	.0106	.0460	.32	.00016	.005	.0324

Surface longitudinal diffusion coefficient, ε_{xs}, in ft^2/sec = 0.03354

Table 11. *Velocity-concentration covariance data, 6-inch cobble boundary*

Station (ft)	Cross correlation coefficient R	Absolute turbulent intensity $\sqrt{\overline{u^2}}$ (ft/sec)	Concentration intensity $\sqrt{\overline{c^2}}$ (units)	Velocity concentration covariance $\overline{uc}$ (ft·units/sec)	Concentration gradient $\frac{\partial \overline{C}}{\partial x}$ (units/ft)	Longitudinal diffusion coefficient ε_x (ft^2/sec)
(1)	(2)	(3)	(4)	(5)	(6)	(7)
2	------	0.0824	10.140	------	-----	------
3	------	.0630	4.930	------	-----	------
4	------	.0785	3.480	------	-----	------
5	------	.0799	3.190	------	-----	------
6	------	.0764	1.450	------	-----	------
8	------	.0555	.696	------	-----	------
10	0.0932	.0694	.580	0.0374	0.103	0.0363
12	.0674	.0668	.348	.0157	.078	.0203
14	.1011	.0759	.261	.0203	.056	.0359
16	.0798	.0897	.188	.0135	.027	.0498
18	.0312	.0862	.145	.0039	.017	.0230
20	.0230	.0956	.142	.0031	.010	.0310

Surface longitudinal diffusion coefficient, ε_{xs}, in ft^2/sec = 0.03089

data for stations 10 through 20, the writer felt that it was better to eliminate the points.

Diffusion of heated water and salt solution jets.--Because of the large quantity of data only a representative sample of the jet data will be presented. The complete data is available separately as a U.S. Geological Survey open-file report (McQuivey, Keefer, and Shirazi, 1971) and also as a U.S. Geological Survey Professional Paper. Presented here are several examples of raw data, an example of the A and B variances plotted against distance, and a tabulation of the diffusion coefficients from the computer output. Also presented are several log-log plots of temperature at the plume axis versus dimensionless distance.

Figures 30 through 33 present tracings of actual conductivity probe output smoothed by the averaging circuit. The data were taken downstream of the small nozzle over the 6-inch cobble boundary (RB1). The dispersant was salt solution at a jet strength of 4.69. Figure 30 represents the vertical concentration profile at 1.0 foot downstream of the nozzle. Figure 31 represents the horizontal concentration profile at the same station. The numbers and checks on the trace show the location of the probe tip below the water surface or the location left or right of centerline, respectively. Figures 32 and 33 represent the vertical and horizontal concentration profiles 8 feet below the nozzle for the same conditions. The salt solution is spread almost uniformly throughout the vertical, but mixing is still going on as evidenced by the roughness of the trace. The lateral trace shows that material had not yet reached the sidewalls of the flume.

Figure 34 presents a typical set of A and B variances plotted versus station below the nozzle. The data are for the smooth boundary

(S1) medium nozzle at a jet strength of 5.84 using hot water as the dispersant. The upper line is the trend line of the variance of the horizontal temperature profiles. The lower line is for the variance of the vertical temperature profiles. It can be seen that in general the B variance was not as great as the A variance indicating little or no reflection of material off the boundaries. The closeness of the points indicates that the data were very close to normally distributed (~ ±10 percent). This was true of the data for all nozzles and jet strengths in general. The scatter of the points about the trend line, ±20 percent maximum, was also typical of the data in general.

Table 12 gives the 69 vertical and lateral diffusion coefficients obtained from graphs such as figure 34.

In addition to the diffusion coefficients a second good index of diffusion is the rate of decay of the temperature excess or concentration along the axis of a diffusing plume. Presented in figures 35, 36, and 37 are plots of the log of the axis temperature excess, T_{max}, versus the log of the dimensionless distance below the nozzle, x/d. All three figures are from medium nozzle data. Figure 35 is for run S1, figure 36 for run TR1, and figure 37 for run RB1. Data from four jet strengths are shown on each figure.

The slope of the log plots are independent of jet strength for a given boundary but increases as the boundary roughness is increased. As shown on the figures the slope of the RB1 lines is 1.65 times the slope of the S1 lines and 1.16 times the slope of the TR1 lines.

This completes the data presentation. In the following chapter an analysis will be made to show the relationship between the turbulence characteristics and the diffusion coefficients from the various experiments.

Table 12. *Diffusion coefficients for heated water and salt solution*

Nozzle size	Smooth boundary (S1)						3/4-inch rock boundary (TR1)						6-inch cobble boundary (RB1)					
	Heat			Salt solution			Heat			Salt solution			Heat			Salt solution		
	Jet strength	ϵ_y	ϵ_z	Jet strength	ϵ_y	ϵ_z	Jet strength	ϵ_y	ϵ_z	Jet strength	ϵ_y	ϵ_z	Jet strength	ϵ_y	ϵ_z	Jet strength	ϵ_y	ϵ_z
Small	1.11	0.00190	No data	0.96	0.00271	No data	1.22	0.00320	0.00694	1.10	0.00236	0.00725	1.00	0.00330	0.01040	1.00	0.00437	0.01161
	2.56	.00212	0.00342	2.30	.00232	0.00355	2.73	.00308	.00689	3.09	.00238	.00796	2.69	.00327	.01049	2.84	.00419	.01210
	4.34	.00208	.00363	4.30	.00245	.00380	5.12	.00328	.00719	5.20	.00225	.00710	4.86	.00321	.00992	4.69	.00344	.01135
	7.15	.00189	.00380	6.26	.00265	.00391	9.15	.00331	.00683	9.05	.00215	.00752	8.68	.00319	.01055	8.19	.00377	.01068
Medium	1.52	0.00188	0.00382	0.64	0.00250	0.00401	1.48	0.00283	0.00641	1.48	0.00232	0.00771	1.88	0.00311	0.01120	1.02	0.00359	0.01290
	2.43	.00198	.00392	2.20	.00255	.00410	2.83	.00330	.00678	3.11	.00214	.00664	2.52	.00314	.01010	2.72	.00368	.01237
	3.82	.00198	.00381	3.85	.00248	.00388	4.83	.00272	.00755	5.10	.00202	.00720	4.44	.00317	.01115	4.57	.00338	.01217
	5.84	.00210	.00423	6.76	.00238	.00470	8.10	.00306	.00738	7.90	.00230	.00708	7.63	.00300	.01100	7.60	.00400	.00176
Large	0.64	0.00211	0.00347	0.27	0.00279	0.00436	0.49	0.00305	0.00678	0.41	0.00241	0.00714	0.59	0.00342	0.01086	0.50	0.00386	0.01270
	1.20	.00178	.00422	.93	.00270	.00470	1.07	.00288	.00770	1.23	.00236	.00752	1.07	.00338	.01110	1.12	.00420	.01216
	1.72	.00199	.00335	1.77	.00269	.00388	2.09	.00285	.00666	2.15	.00202	.00767	1.88	.00294	.01096	1.92	.00360	.01200
	2.81	.00187	.00369	2.85	.00265	.00435	3.37	.00297	.00704	3.80	.00200	.00690	3.332	.00328	.01083	3.26	.00433	.01140

Chapter V

DISCUSSION OF RESULTS

As stated in the introduction, the primary purpose of this report is to develop readily usable Eulerian-Lagrangian relations which can be used to predict the turbulent diffusion coefficients in the vertical, lateral, and longitudinal coordinate directions from the statistical properties of turbulence measurements in the Eulerian framework. The discussion is divided into three general areas. First, the lateral, longitudinal, and vertical diffusion coefficients will be analyzed using an extension of Philip's (1967) hypothesis. Included is a discussion of the applicability of space-time correlations for predicting the Lagrangian time scale. Next, the Boussinesq form of longitudinal diffusion coefficient will be discussed in terms of the velocity-concentration covariance measurements. Finally, some general comments are made on the relation between longitudinal dispersion and turbulent diffusion, and on the diffusion of turbulent jets.

Diffusion and Philip's hypothesis

A brief review of the theory of Chapter II is in order so that the reader may more clearly understand the problem of relating the turbulent diffusion coefficients to the statistical properties of Eulerian turbulence measurements. The fundamental connection between the turbulent diffusion coefficients and the turbulent velocity fluctuations in homogeneous turbulence is established by equations 23 and 24:

$$\varepsilon_{ij} = \frac{1}{2} \frac{d \overline{\sigma_{ij}^2}}{dt} \quad , \tag{23}$$

and

$$\overline{\sigma_{ij}^2} = 2\left(\overline{u_i^2} \cdot \overline{u_j^2}\right)^{\frac{1}{2}} \int_0^t \int_0^t \left[R_{L_{ij}}(\tau) + R_{L_{ji}}(\tau)\right] d\tau \, dt^* \quad . \qquad (24)$$

Both of these equations are Lagrangian in nature. That is, the u_i and $R_{L_{ij}}(\tau)$ are velocities and correlations of a single particle traveling with the flow field and not velocities and correlations at a single point. These relations are deceptively simple. No current experimental techniques allow ready evaluation of the Lagrangian velocity components. The Lagrangian correlation function is thus also not readily measurable. Eulerian velocities and correlations, at least in the longitudinal direction, are measured with relative ease. If use is to be made of equations 23 and 24 assumptions are then necessary about the relation between Lagrangian properties (measured by following single particles) and Eulerian properties (measured by watching many particles move past a point).

The first such assumption that will be made is that the time-average velocity fluctuations, the $\overline{u}_i$ components, are the same in either frame of reference. This means that time and space averaging are equivalent. That is, by following one particle and averaging its velocity as it travels throughout the flow field we should get the same value for $\sqrt{\overline{u_i^2}}$ as we would by time averaging the u_i of many particles passing a single point. In a uniform velocity field this would seem justified. In a shear flow this will be an accurate assumption only if Lagrangian particles avoid the regions near the walls and bed.

The next assumption to be made is the form of the relation between the Eulerian and Lagrangian correlation function. In order to attack

this question Philip (1967) considered the problem in a field of homogeneous, isotropic turbulence with zero mean motion. This allowed consideration of the longitudinal velocity fluctuations only. His argument was that when making Eulerian correlation measurements between velocities separated in space and time [say from point (0,0,0) to point (x,r,t)], occasionally the same fluid particle will have been present at both points. Thus on these rare occasions we will have made both an Eulerian and a Lagrangian measurement. By making a sufficiently large number of these measurements it is possible to generate a new correlation function from these rare occasions when Eulerian and Lagrangian coincide. Philip next assumed that the correlation of the velocities on these rare occasions could be replaced by the correlation at any time. By integrating over all possible positions (x,r,t) with weighting equal to the probability of the Eulerian-Lagrangian coincidence, he developed the following identity:

$$R_L(t) = \int_{-\infty}^{\infty} \int_{0}^{\infty} \theta(x,r,t)\ R_E(x,r,t)\ dr\ dt \quad , \tag{57}$$

where $\theta(x,r,t)$ is the probability density function of the Eulerian-Lagrangian coincidence. By taking $\theta(x,r,t)$ to be a three-dimensional Gaussian function and assuming a mathematically convenient and physically reasonable form for $R_E(x,r,t)$ he was then able to generate R_L by numerical methods. After transforming to a space with mean motion this led to an Eulerian-Lagrangian time scale relation of the form

$$\frac{T_L}{T_E} = \left(1 + \frac{\omega^2}{\overline{u^2}}\right)^{\frac{1}{2}} F(\omega) \quad , \tag{31}$$

where ω and $F(\omega)$ are functions of the absolute turbulence intensity $\sqrt{\overline{u^2}}$ and the time scale ratio T_L/T_E. The nature of Philip's relation suggests a dependence of T_L/T_E on the inverse of the turbulence intensity. This dependence is verified here for the surface of an open channel.

The relation proposed by Philip is shown in figure 38. Also shown on the figure are data from this study and from the work of Engelund, Mickelsen, Hay and Pasquill, and Durst, as reported by Philip (1970). Estimates of the Lagrangian time scale were computed from equation 28 written for the longitudinal direction at the water surface as

$$T_{L_x} = \frac{\varepsilon_{xs}}{\overline{u^2}} \quad . \tag{5}$$

The surface turbulent diffusion coefficients, ε_{xs}, from the particle experiments were divided by the surface turbulent intensity extrapolated from figure 12. This assumes that Lagrangian and Eulerian velocity fluctuations are the same as discussed above. The Eulerian time scale values were obtained from the autocorrelation functions of the longitudinal turbulence intensity records at the channel centerline. Since no definite variation of T_E with depth could be found, a depth average value was used. The agreement with Philip's relation is quite good. The maximum deviation from the line is 30 percent. It might be noted that Philip's relation appears to be somewhat too steep. If a least-squares straight line were fitted through the data points a more accurate fit of the data could be obtained. This would be important when using the relation to predict longitudinal turbulent transfer coefficients as described further on. Some of the inaccuracy is probably due to the fact that turbulence at the water surface is

approximately homogeneous but anisotropic. Thus $\sqrt{\overline{u^2}}$ is not exactly equal to the "intensity of turbulence" which Philip used.

Extension of Philip's concept to Eulerian-Lagrangian relations within the flow field is a much more complex problem, both experimentally and theoretically. First, turbulence in an open channel, except near boundaries, is homogeneous but anisotropic in the x-z plane and both nonhomogeneous and anisotropic in the x-y plane. Second, no direct means of obtaining either the Eulerian velocity or the scale in the y and z directions is available. The root-mean-square values of the velocity fluctuations, $\sqrt{\overline{u^2}}$ and $\sqrt{\overline{w^2}}$, could be approximated as fixed percentages of $\sqrt{\overline{u^2}}$ on existing experimental grounds, but no theory exists for a lateral or vertical Eulerian time scale. Thus even if a theoretical relation between the vertical or lateral velocity fluctuations $\overline{v^2}$ and $\overline{w^2}$ and the ratio of the time scales T_{L_y}/T_{E_y} and T_{L_z}/T_{E_z} could be found it would be technically infeasible to check. Justification is needed for relating vertical and lateral time scales and diffusion processes to the readily measurable longitudinal Eulerian properties of the flow.

In order to make such a justification we must look at the effect of anisotropy and inhomogeneity on the flow field. Anisotropy of a homogeneous turbulence field means that the time average velocity fluctuations are no longer equal, that is $\sqrt{\overline{u^2}} \neq \sqrt{\overline{v^2}} \neq \sqrt{\overline{w^2}}$, but maintain some constant ratio. That is, $\sqrt{\overline{v^2}} = K_1 \sqrt{\overline{u^2}}$, and $\sqrt{\overline{w^2}} = K_2 \sqrt{\overline{u^2}}$. This being true it is not unreasonable to expect some constant relation between the correlation functions and time scales in the three directions. If such a constant relation exists, then whatever connection exists between T_{L_y}/T_{E_y} and $\sqrt{\overline{v^2}}$ or T_{L_z}/T_{E_z} and $\sqrt{\overline{w^2}}$ must differ at most

by some constant from the relation between T_{L_y}/T_{E_y} or T_{L_z}/T_{E_z} and $\sqrt{\overline{u^2}}$. Since with the exception of the region near the sidewalls open channel flow is approximately homogeneous but anisotropic in the x-z plane we might expect a dependence of T_{L_z}/T_{E_z} on $\sqrt{\overline{u^2}}$ similar in form to that proposed by Philip for isotropic turbulence. Such a relation is not measurable, however, since neither T_{L_z} or T_{E_z} are measurable. T_{L_z} could be approximated by dividing ε_z by $K_2\ \overline{u^2}$, analogous to equation 58, but the value for K_2 is not known for an open channel. However, by defining a new time scale, T_{A_z} as

$$T_{A_z} = \frac{\varepsilon_z}{\overline{u^2}} \quad , \tag{59}$$

we bypass the problem. If the above assumptions are correct, this new time scale should differ at most by some constant from the actual lateral Lagrangian time scale, T_{L_z} . It seems reasonable that the ratio of this new time scale to the longitudinal Eulerian time scale, T_{A_z}/T_E might show a dependence on $\sqrt{\overline{u^2}}$.

The effect of inhomogeneity is difficult to approach theoretically. When inhomogeneities are present no fixed relation exists between the velocity fluctuations in the three coordinate directions. Thus there is no a priori reason to expect a dependence on the Eulerian-Lagrangian time scale ratio in the vertical direction, T_{L_y}/T_{E_y} on $\sqrt{\overline{u^2}}$. To bypass this problem we must resort to heuristic arguments. Once again there is no way of directly measuring a value for the Lagrangian time scale or the Eulerian time scale in the y direction. It seems plausible, then, to resort to a time scale based on the longitudinal

intensity and the y-direction diffusion coefficient. This time scale is defined as follows:

$$T_{A_y} = \frac{\varepsilon_y}{\overline{u^2}} \quad , \tag{60}$$

where ε_y is the depth average turbulent diffusion coefficient and $\overline{u^2}$ is a depth-averaged value of the turbulent velocity fluctuations. By depth averaging, the effect of inhomogeneity in the y direction is removed since the velocity and turbulence structure do not vary from station to station in a steady, uniform open-channel flow. We might now expect a variation of this depth average time scale with depth-averaged intensity of turbulence. Experimental evidence from this study will now be presented to show that relations such as equations 59 and 60 do produce workable results.

The first application of the analysis based on the new time scales is to lateral diffusion at the water surface. Shown in figure 39 is the ratio of the lateral integral time scale to the longitudinal Eulerian integral time scale T_{A_z} / T_E versus the inverse of the longitudinal turbulent intensity at the water surface, $1/\sqrt{\overline{u^2}}$. Also shown is a line with the same slope as Philip's relation. The data are within ±20 percent of a straight line with Philip's slope and once again a line of less slope would produce a better fit to the data.

A similar analysis was next made on the depth-averaged diffusion coefficients obtained from the jet-diffusion studies and the velocity-concentration covariance measurements. The y and z coefficients are the mean value of the 12 obtained for each boundary condition for the 3 nozzles at 4 discharges. The reason a simple average was used is

discussed in the "Jet diffusion" section. In general the depth-averaged values of the turbulent diffusion coefficients, ε_i, tended to be somewhat higher than the surface values, ε_{is}. For the smooth boundary (S1), ε_z exceeded ε_{zs} by 8.7 percent and ε_x exceeded ε_{xs} by 28.7 percent. For the 6-inch cobble boundary (RB1), ε_z exceeded ε_{zs} by 7.2 percent and ε_x exceeded ε_{xs} by 5.8 percent. Figure 40 shows the relation between T_{A_y}/T_E, T_{A_z}/T_E, or T_{L_x}/T_E, and the depth-average value of $1/\sqrt{\overline{u^2}}$. The time scale ratios were obtained from equation 62 with the centerline value of $\sqrt{\overline{u^2}}$ averaged at 9 dimensionless depths, 0.1 to 0.9. It should be remembered that T_E is still a value obtained from longitudinal velocity correlations.

The closeness of the horizontal and vertical data to straight lines is quite good. The maximum deviation is 23 percent low for the smooth boundary heat data in the y direction. In fact, most of the deviation is due to the fact that with a single exception the salt solution diffused faster than the heated water. On the average (both y and z direction) ε_i for salt exceeded ε_i for heat by 15.1 percent. This fact has significance on its own since it is sometimes reported (Forstall and Shapiro, 1950) that ε_i for heat and mass are equal.

For the longitudinal direction the T_{L_x}/T_E versus the depth average of $1/\sqrt{\overline{u^2}}$ relation is less satisfactory. Because the points were obtained from the average ε_x values in the velocity-concentration covariance measurements, this is not surprising. The experimental error in the measurements is not small. These errors will be discussed further in the next section.

By now the reader may legitimately ask, "What is all this good for?" The importance of this analysis is that diffusion coefficients

can be obtained from readily made Eulerian turbulence characteristics by reversing the process used to generate figures 38, 39, and 40. First, the longitudinal turbulence intensity is measured at the desired location in the flow, or at sufficient points to obtain a depth-average value of $\sqrt{\overline{u^2}}$. Next the Eulerian time scale, T_E , is determined from the autocorrelation of the turbulence signal (depth average for depth-average coefficients). Next the proper figure, 38 through 40, is entered to determine T_{L_i} or T_{A_i} over T_E . From this ratio, T_{L_i} or T_{A_i} is determined from the relation

$$\varepsilon_i = \overline{u^2}\, T_{L_i} \quad \text{or} \quad \varepsilon_i = \overline{u^2}\, T_{A_i} \quad . \tag{61}$$

Figures 38-40, particularly figure 38, are substantiated by considerable experimental evidence in addition to that from this study. Turbulent diffusion coefficients in the atmosphere as well as in open channels could be predicted (at least in the longitudinal direction) from such relations since both types of data are shown (Durst's data are large scale meteorological and Mickelsen's are small scale wind tunnel). This technique makes possible the prediction of diffusion coefficients at field sites or in models from turbulence measurements rather than by empirical formulas. Turbulence measurements for use in predicting transfer coefficients should be somewhat less involved than making actual tracer measurements to determine rates of spread. Applications might include design of sewer or powerplant outfalls along rivers. Field application to atmospheric diffusion processes will require more readily usable turbulence measuring techniques than are now available. Prediction of wind tunnel transfer coefficients for use in modeling atmospheric processes should currently be practical.

Space-time velocity correlations

The purpose of the space-time velocity correlation measurements was to determine to what degree of approximation they could be used as a substitute for Lagrangian correlation measurements. This comparison is made by checking the Lagrangian time scales, T_{L_x}, obtained through the diffusion measurements and equation 58 against the time scale values obtained from integrating the envelope curves in figures 21 through 26 in Chapter IV. Because of the similarity in roughness and turbulence characteristics the 3/4 - inch rock boundary Lagrangian time scale was estimated from the 1 1/2 - inch rock boundary data. The results are shown in table 13. For the smooth boundary (S1) the Lagrangian time scale of 13.52 seconds exceeds the average space-time integral scale of 5.03 seconds by a factor of 2.7. For the 3/4 - inch rock boundary (TRI) the Lagrangian time scale of 7.68 seconds exceeds the average space-time integral scale of 3.80 seconds by a factor of 2.02. Had these values been used to predict the longitudinal diffusion coefficient from equation 63 the results would have been low by the same factors. This is in direct contrast to the results of Baldwin and Mickelsen (1963) whose results were overpredicted by roughly the same amount.

Baldwin and Mickelsen's results can be explained by considering the Eulerian-Lagrangian relation of Philip. From the properties of the space-time correlation it can be seen that the space-time integral scale is always greater than or equal to the Eulerian integral scale, T_E. This is because the $R_u(0,\tau)$ space-time correlation curve is the autocorrelation curve and hence contains the same area as $R(\tau)$, that is T_E. Also for any small finite probe spacing, ξ_1, $R_u(\xi_1,\tau)$ will have some finite area unless the turbulence were to decay in zero time.

Table 13. *Space-time and Lagrangian time scales*

Boundary condition	Longitudinal space-time integral time scale (secs)			Lagrangian time scale T_{L_x} (secs)
	0.15 ft Below water surface	0.45 ft Below water surface	0.75 ft Below water surface	
S1	5.30	5.10	4.70	13.52
TR1	3.50	4.30	3.60	7.68

Thus an envelope curve of $R_u(\xi,\tau)$ must have a greater area contained within it than the autocorrelation and hence a bigger time scale. Now, by considering figure 38 it can be seen that for flows where the reciprocal of the turbulent intensity, $1/\sqrt{\overline{u^2}}$ is less than 2.1 that T_{L_x}/T_E is less than one. Thus T_{L_x} is less than T_E and must therefore be less than the space-time integral scale also. How this might be true physically is difficult to visualize, but the result is consistent with experimental results.

Longitudinal diffusion and the velocity-concentration covariance

As stated in Chapter II, considerable simplification can be made in the Eulerian diffusion equation by assuming that the principal axes of the diffusion coefficient tensor coincide with the axes of the flow field. This assumption about the principal axes is valid as long as the eddies in the flow field have no preferred orientation. It might be reasonable to argue that the orientation of the principal axes is a random variable in the same sense that the orientation of any particular eddy is random. Then the off-diagonal terms would not necessarily equal zero, except perhaps in an average sense at points in the flow field where the orientation of the principal axes of diffusion averaged over many eddies happens to coincide with the axes of the flow field. At points in the flow where the preferred orientation is skewed, the off-diagonal terms in the diffusion tensor would not be zero, even in an average sense (personal communication, Sayre, 1969). At any rate, by making this simplification it becomes possible to evaluate the turbulent diffusion coefficients directly from the relation

$$\varepsilon_i = \frac{-\overline{u_i c}}{\partial \overline{C}/\partial x_i} , \qquad (62)$$

providing $\overline{u_i c}$ can be measured.

Using the technique described in Chapter III it is now possible to evaluate the longitudinal velocity-concentration covariance. This allows direct evaluation of ε_x from equation 62. By comparing the results with values of ε_{xs} obtained from the floating particle studies it becomes possible to qualitatively examine the validity of the Boussinesq-type mass transfer coefficient. Figures 41, 42, and 43 show the results of such an analysis for runs S1, R1, and RB1. Plotted in the figures are the longitudinal turbulent diffusion coefficient, ε_x, obtained from $\overline{uc}$ versus the station below the injector nozzle (data in tables 9, 10, and 11, Chapter IV). Also shown is the surface value of ε_{xs}.

For the smooth boundary, figure 41, 10 of the 12 data points lie within ±25 percent of the surface value of ε_{xs}. The longitudinal diffusion coefficient within the flow is somewhat greater than ε_{xs}, the mean value being 0.0118 compared to 0.00916. For the 1½-inch rock boundary, figure 42, 10 of the 13 data points lie within ±25 percent of the surface value of ε_{xs}. Again the trend for the values obtained from the velocity-concentration covariance is greater than the ε_{xs} values, the mean value being 0.0366 compared to 0.0335. For the 6-inch cobble boundary, figure 43, 5 of the 6 data points lie within ±30 percent of the surface values of ε_{xs}.

The scatter of the results could be due to a number of causes. Most obvious is experimental accuracy. Measurements of the longitudinal

turbulent intensity are considered good to ±15 percent under ideal conditions. Such measurements require accurate calibration of the hot-film and operation in clean water at constant temperatures. The turbulence level must be such that $\overline{U}$, the local mean velocity exceeds $\sqrt{\overline{u^2}}$, the fluctuating component by approximately an order of magnitude. All of these criteria are met by this study and indicate that the turbulence portion of the covariance is as good as is technically feasible. The conductivity probe was conservatively designed in terms of frequency response and was considerably more streamlined than the hot-film probe. As a technical instrument it was at least as good as the hot-film for the job it was intended to do. The clean water and constant temperature criteria applied also to the accurate operation of the conductivity probe. The error encountered in the concentration fluctuation measurements should be less than or equal to the error in the velocity fluctuation measurements. As indicated in the experimental apparatus section, no significant blockage or heat transfer effects could be detected when the probes were operated together. If the spacing of the probes was not greater than the smallest scale eddies responsible for mixing then the covariance measurements should be accurate to ±20 percent.

With error of this magnitude it would be desirable to have an independent check on the quality of the covariance measurements. Such a check is available through basic theory and the results from the "Diffusion of turbulent jets" section which follows this by several pages. In the turbulent jet section it is shown that the concentration along the axis of a diffusing plume decays as a power law function of the distance below the injector nozzle. The exponent of the power law

is a function of the channel shear velocity. This means that the concentration gradient along the plume axis can also be expressed as a power law function of the distance as follows:

$$\frac{\partial C_{max}}{\partial x} = A\, b\, x^{(b-1)} \quad , \tag{63}$$

where A is a constant and b is the decay exponent. Because all the covariance measurements were made along the axis of a diffusing plume, $\partial C_{max}/\partial x$ may be substituted for $\partial \overline{C}/\partial x$ in equation 62 written for the longitudinal direction to give the following expression:

$$\varepsilon_x = \frac{\overline{uc}}{A\, b\, x^{(b-1)}} \quad . \tag{64}$$

Sayre (1968) states that there is no reason to expect a variation of ε_x in the longitudinal direction at a given level in the flow. Thus by replacing $A\, b\, \varepsilon_x$ by a constant, k_3, we find the following expression for $\overline{uc}$ as a function of x

$$\overline{uc} = k_3\, x^{(b-1)} \quad . \tag{65}$$

This means that a log-log plot of $\overline{uc}$ versus x should be a straight line with slope of b-1. The values of the exponent b are well established by 24 independent graphs for each of the three boundary conditions. The behavior of $\overline{uc}$ as indicated by equation 65 and the established exponents would thus substantiate the covariance measurements and the Boussinesq-type transfer coefficient. In addition, the behavior of $\overline{uc}$ along the axis of a plume would then be coupled to a measurable mean flow parameter because the exponent b is shown to be a linear function of the shear velocity, U_*, in the "Diffusion of turbulent jets" section. Shown in figure 44 is a log-log plot of $\overline{uc}$ versus x for runs

S1, R1, and RB1. Also shown are lines with slopes of -2.04, -2.46, and -2.705, the (b-1) values for the three runs. The closeness of the data to the lines is remarkably good. The average deviation of the points from the lines is ±21.6 percent. The "worst" point is the 1-foot station for run S1 which misses the line by a factor of 3. These results support the ±20 percent value for accuracy of the covariance measurements.

While experimental technique is certainly a major source of uncertainty, it would not seem to account for all the scatter in the results. We must then look at the assumptions leading to equation 64. If the axes of the diffusion coefficient tensor do not align with the axis of the flow, then the off-diagonal turbulent diffusion coefficients are not zero and equation 62 is not valid, or at best is only an approximation. The increasing scatter of the data as the boundary roughness is increased may indicate that the axis-alignment assumption becomes less and less valid for flows with increasing turbulence levels. When considering this question it is important to remember that all the covariance measurements were made on the axis of a diffusing plume. The larger scatter in the results at higher roughness may be due to meandering of the plume axis. In fact, it is conceivable that equation 62 would give much worse results elsewhere in the flow field.

With the above discussion in mind, only two things may be safely concluded at this time. First, the single-electrode/hot-film technique is a valid and useful new tool for the study of turbulent mass transfer. Second, under the restrictions of this study, that is, along the axis of a plume diffusing at mid-depth of a steady, uniform open-channel flow, the Boussinesq-type mass transfer coefficient is valid. The

small number of measurements and the restrictive conditions precludes broad generalization on the behavior of the velocity-concentration covariance with roughness, velocity, or other mean flow parameters. The results must still be considered significant, however. The difficulty in evaluating ε_x from such an experiment is analogous to evaluation of the coefficient of viscosity with precision from the equation

$$\tau_{ij} = \mu\left(\frac{\partial u_i}{\partial x_j} + \frac{\partial u_j}{\partial x_i}\right) \tag{66}$$

in a non-uniform laminar flow.

It is hoped that this study will encourage others to use this technique to study the turbulent mass transfer term in more detail. A first series of experiments should include measurement of $\overline{uc}$ throughout the flow field to determine where the Boussinesq-type transfer coefficient is valid. The variation of $\overline{uc}$ with roughness could then be undertaken. The next step would be the study of the vertical and lateral covariance terms $\overline{vc}$ and $\overline{wc}$. Measurement techniques for direct recording of v and w are currently being developed. The combination with the single-electrode probe should prove to be relatively easy. Such measurements would enable a comprehensive study of the behavior of the diffusion tensor.

Dispersion

The data from this study afford a unique opportunity to study the effect of longitudinal diffusion on dispersion. It has been accepted for some time that the dominant mechanism in dispersion is the variation of the mean velocity within a cross section, both vertical and lateral. The role of the longitudinal turbulent velocity fluctuations

is assumed to be small. The turbulent transfer coefficient, ε_x, is approximated by the depth-average value of the vertical transfer coefficient, ε_y. Using this approximation, ε_x is approximately 1 percent of D_x, the dispersion coefficient (Sayre and Chang, 1968). Using values from table 8, Chapter IV, and the results of the velocity-concentration covariance study, it will be seen that this is a poor approximation. For runs S1 and S2 the surface diffusion coefficients were 4.1 percent and 5.7 percent of D_x, respectively. For runs R1 and R2 the surface diffusion coefficients were 12.2 percent and 10 percent of D_x, respectively. For runs RB1 and RB2 the surface diffusion coefficients were 3.52 percent and 3.53 percent of D_x, respectively. The depth-average values, ε_x, obtained from the $\overline{uc}$ study are even higher percentages of D_x, being 5.23 percent, 13.13 percent, and 3.73 percent for runs S1, R1, and RB1, respectively. Thus, while neglecting or minimizing the effect of ε_x on dispersion may not cause large errors, the effect is greater than previously thought.

A second interesting analysis of the dispersion data involves comparison of the coefficients to the classic prediction formulas involving a product of the shear velocity, U_*, the normal depth, Y_N, and a constant (Elder, 1959; Sayre and Chang, 1968). Shown in figure 44 is a plot of D_x for the seven runs in this study versus $Y_N U_*$. Also shown are two lines with slopes 5.3 and 7.2, approximately the range of values of the constant in the prediction equation. For 5 of the 7 runs, S1, S2, TR1, R1, and R2, the predicted value lies within ±40 percent of the measured values. For the two 6-inch cobble runs, RB1, and RB2, the error is between 30 percent and 50 percent. One cause for this discrepancy is lateral velocity variations. A second possibility is the

large amount of dispersant which becomes entrapped in the pore spaces and dead zones of the higher boundary roughnesses. This entrapped material slowly diffuses into the flow producing long "tails" on the $\overline{C}$ versus t curves. These "tails" greatly increase the variances of the curves and result in large values for D_x. Over extremely rough boundaries the simple prediction formulas are approximations at best. More sophisticated analysis such as that of Fischer (1966) is required. Miller (personal communication, 1971) studied mixing over a wide range of roughness in a 2-foot wide flume and reached similar conclusions.

Diffusion of turbulent jets

In addition to the long-time turbulent diffusion coefficients used in the Philip's hypothesis section, the jet studies offer useful insight into the behavior of a diffusing plume at stations close to the nozzle. The first area looked at was the effect of jet strength (ratio of injection to mean stream velocity, U_{jet}/U_{xs}) on mixing. To determine the effect the depth-averaged diffusion coefficients in the y and z directions were plotted against jet strength. The results are illustrated in figures 45 and 46. From the figures it can be seen that within ±10 percent the jet strength has no effect on the diffusion coefficients in either the y or z direction. Once again the tendency for the salt solution to diffuse 15 percent faster than the heated water can be seen. The writer could find no satisfactory explanation for this difference. Density effects were not considered because the maximum measured plume rise for a heated water jet was 0.05 feet (5 percent of the normal flow depth). This was at the farthest station from the injector nozzle used in the diffusion coefficient calculations. This would seem to indicate that the turbulent Prandtl number (ratio

of heat transfer coefficient to momentum transfer coefficient) is less than the turbulent Schmidt number (ratio of mass transfer coefficient to momentum transfer coefficient). It has sometimes been indicated that the two are equal (Forstall and Shapiro, 1950).

A second useful result of the jet studies is the effect of channel roughness (changes in ambient turbulence level) on the decay rate of centerline temperature or concentration in a diffusing plume. It has been known for some time that the maximum temperature excess or concentration versus dimensionless distance below the nozzle can be plotted as a straight line on log-log paper as was done in Chapter IV (Albertson and others, 1948; Forstall and Shapiro, 1950; and others). This indicates that the decay is some power law of the form

$$C_{max} \text{ or } T_{max} = A\left(\frac{x}{d}\right)^{b} , \qquad (67)$$

where A and b are constants. The exponent b is the slope of the log-log plot. Apparently because most previous studies have been conducted using air as a medium (for example, Bradbury and Riley, 1967), no one has studied the effect of roughness (increased ambient turbulence level) on the exponent b. To determine this effect, the exponent for runs S1, TR1, and RB1 is plotted as a function of the shear velocity in figure 47. Within 3 percent the data fall on a straight line through the origin. While the data are not numerous enough to state flatly that this is a universal relation, the result is encouraging. Further information such as this would be useful in the design of jet type outfalls for sewage or power plant coolants. By determining the shear velocity of the dispersing stream, it would be possible to predict the rate of decay of the plume-axis concentration or temperature. It is

interesting to note that the decay exponent can be related to a simple mean-flow parameter such as the shear velocity when a similar analysis for the dispersion process (that is, D_x versus $Y_N U_*$) produced such poor results.

A final result which may be extracted from the data is a check on Forstall and Shapiro's prediction of the length of the core region of a jet (equation 36). This is the distance from the nozzle to the point where the axis temperature or concentration is no longer equal on the average to the injection value. Equation 36 suggests that the core length divided by the nozzle diameter is a linear function of the jet strength. Shown in figure 48 is the result of plotting the log of x_c/d versus the log of the jet strength for runs S1, TR1, and RB1. The data points were obtained by extrapolating relations such as figures 35 through 37 back to the injection temperature and reading the x/d value. The data for all three boundary roughnesses fall on straight lines. This indicates that x_c/d is related to the jet strength by a power function of the form

$$\frac{x_c}{d} = B\left(\frac{U_{jet}}{U_{xs}}\right)^{\Omega} \quad , \tag{68}$$

where Ω and B are constants depending on the boundary roughness. The Ω values for these experiments are 0.607, 0.493, and 0.482 for runs S1, TR1, and RB1, respectively. This type of relation would seem to make better sense than Forstall and Shapiro's on the grounds that the core length increases with increasing jet strength rather than decreasing. The core length also decreases more rapidly with jet strength over a rougher boundary.

A short summary of the implications of the results of the jet studies is now in order. First, since the turbulent transfer coefficients in both the lateral and vertical direction appear to be independent of jet strength, nothing appears to be gained by designing jet-type fluid mixers which inject at higher than stream velocity. Second, the dependence of the axis temperature or concentration decay rate of a jet on the shear velocity of an open channel may prove useful in the design of jet-type outfalls for sewers or powerplants. The power law relation between the jet strength and the core length may also be useful in such designs. By predicting the axis temperature or concentration decay rate from equation 67, the core length of the jet from equation 68, and the remainder of the temperature or concentration field by methods such as Albertson and others' or Forstall and Shapiro's, it should be possible to predict with reasonable accuracy the diffusion pattern in an open channel.

Chapter VI

SUMMARY AND CONCLUSIONS

Diffusion and Philip's hypothesis

The results of this study verify Philip's (1967) concept relating the ratio of Eulerian to estimated Lagrangian time scales in the longitudinal direction and the reciprocal of the longitudinal turbulent intensity. The relation appears to be somewhat steeper in slope than actual data. It may be used to predict with ±30 percent accuracy longitudinal turbulent diffusion coefficients at the water surface and in the flow field.

A similar concept is developed using an integral time scale based on the longitudinal turbulent intensity which may be used to predict both surface and depth-averaged turbulent diffusion coefficients in the vertical, lateral, and longitudinal directions for floating particles and heated water and salt-solution jets within ±25 percent accuracy. The concept developed appears to apply to both open channels and the atmosphere. Data indicate no scale effect in the relations which should thus be good for both model and prototype predictions of turbulent transfer coefficients.

Space-time velocity correlations

Space-time velocity correlation measurements in the longitudinal direction were made over the smooth and 3/4-inch rock roughnesses. Time scale values obtained from these measurements were 200 to 250 percent low compared to the Lagrangian time scales estimated from diffusion measurements. This is in contrast to the results of Baldwin and Mickelsen whose results were approximately the same amount high.

The Eulerian-Lagrangian relation of Philip suggests a dependence of the Lagrangian and space-time scales on the longitudinal turbulence intensity which would result in such a discrepancy.

Longitudinal diffusion and the velocity-concentration covariance

A procedure was developed for measuring the longitudinal velocity-concentration covariance using a bridge unit and single-electrode conductivity probe and a hot-film anemometer and parabolic sensor. Comparison of the behavior of the covariance term along the axis of a diffusing jet with a theoretical model indicates a ±20 percent accuracy for the measurement technique. The theoretical model also provides an indirect connection between the covariance term and the channel shear velocity. The longitudinal turbulent diffusion coefficient was computed at a number of points along the axis of a diffusing salt-solution plume using a Boussinesq-type formula. Comparison of the results with surface diffusion coefficients indicate that within ±25 percent uncertainty, the Boussinesq model is adequate to describe scalar transport along the axis of a diffusing plume. The limited amount of data did not allow great generalization on the behavior of the longitudinal velocity-concentration covariance in an open channel. Suggested future research includes measurement of the covariance throughout the flow field in a diffusing plume and the extension of the measurement technique to the lateral and vertical covariance terms. The single-electrode probe/hot-film sensor technique offers a valid and useful new tool for the study of turbulent mass transfer.

Dispersion

Comparison of the longitudinal turbulent diffusion coefficient to the one-dimensional dispersion coefficient indicates that turbulent diffusion may account for as much as 13 percent of the dispersion process. The data indicate that predicting the dispersion coefficient from classic formulas such as $D_x = 5.3\ Y_N\ U_*$ may result in values as much as 50 percent low over the roughest boundary. This discrepancy may be attributed to secondary flow and storage and release of dispersant in dead zones in the rough surface. More accurate analysis techniques such as that of Fischer (1966) should be used for determining D_x in rough channels.

Diffusion of turbulent jets

Within an accuracy of ±10 percent the jet strength (ratio of jet velocity to free stream velocity) was found to have no influence on the diffusion coefficients for jets of heated water and salt solution. Jet strengths ranged from 0.5 to 9.0. The results indicate that nothing is gained by designing jet-type outfalls which inject at greater than stream velocity. Salt solution diffuses approximately 15 percent faster than heated water. The decay of temperature excess or concentration along the axis of a diffusing plume was found to follow a power law of the form C_{max} or $T_{max} = A(x/d)^b$. The exponent b is a linear function of the shear velocity, U_*. The length of the core region of the jet was found to be a power law function of the jet strength of the form $x_c/d = B(U_{jet}/U_{xs})^{\Omega}$. The exponent Ω is a function of the boundary conditions and varied from 0.48 to 0.61 for the range of roughnesses used. By using these two relations in conjunction with the results of other experimentors such as Albertson and other, or Forstall and

Shapiro, it should be possible to predict with reasonable accuracy the core length, temperature excess or concentration decay rate, and complete diffusion pattern in an open-channel flow.

Future studies

Two distinct areas for future research are suggested by this study. The first, and more practically-oriented area, would be the extension of average-time-scale analysis to field studies of mixing in rivers and in the atmosphere. Simultaneous measurements of turbulence characteristics and diffusion coefficients under field conditions would allow better definition of the relation between the time-scale ratio and the turbulent intensity. Such studies could also be used to extend knowledge on the relation between turbulence and mean flow parameters such as velocity and roughness. Such information could be of great value in the prediction of dispersion processes in real-world situations.

The second, and more theoretically-oriented area, would be a detailed study of the covariance terms in the Reynolds-averaged Eulerian diffusion equation using the hot-film single-electrode probe technique. A first series of measurements should include measurement of the longitudinal covariance term throughout the flow field to determine where the Boussinesq-type transfer coefficient is valid. The variation of the covariance terms with roughness might then be undertaken. More sophisticated anemometry equipment is available which allows measurement of all three velocity components. By combining this with the single-electrode probe, simultaneous measurements of all three covariance terms could be made. Such measurements would allow a comprehensive study of the behavior of the diffusion tensor.

LITERATURE CITED

LITERATURE CITED

Albertson, M. L., Dai, Y. B., Jensen, R. A., and Rouse, H., 1948, Diffusion of submerged jets: Am. Soc. Civil Engineers Trans., v. 74, p. 639-697.

Baldwin, L. V., and Mickelsen, W. R., 1963, Turbulent diffusion and anemometer measurements: Am. Soc. Civil Engineers Trans., v. 128, p. 1595-1631.

Batchelor, G. K., 1949, Diffusion in a field of homogeneous turbulence: Australian Jour. Science Research, v. 2, p. 437-450.

Bradbury, L. J. S., and Riley, J., 1967, The spread of a turbulent plane jet issuing into a parallel moving air stream: Jour. Fluid Mechanics, v. 27, p. 381-394.

Elder, J. W., 1959, The dispersion of marked fluid in turbulent shear flow: Jour. Fluid Mechanics, v. 5, pt. 4, p. 544-560.

Engelund, F., 1969, Dispersion of floating particles in uniform channel flow: Am. Soc. Civil Engineers Proc., v. 95, no. HY4, p. 1149-1162.

Fischer, H. B., 1966, Longitudinal dispersion in laboratory and natural streams: Calif. Inst. Technology [Pasadena], Rept. No. KH-R-12, 250 p.

———1967, Transverse mixing in a sand-bed channel: U.S. Geol. Survey Prof. Paper 575-D, p. D267-D272.

———1969, The effect of bends on dispersion in streams: Water Resources Research, v. 5, no. 2, p. 496-506.

Forstall, W., Jr., and Shapiro, A. H., 1950, Momentum and mass transfer in coaxial gas jets: Jour. Appl. Mechanics, v. 17, p. 399-408.

Gibson, C. H., and Schwarz, W. H., 1963, Detection of conductivity fluctuations in a turbulent flow field: Jour. Fluid Mechanics, v. 16, p. 357-364.

Glover, R. E., 1964, Dispersion of dissolved or suspended materials in flowing streams: U.S. Geol. Survey Prof. Paper 433-B, 32 p.

Hinze, J. O., 1959, Turbulence: New York, McGraw-Hill Book Co., 586 p.

Jobson, H. E., and Sayre, W. W., 1970, Vertical mass transfer in open channel flow: Am. Soc. Civil Engineers Proc., v. 96, no. HY3, p. 703-724.

Keeler, R. N., 1964, Mixing and chemical reaction in turbulent flow reactors: Ernest O. Lawrence Radiation Lab. [Livermore, Calif.], Rept. No. UCRL-7852, 180 p.

McQuivey, R. S., 1967, Measurement of turbulence in open-channel flow: U.S. Geol. Survey open-file rept., 200 p.

McQuivey, R. S., and Keefer, T. N., 1971, Measurement of the velocity-concentration covariance: Written communication; to be published in Am. Soc. Civil Engineers Hydraulics Div. Jour.

McQuivey, R. S., Keefer, T. N., and Shirazi, M. A., 1971, Turbulent spread of heat and matter: U.S. Geol. Survey open-file rept., 166 p.

Miller, A. C., 1971, Turbulent diffusion and longitudinal dispersion measurements in a hydrodynamically rough open-channel flow: Dissertation, Colorado State Univ.

Orlob, G. T., 1959, Eddy diffusion in open-channel flow: Univ. Calif. [Berkeley], Water Resources Research Center, Sanitary Eng. Research Lab., Contr. No. 19, 151 p.

Philip, J. R., 1967, Relation between Eulerian and Lagrangian statistics: Physics of Fluids Supp., p. 569-571.

Prych, E. A., 1970, Effects of density differences on lateral mixing in open-channel flows: W. M. Keck Lab. of Hydraulics and Water Resources, Calif. Inst. Technology [Pasadena], Rept. No. KH-R-21, 225 p.

Sayre, W. W., 1968, Dispersion of mass in open channel flow: Colorado State Univ. Hydraulics Paper No. 3, Feb. 1968, 72 p.

———1969, Personal communication, Assoc. Prof. Civil Eng., Univ. Iowa [Iowa City].

Sayre, W. W., and Chang, F. M., 1968, A laboratory investigation of open channel dispersion processes for dissolved, suspended, and floating dispersants: U.S. Geol. Survey Prof. Paper 433-E, 71 p.

Sullivan, P. J., 1968, Dispersion in a turbulent shear flow: Ph.D. Thesis, Churchill College, Univ. Cambridge [Cambridge, England], 197 p.

Taylor, G. I., 1954, The dispersion of matter in turbulent flow through a pipe: Royal Soc. [London] Proc., v. 223A, p. 446-468.

Townsend, A. A., 1956, The structure of turbulent shear flow: Cambridge Univ. Press, p. 172-193.

Vanoni, V. A., 1946, Transportation of suspended sediment by water: Am. Soc. Civil Engineers Trans., v. 111, p. 67-133.

Yotsukura, N., Fischer, H. B., and Sayre, W. W., 1970, Measurement of mixing characteristics of the Missouri River between Sioux City, Iowa, and Plattsmouth, Nebraska: U.S. Geol. Survey Water-Supply Paper 1899-G, 29 p.

APPENDIX I - FIGURES

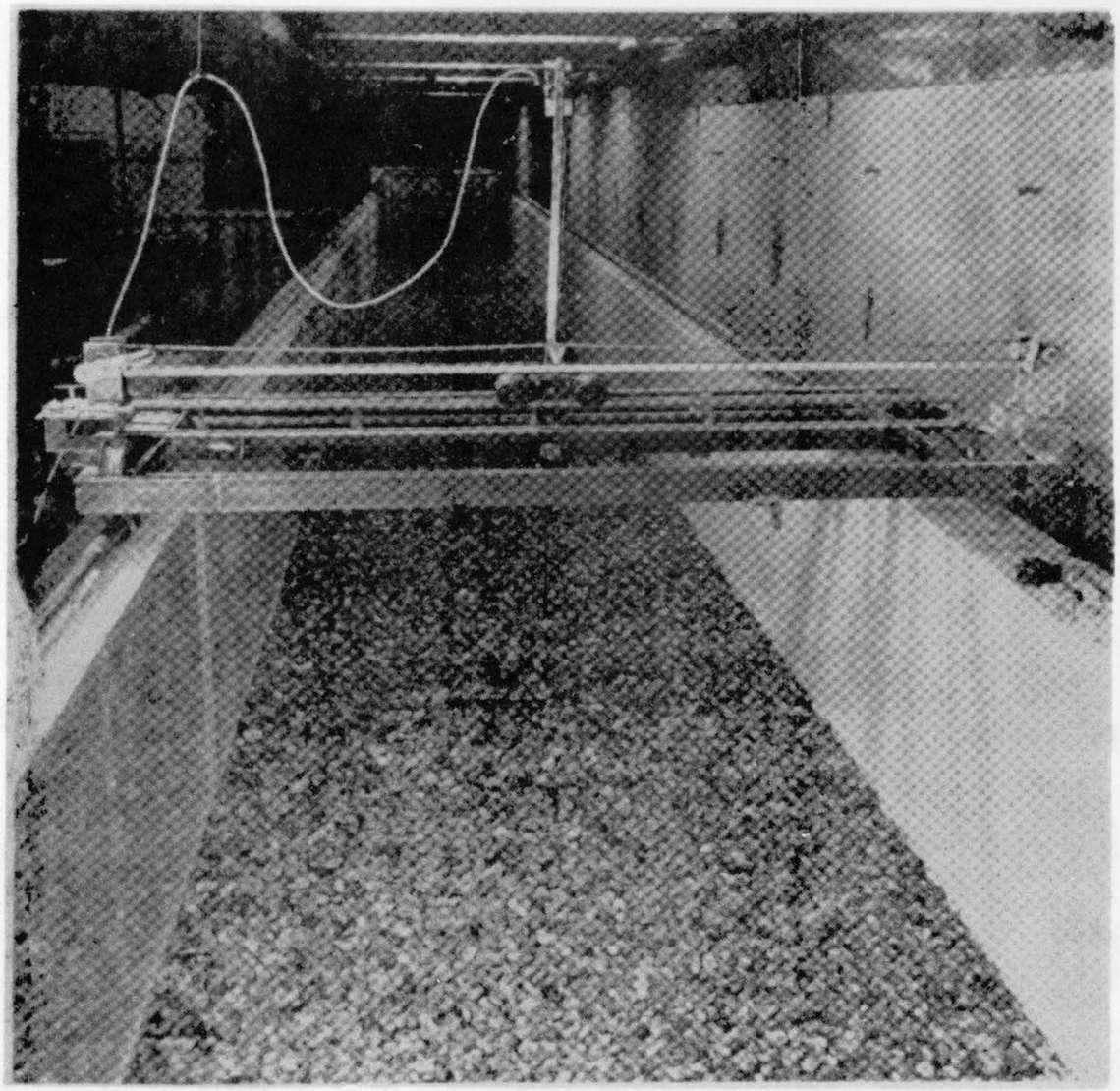

Figure 1. 4-foot wide flume and instrument carriage.

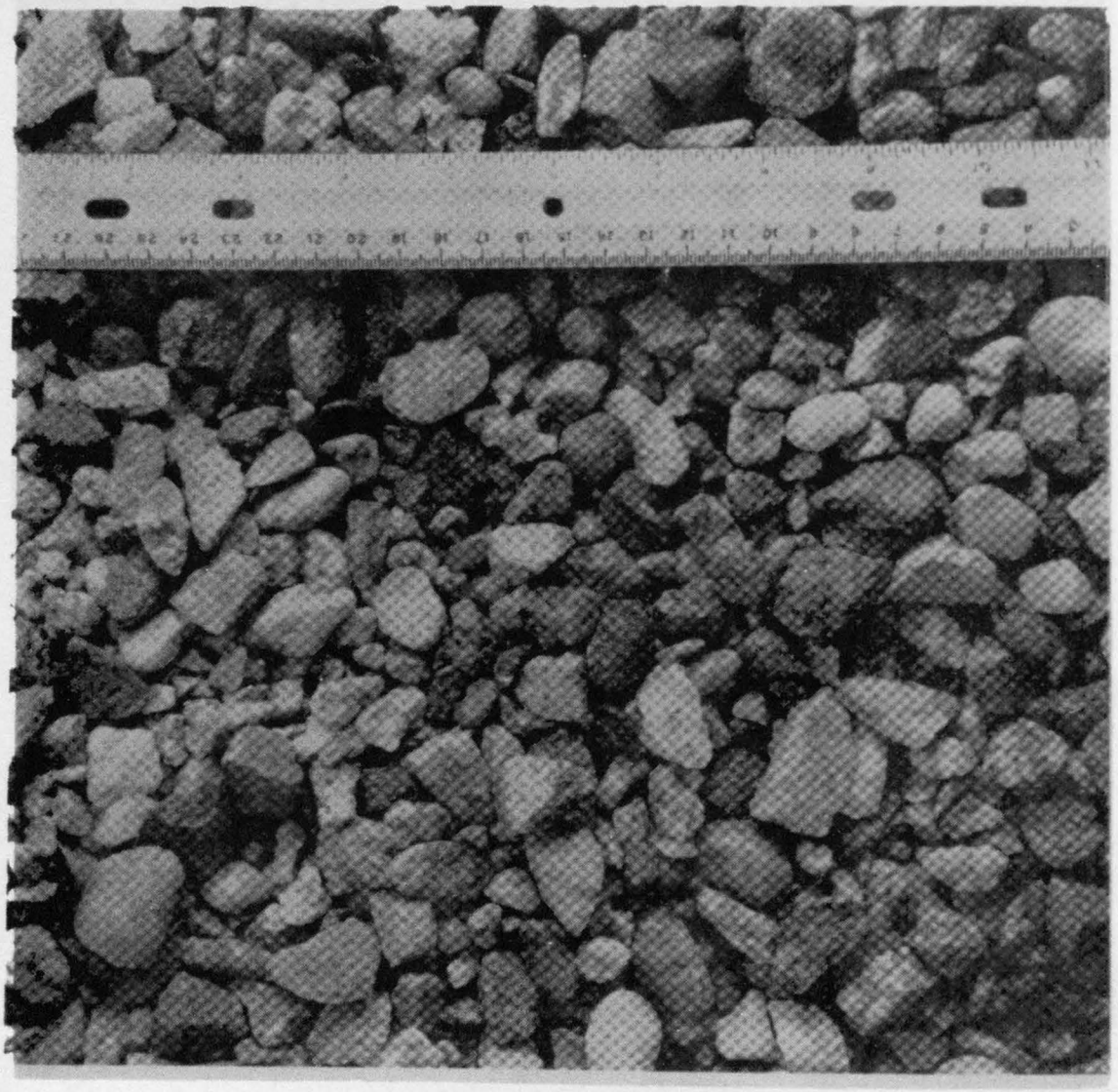

Figure 2. Close-up photograph of 3/4-inch rock roughness.

Figure 3. Close-up photograph of 1½-inch rock roughness.

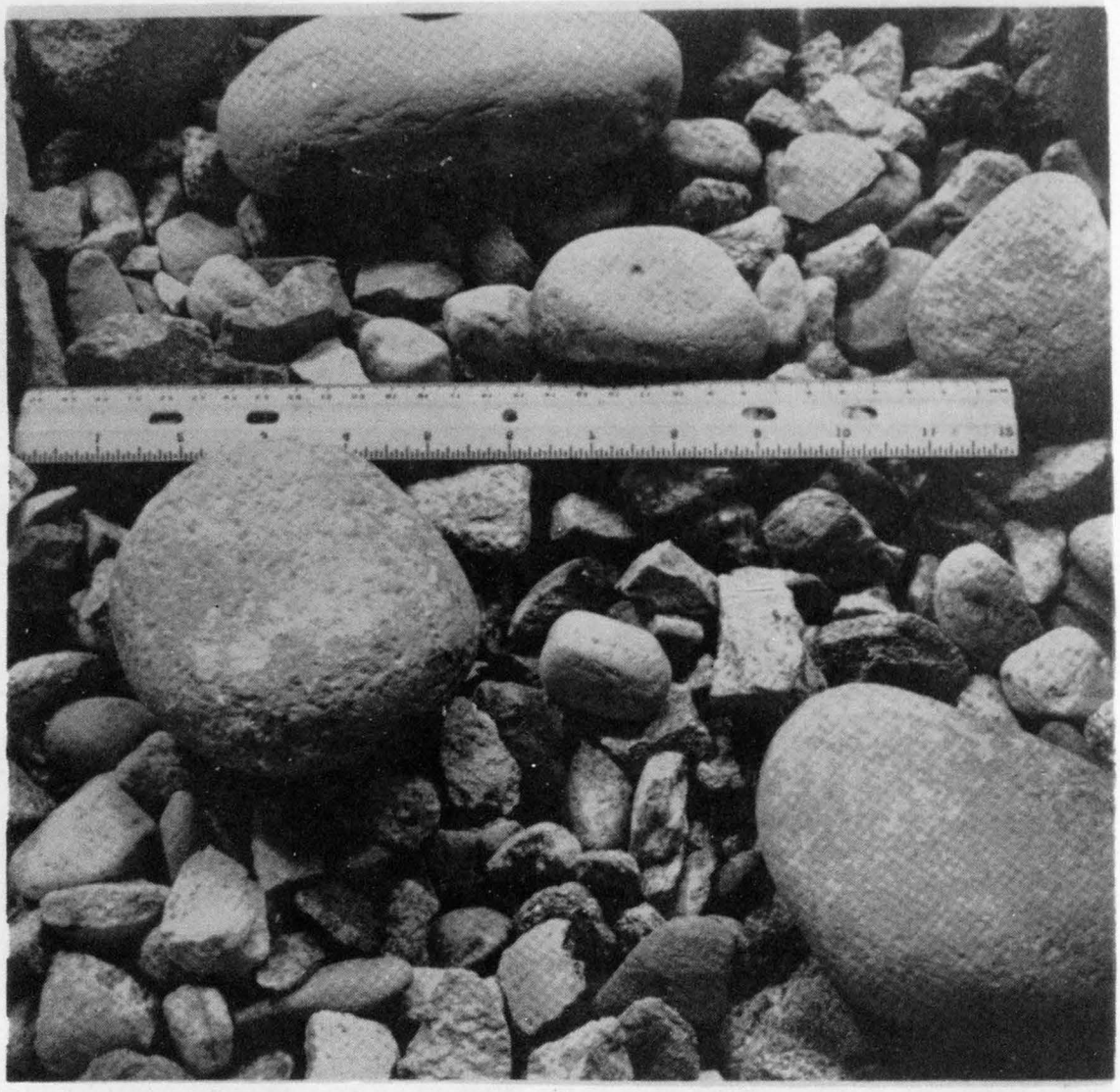

Figure 4. Close-up photograph of 6-inch cobble roughness.

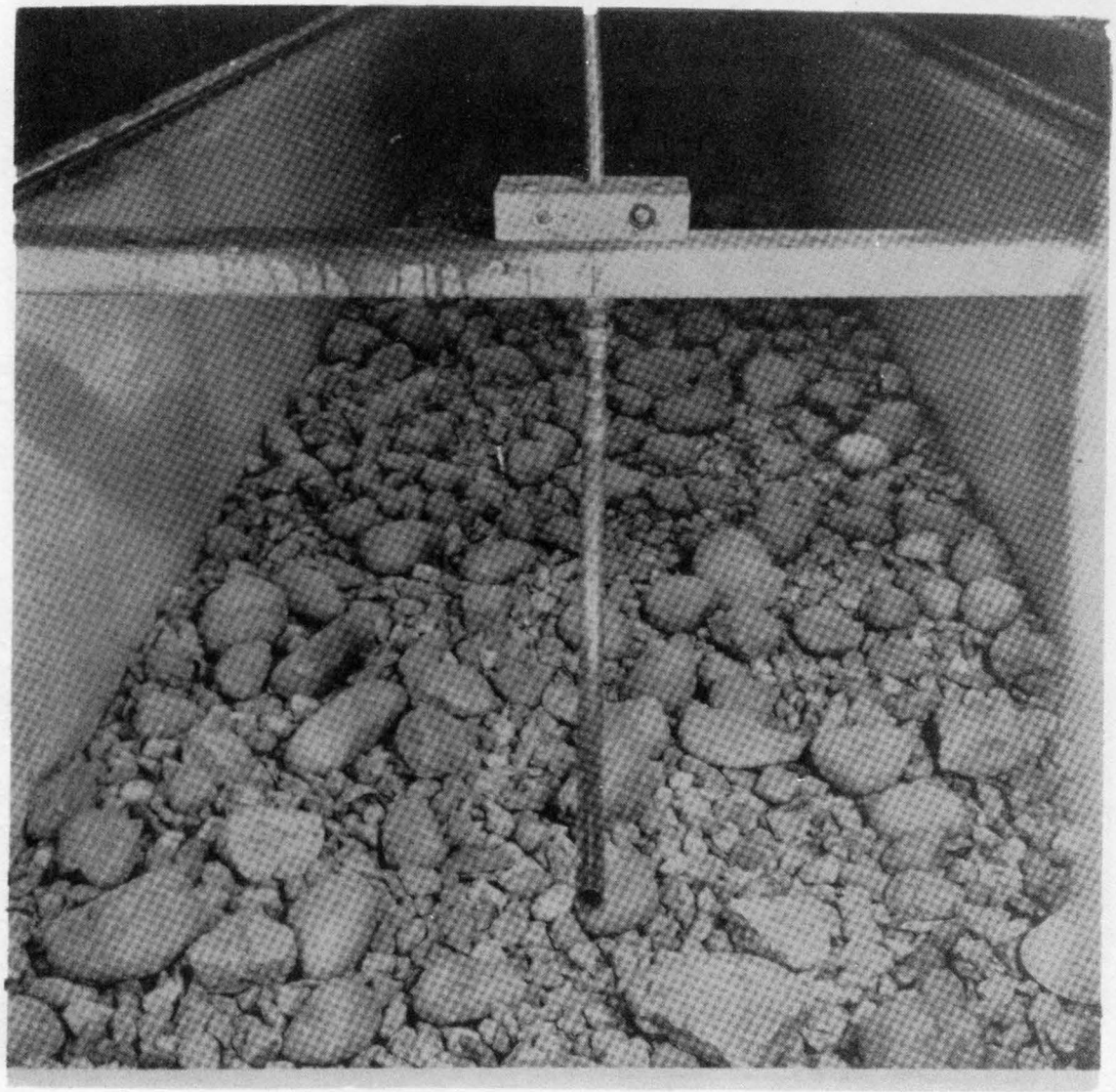

Figure 5. Photograph of 1.882 centimeter nozzle and support system over 6-inch cobble roughness.

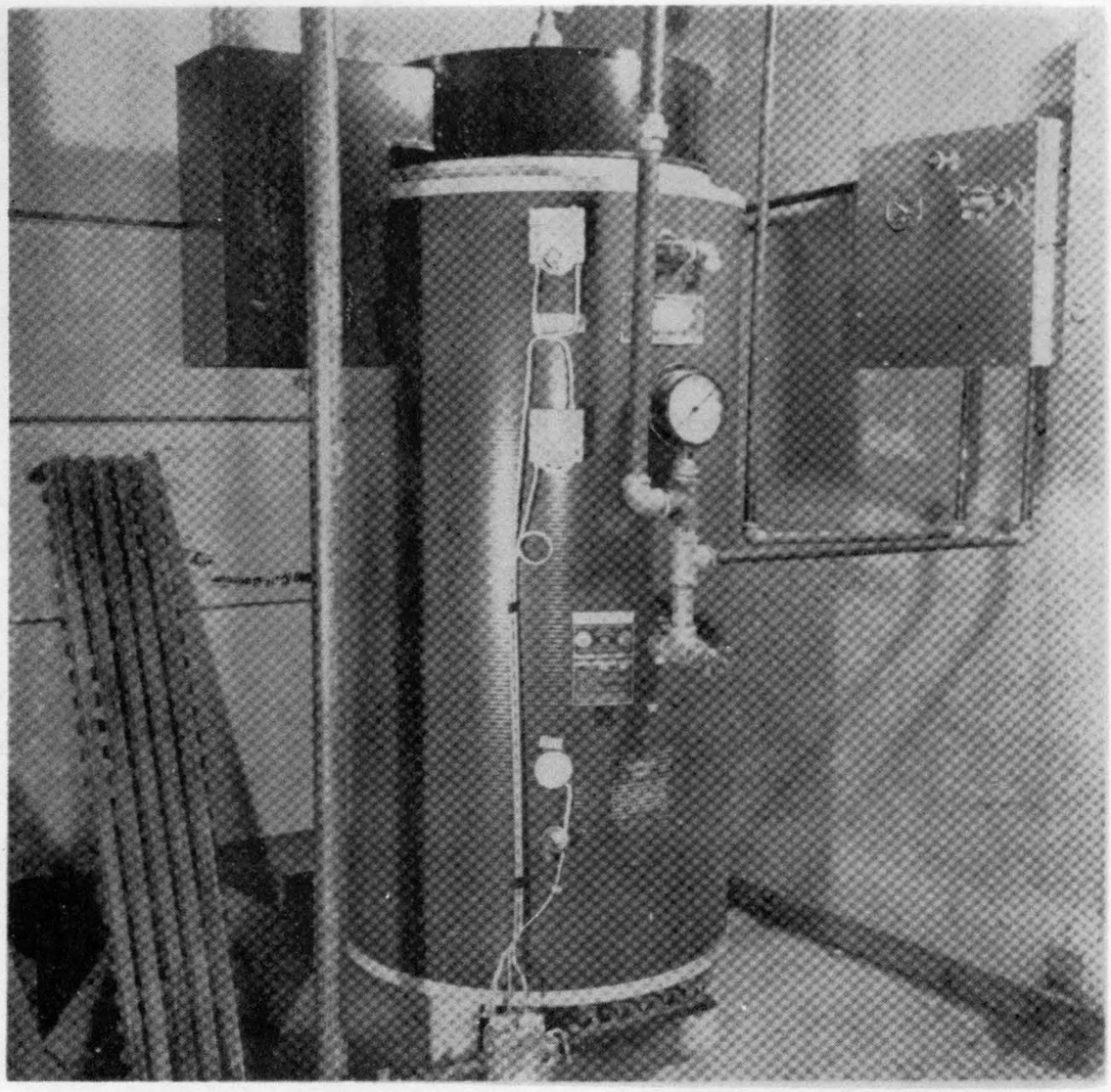

Figure 6. Hot water heater.

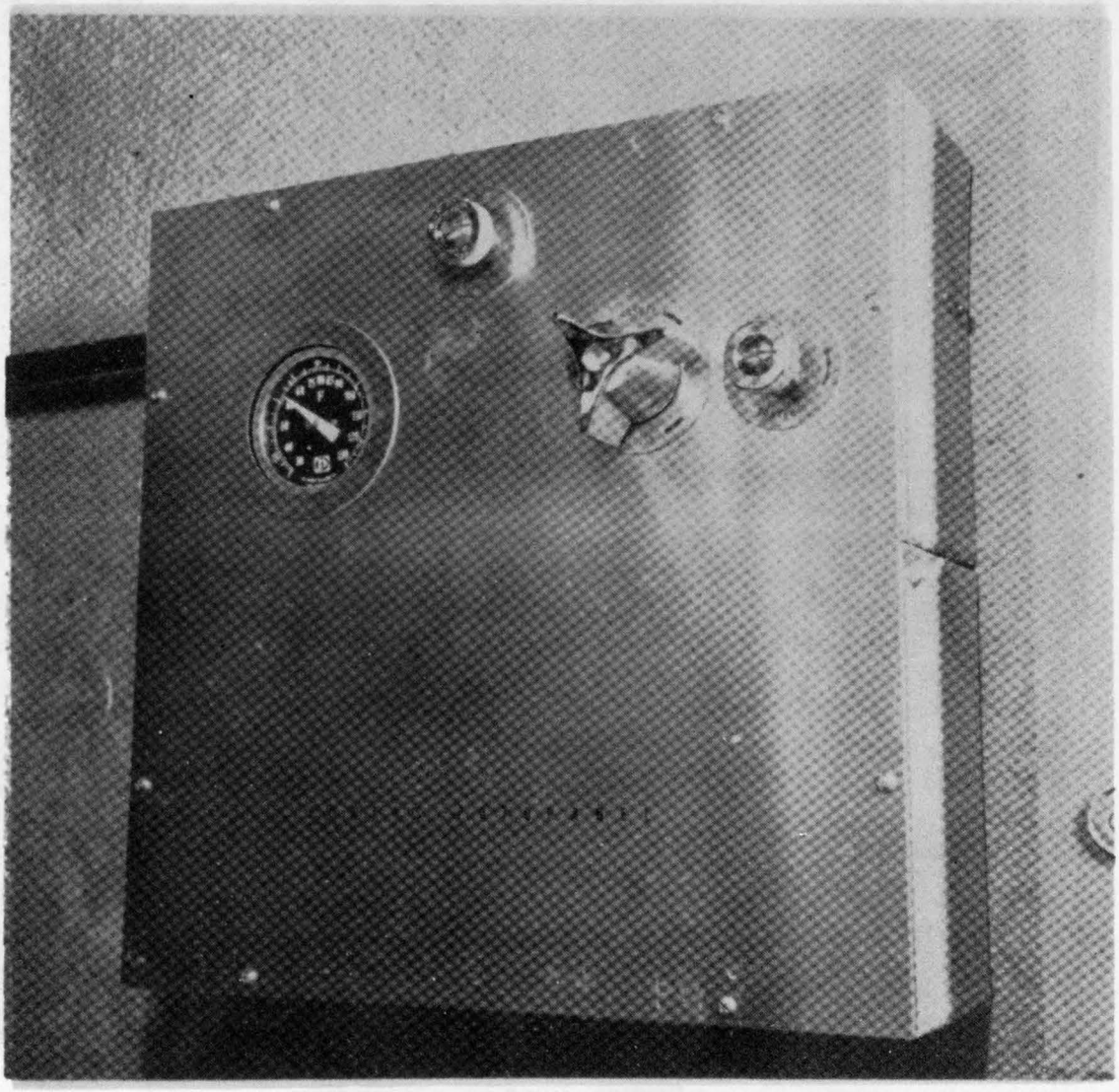

Figure 7. Thermostatic mixing valve.

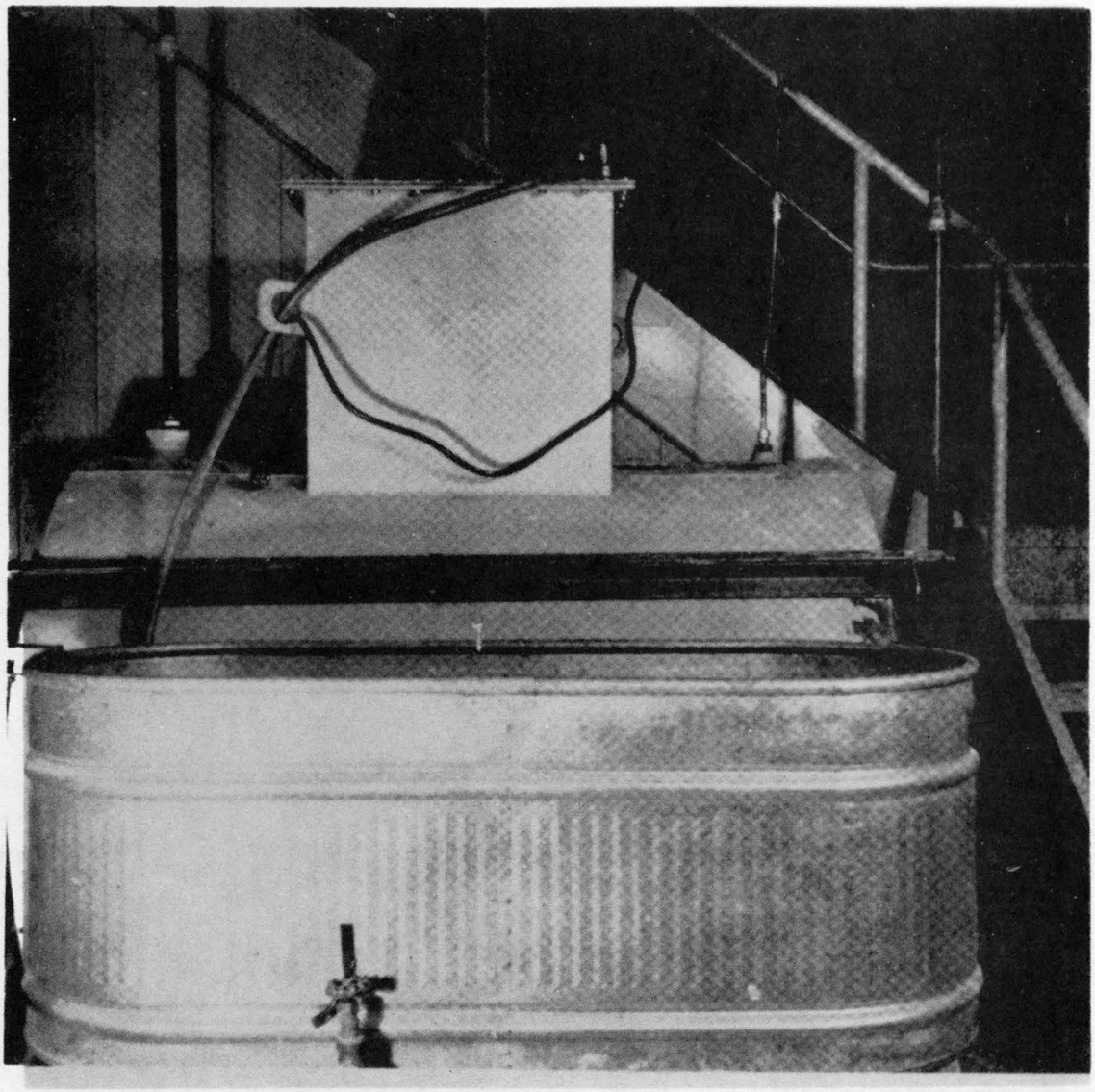

Figure 8. 500-gallon salt solution storage tank.

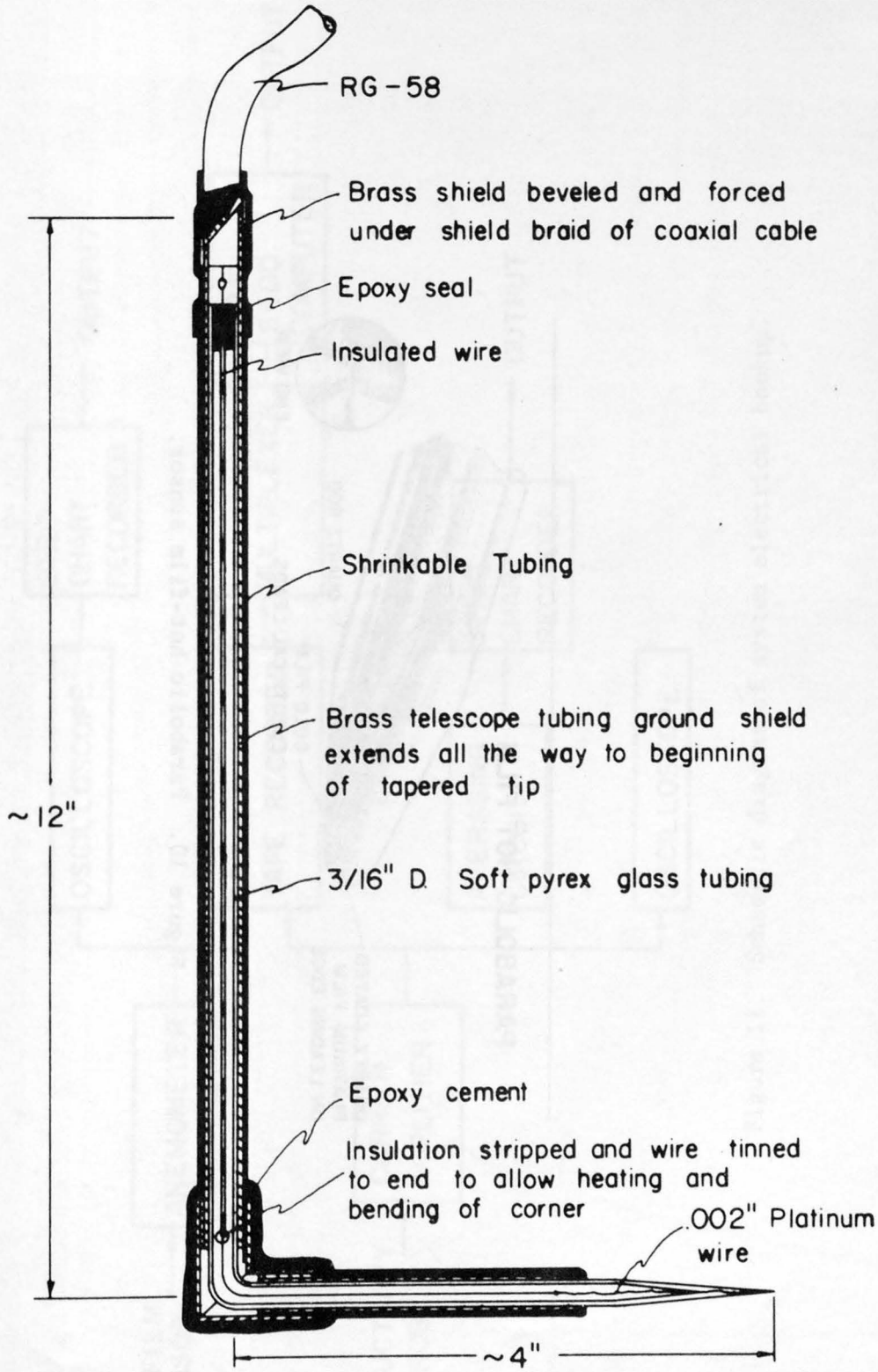

Figure 9. Assembly diagram of single-electrode conductivity probe.

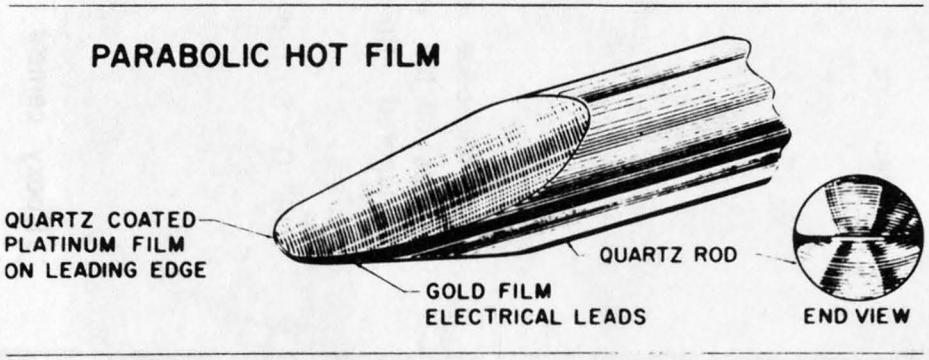

Figure 10. Parabolic hot-film sensor.

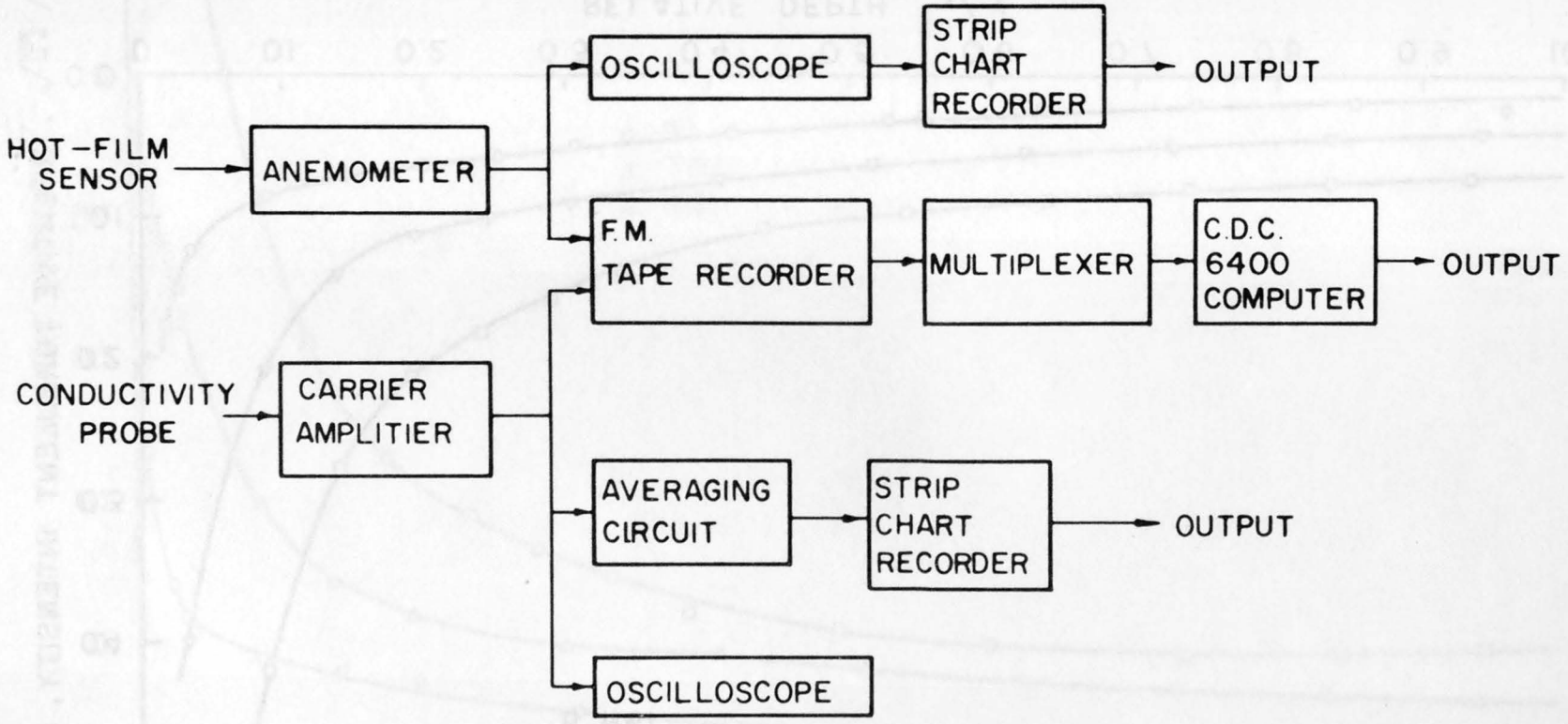

Figure 11. Schematic diagram of system electrical hookup.

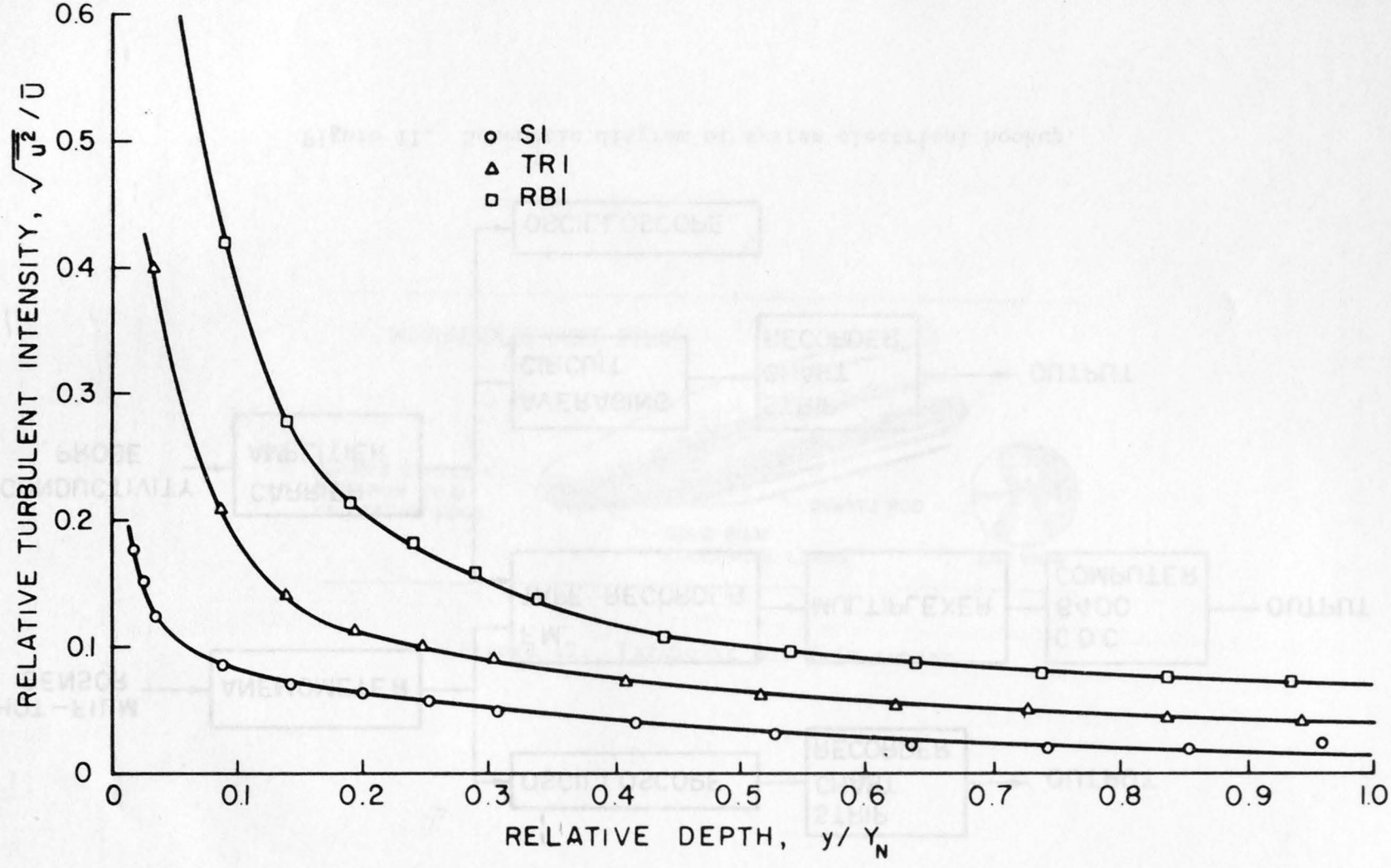

Figure 12. Relative turbulent intensity versus relative depth at channel centerline for runs S1, TR1, and RB1.

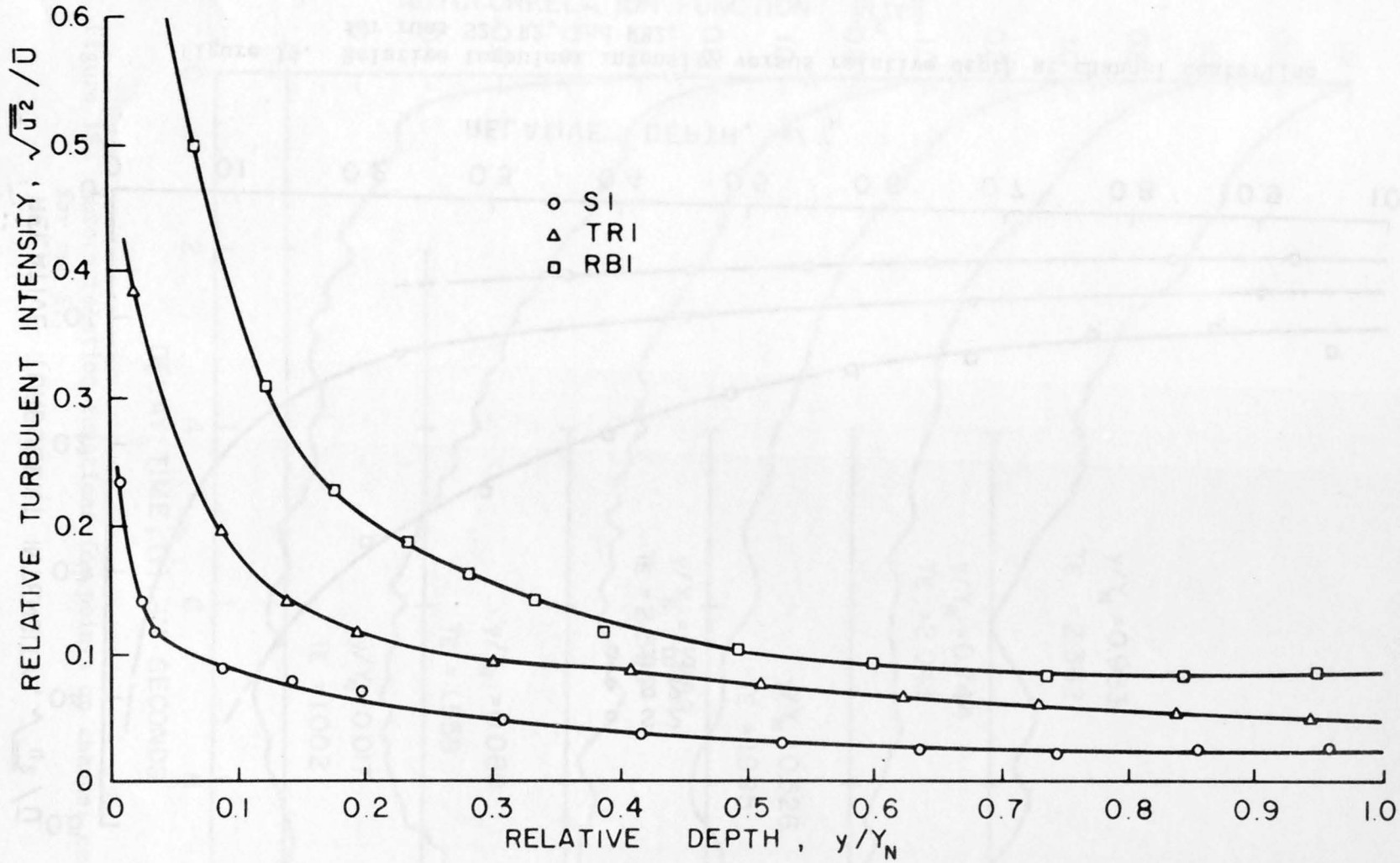

Figure 13. Relative turbulent intensity versus relative depth halfway between channel centerline and flume wall for runs S1, TR1, and RB1.

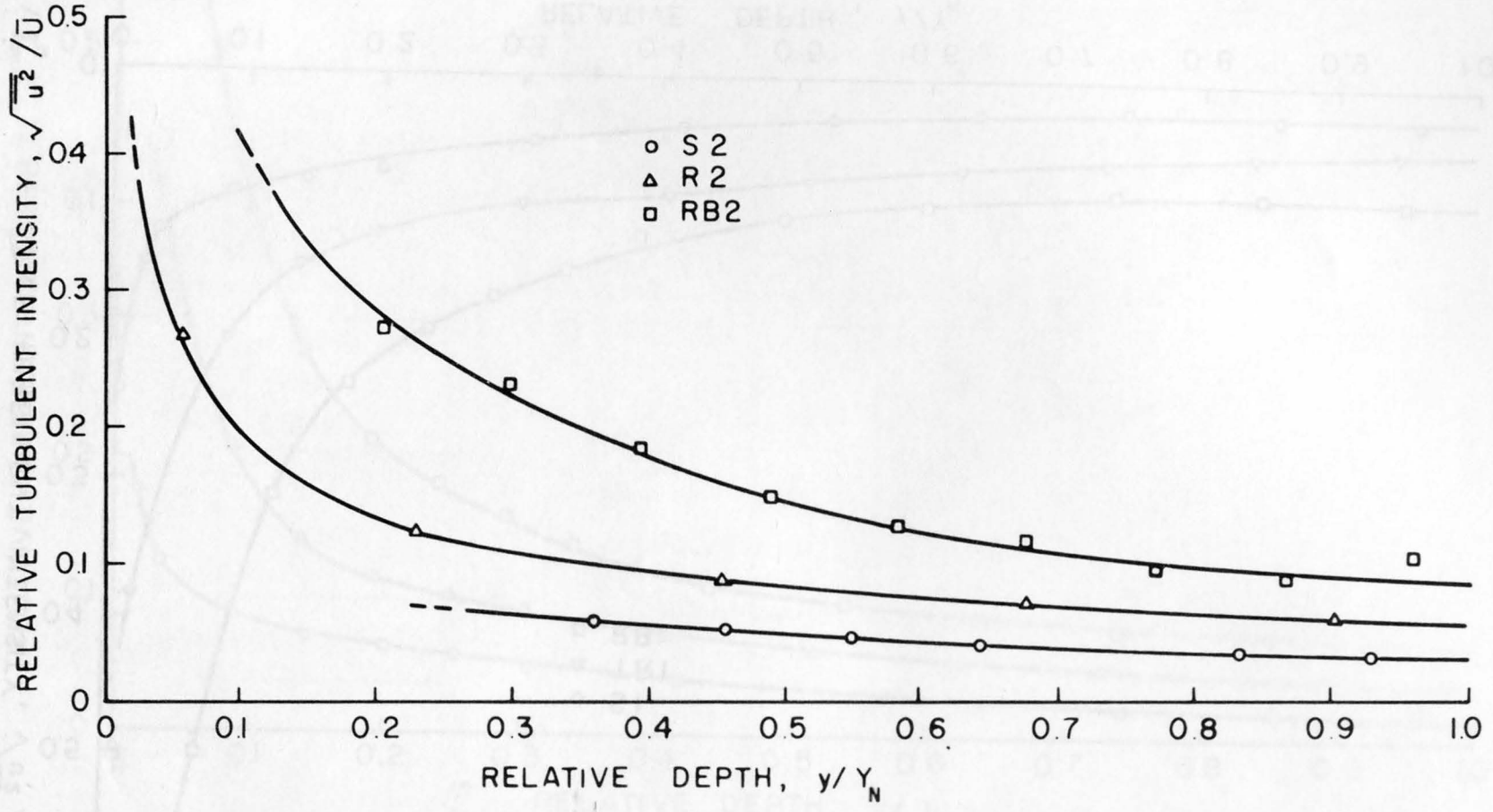

Figure 14. Relative turbulent intensity versus relative depth at channel centerline for runs S2, R2, and RB2.

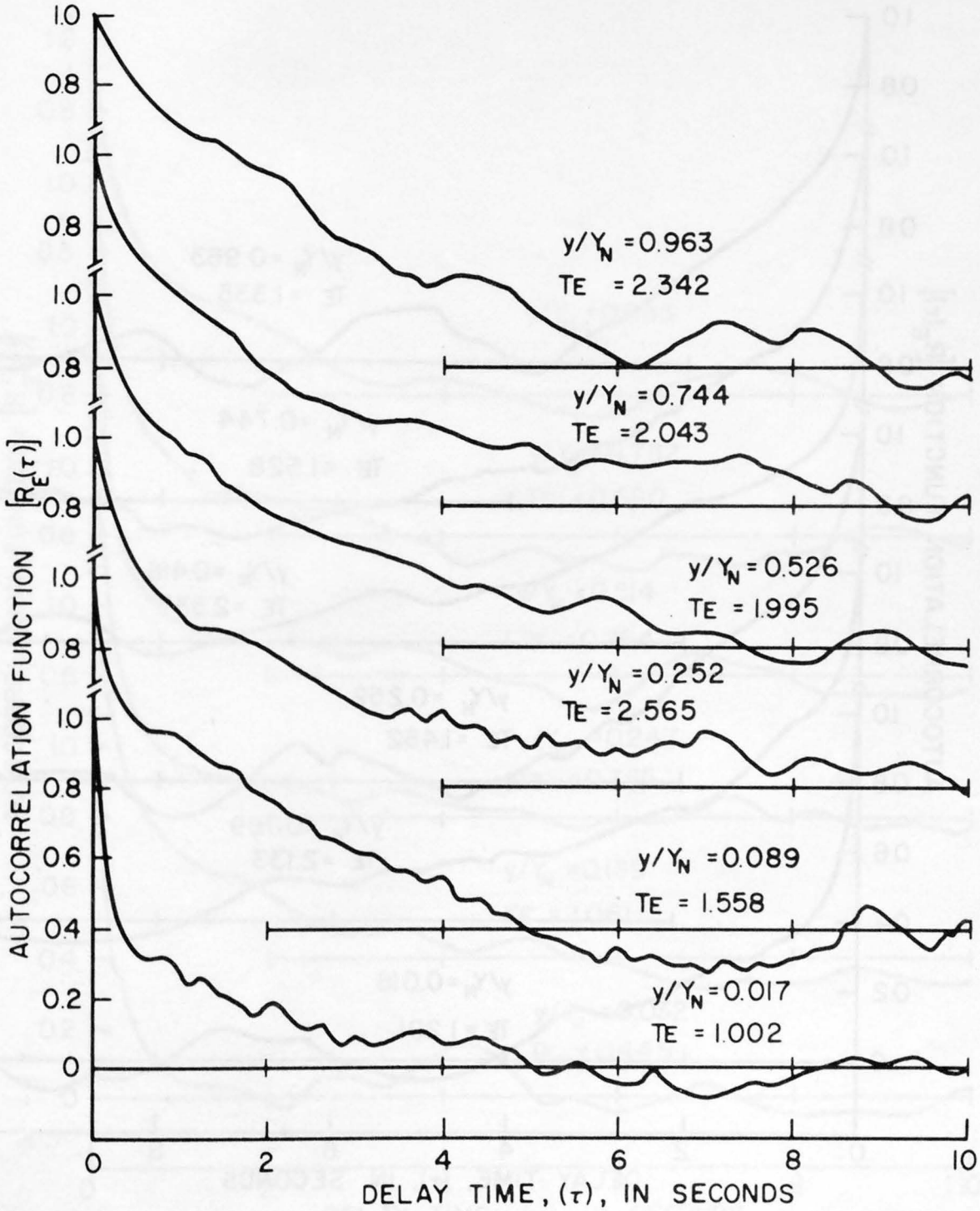

Figure 15. Autocorrelation functions for points on channel centerline for run S1.

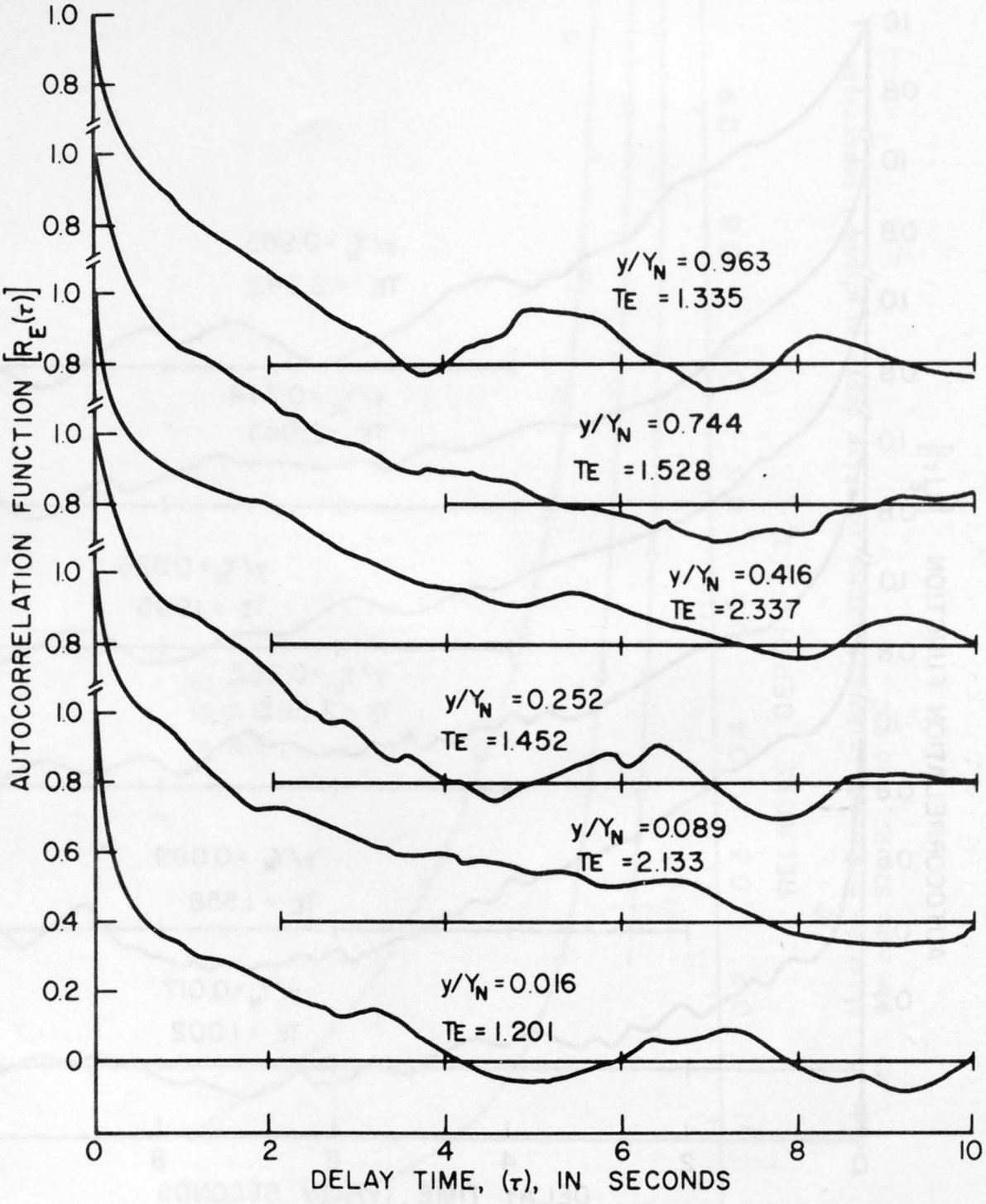

Figure 16. Autocorrelation functions for points halfway between channel centerline and flume wall for run S1.

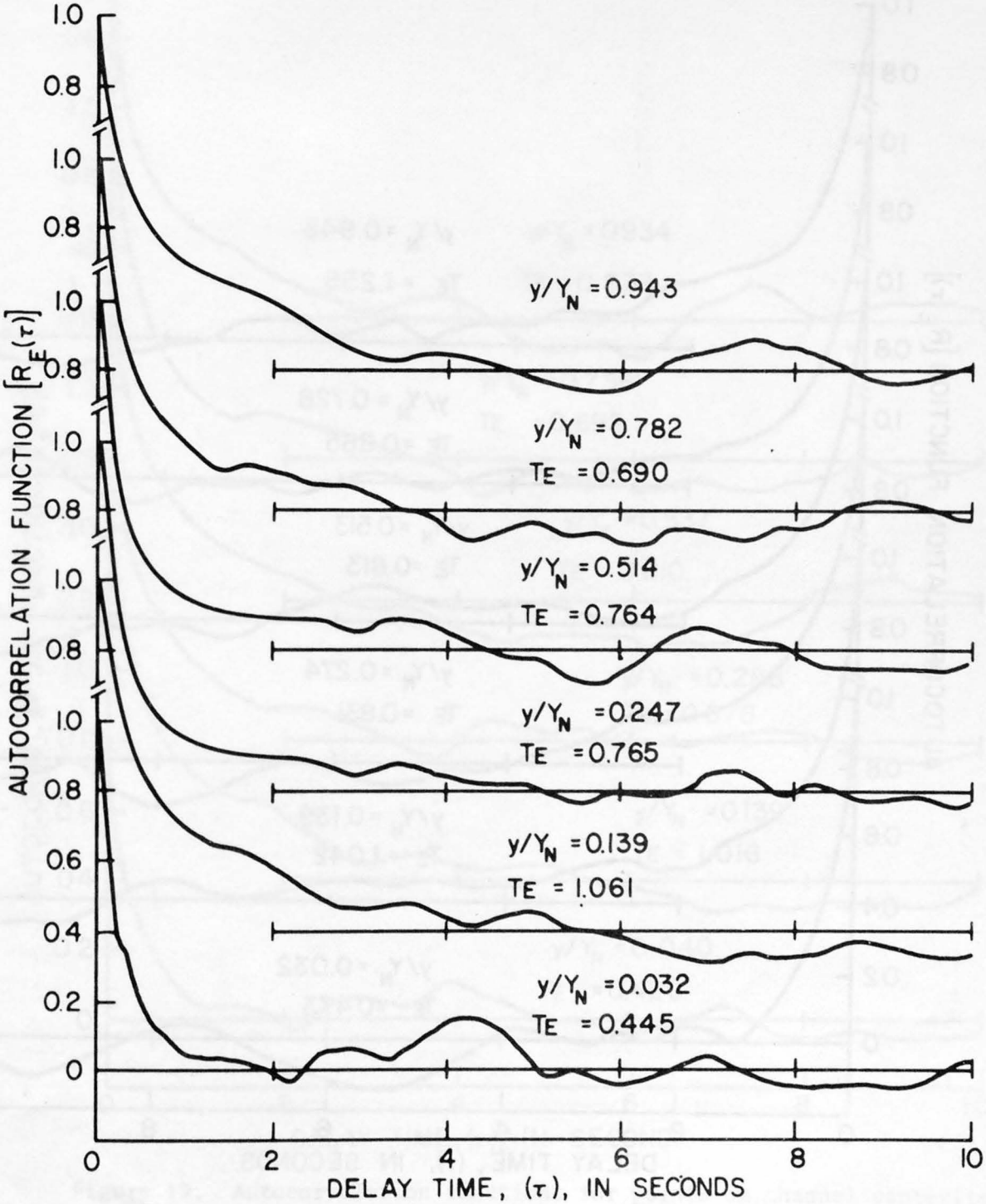

Figure 17. Autocorrelation functions for points on channel centerline for run TR1.

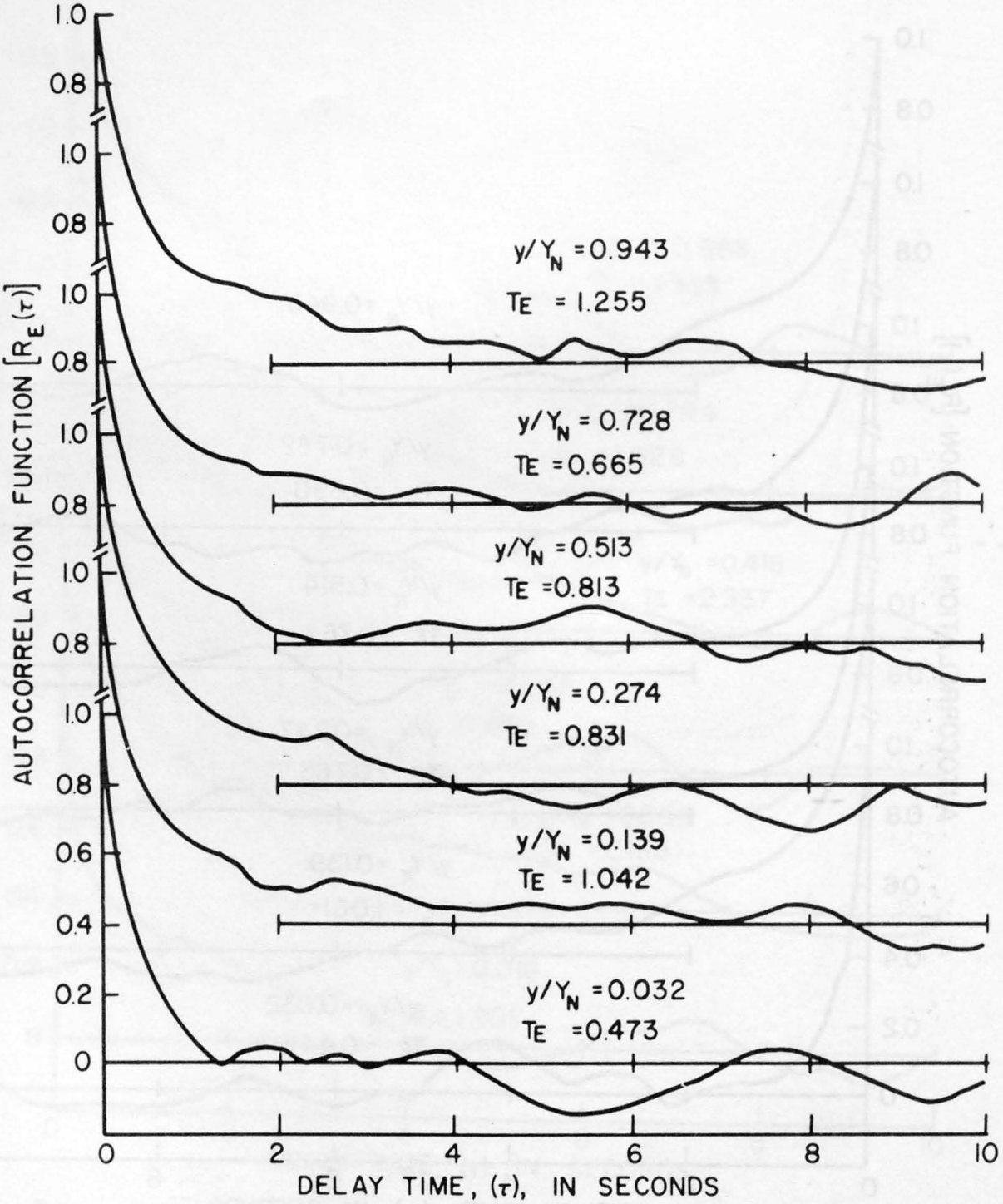

Figure 18. Autocorrelation functions for points halfway between channel centerline and flume wall for run TR1.

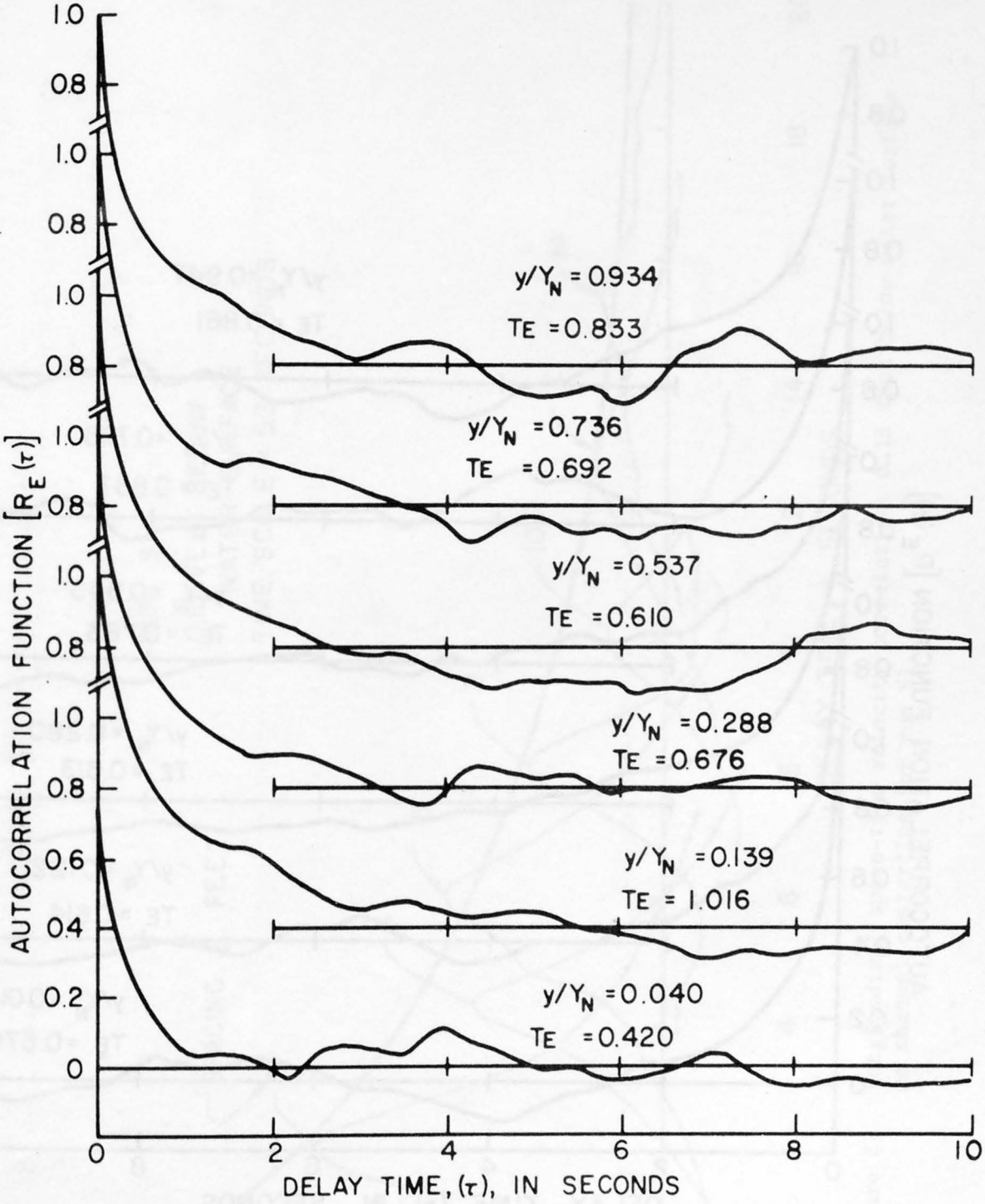

Figure 19. Autocorrelation functions for points on channel centerline for run RB1.

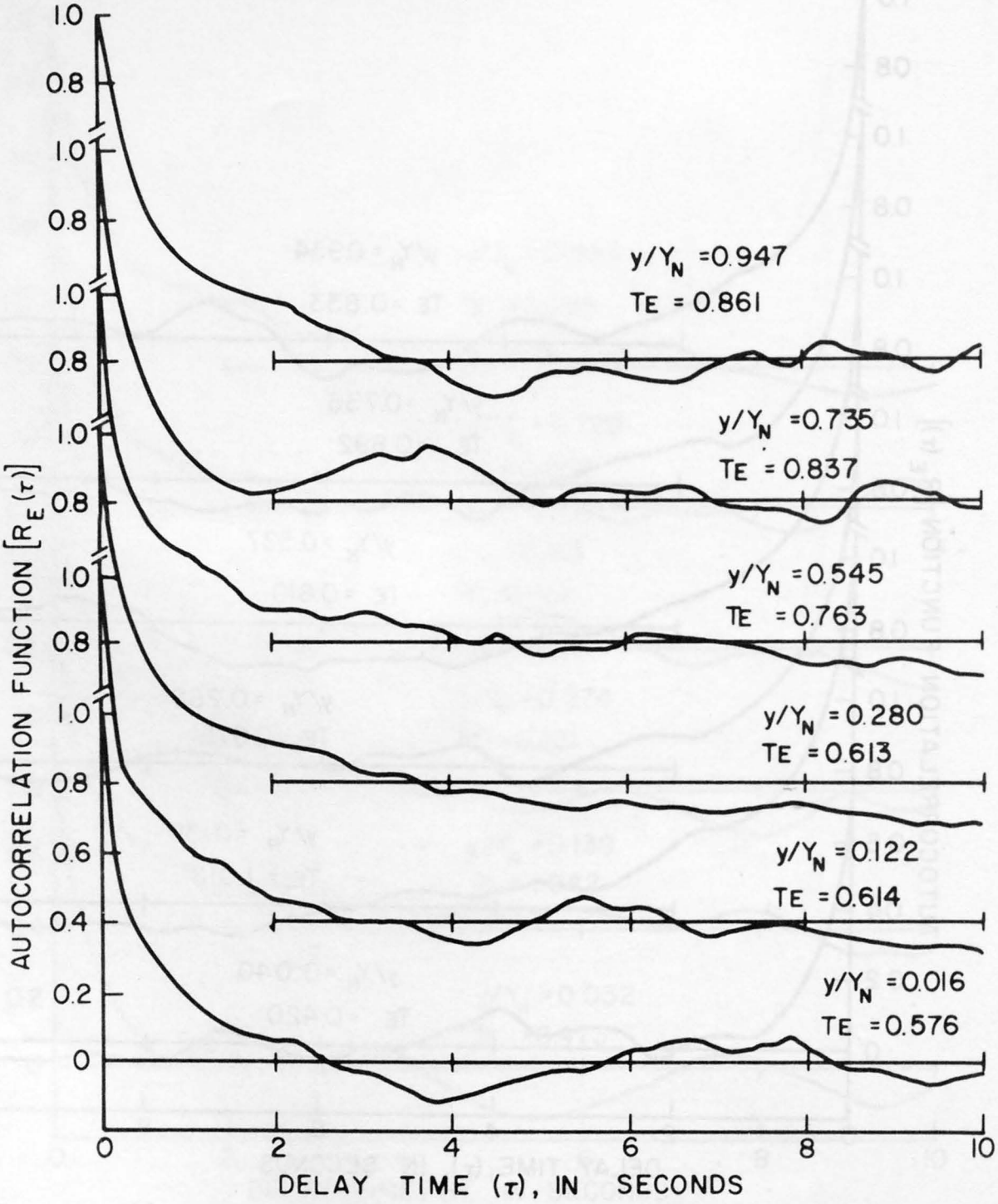

Figure 20. Autocorrelation functions for points halfway between channel centerline and flume wall for run RB1.

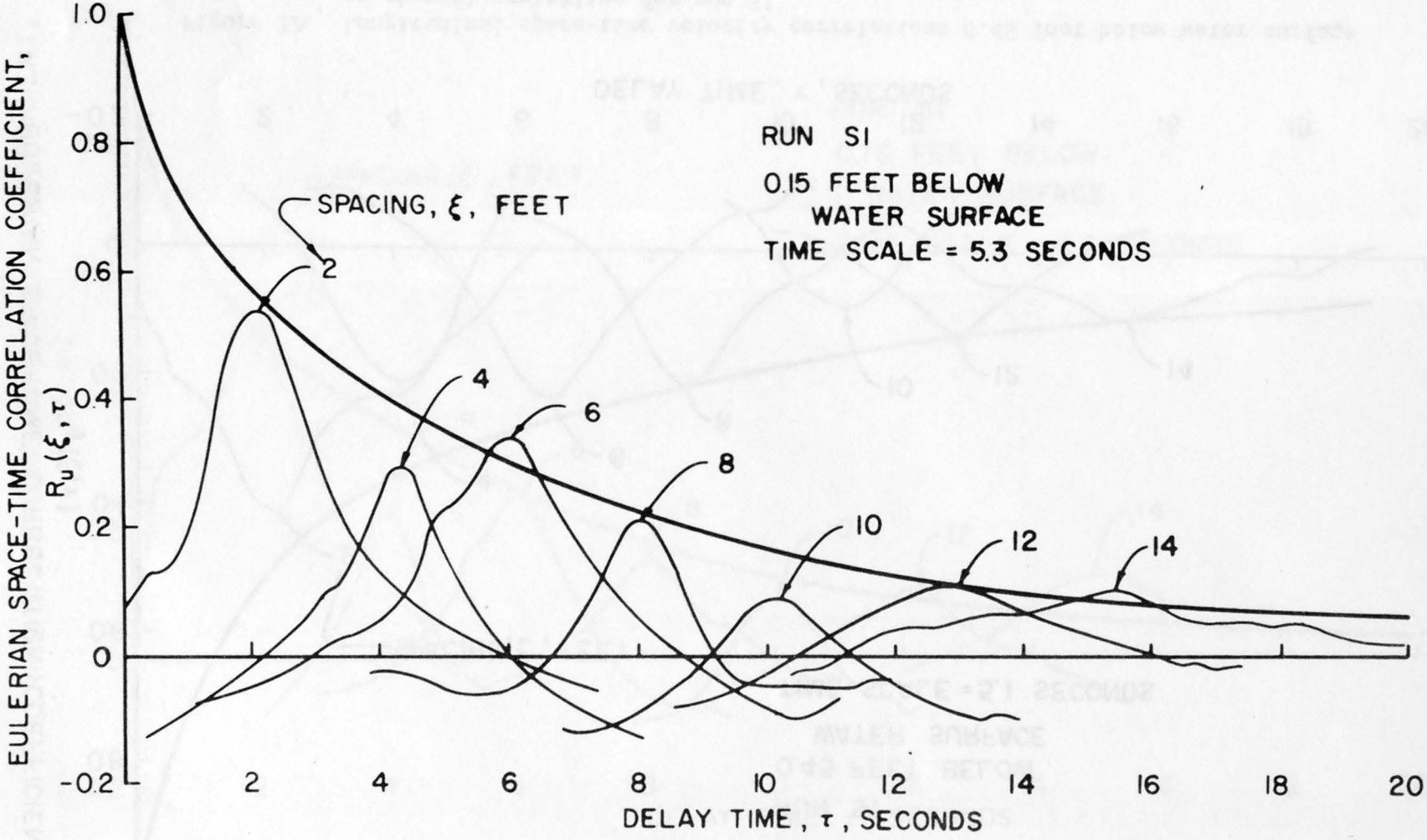

Figure 21. Longitudinal space-time velocity correlations 0.15 foot below water surface on channel centerline for run S1.

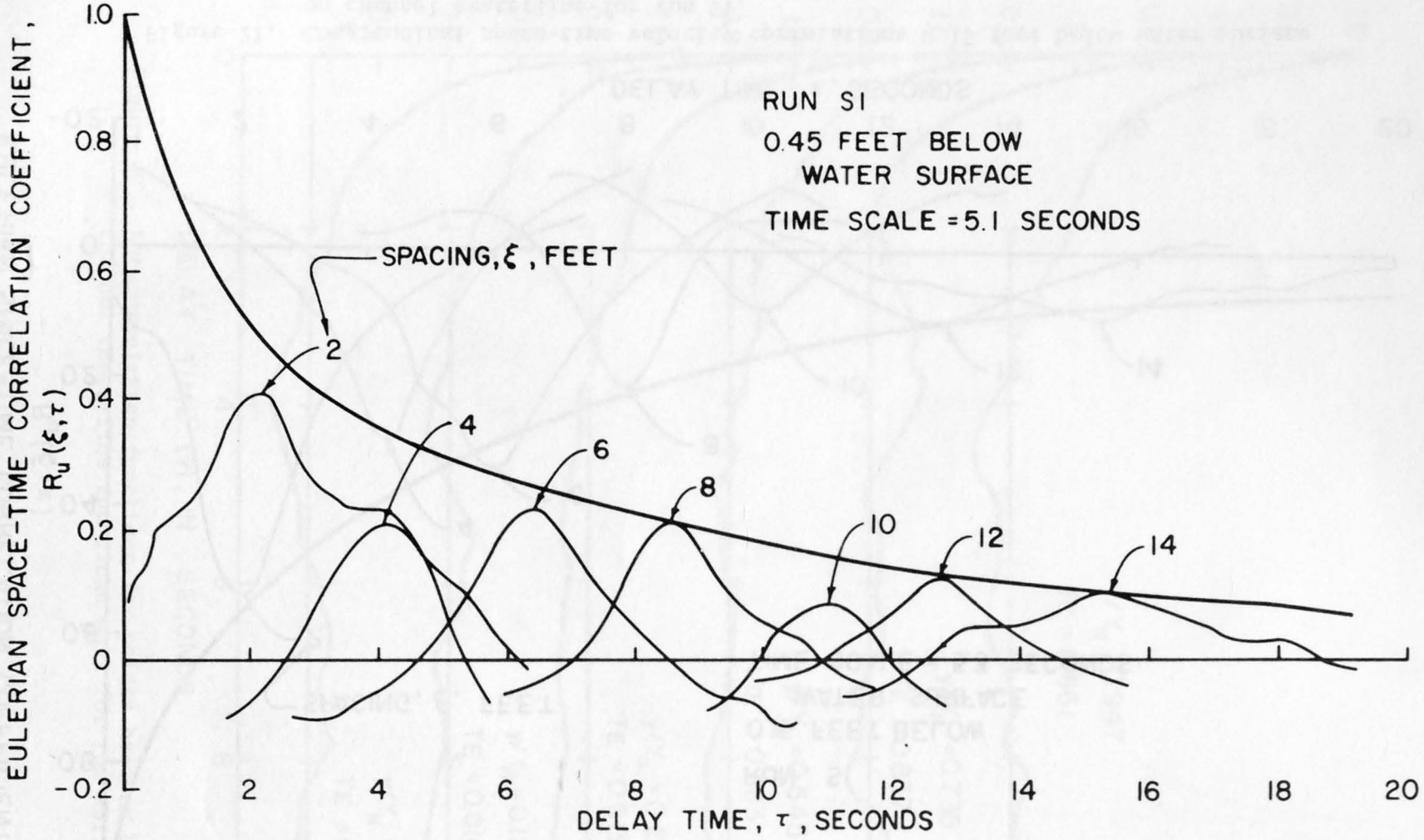

Figure 22. Longitudinal space-time velocity correlations 0.45 foot below water surface on channel centerline for run S1.

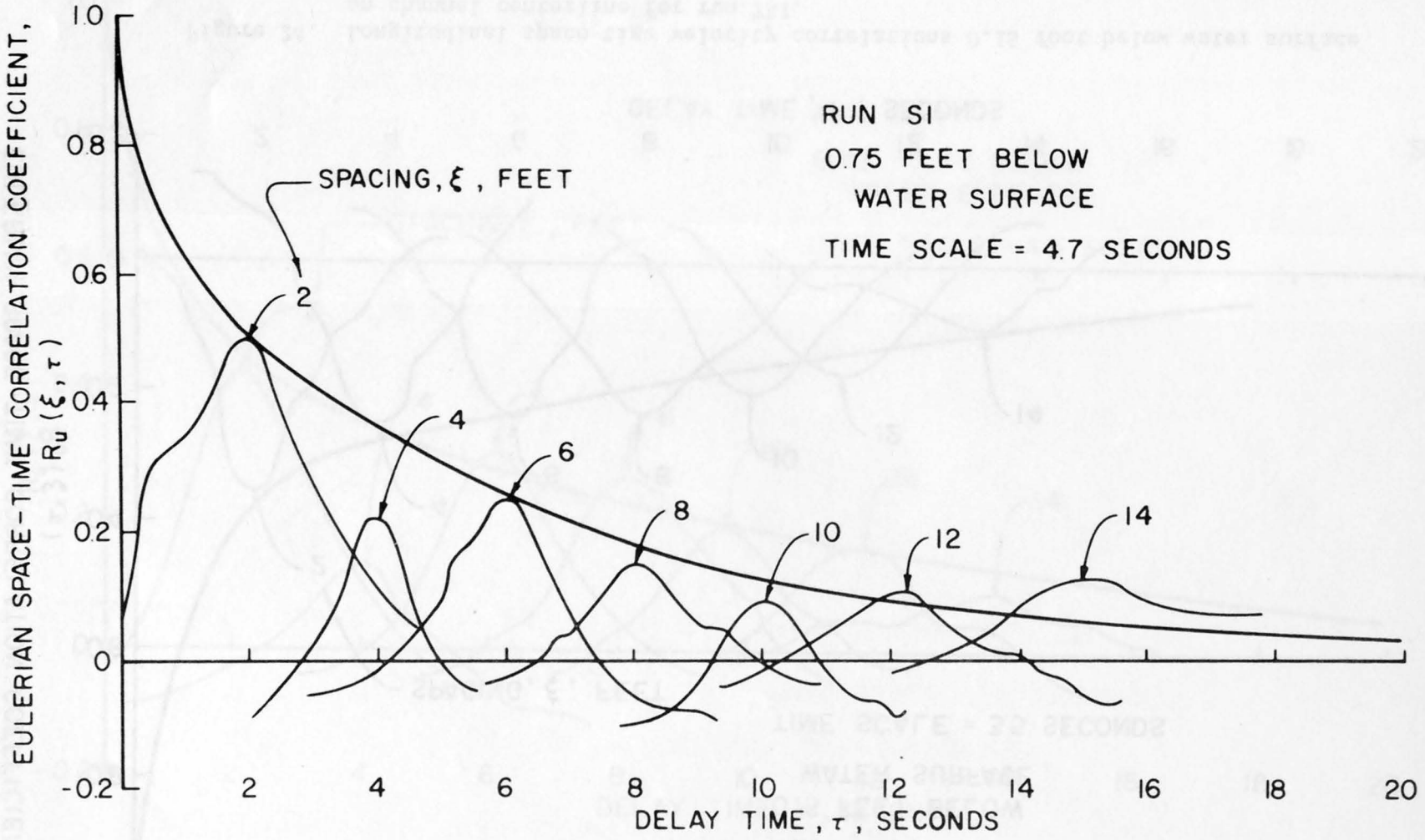

Figure 23. Longitudinal space-time velocity correlations 0.75 foot below water surface on channel centerline for run S1.

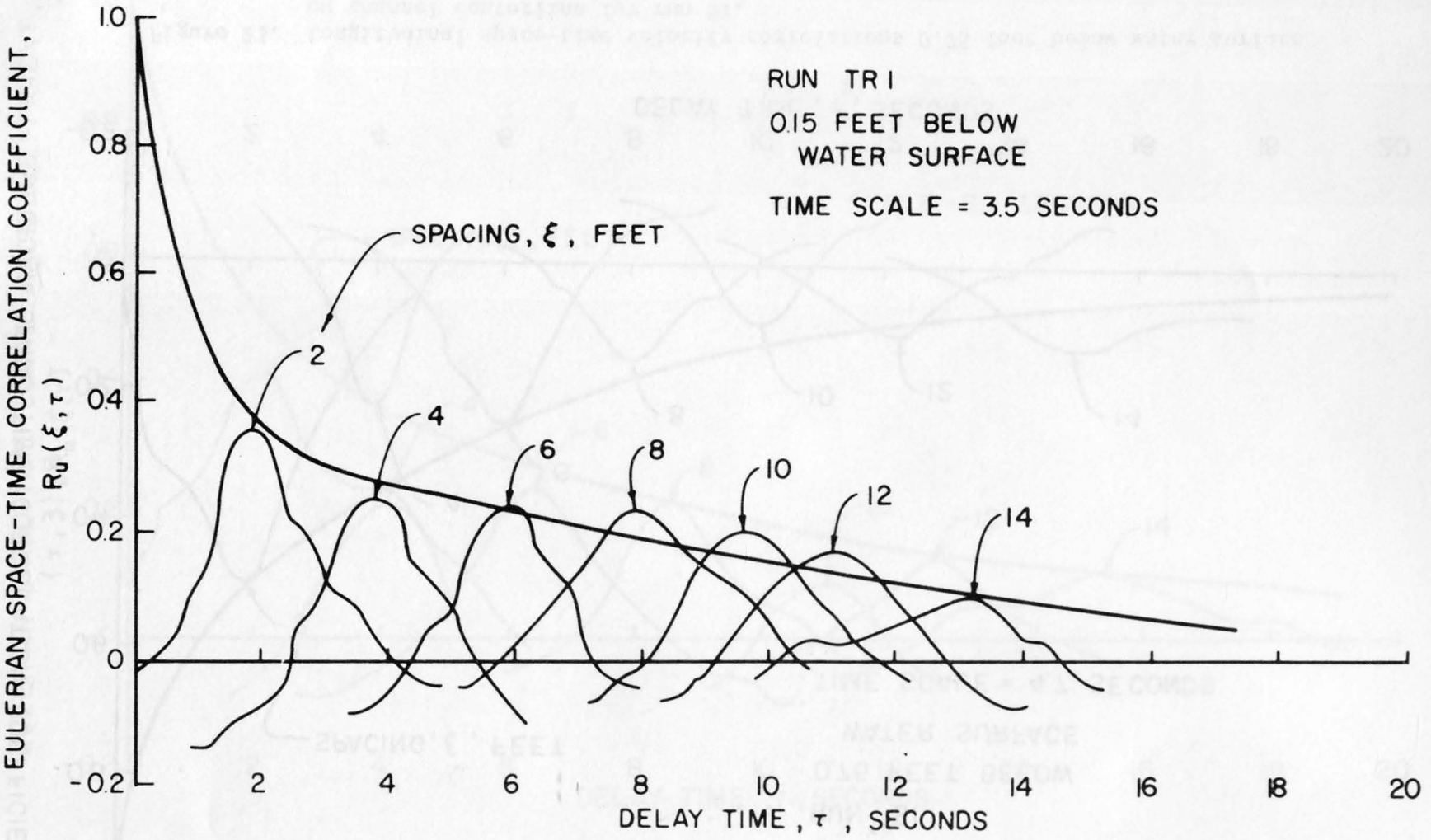

Figure 24. Longitudinal space-time velocity correlations 0.15 foot below water surface on channel centerline for run TR1.

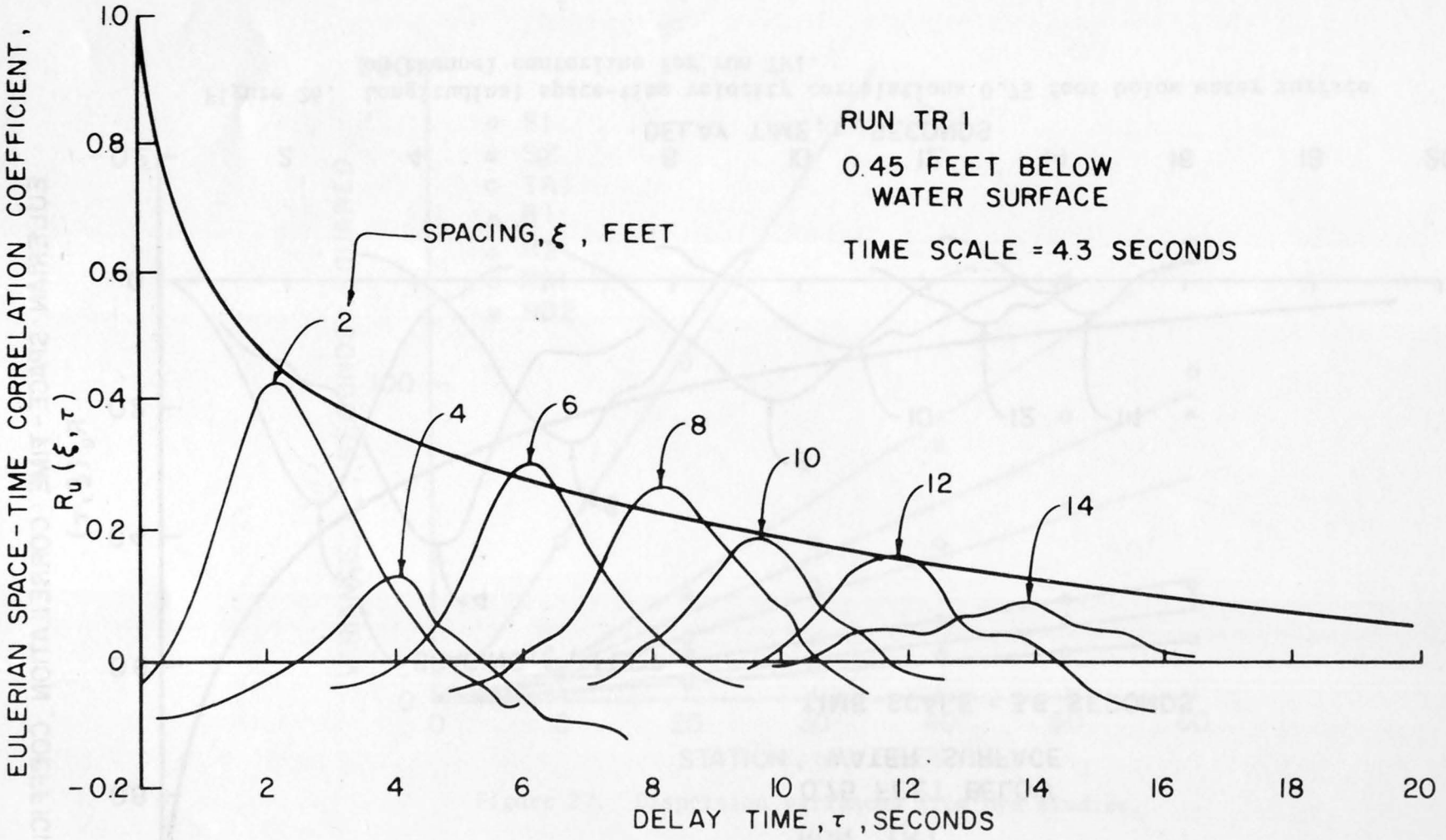

Figure 25. Longitudinal space-time velocity correlations 0.45 foot below water surface on channel centerline for run TR1.

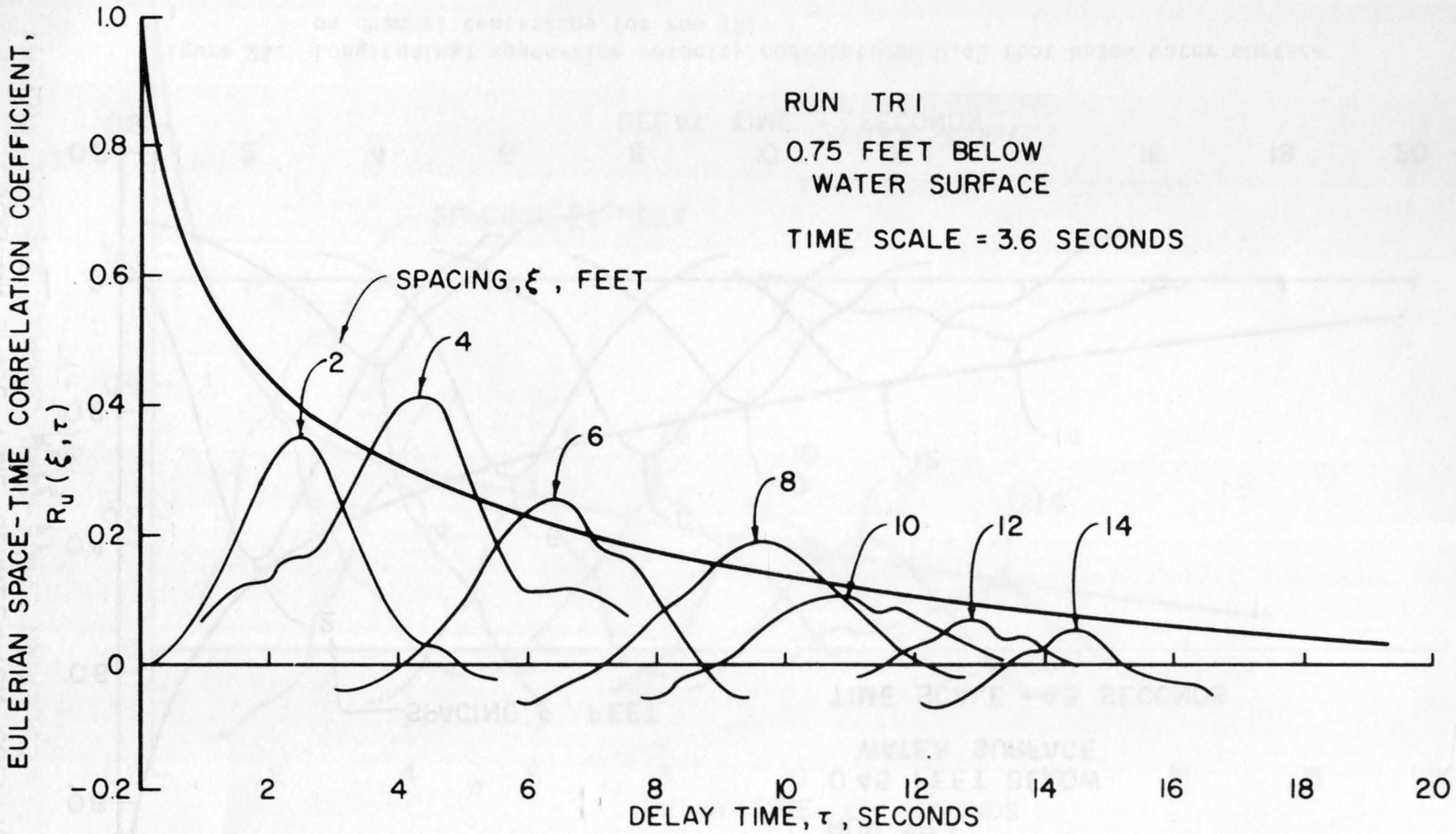

Figure 26. Longitudinal space-time velocity correlations 0.75 foot below water surface on channel centerline for run TR1.

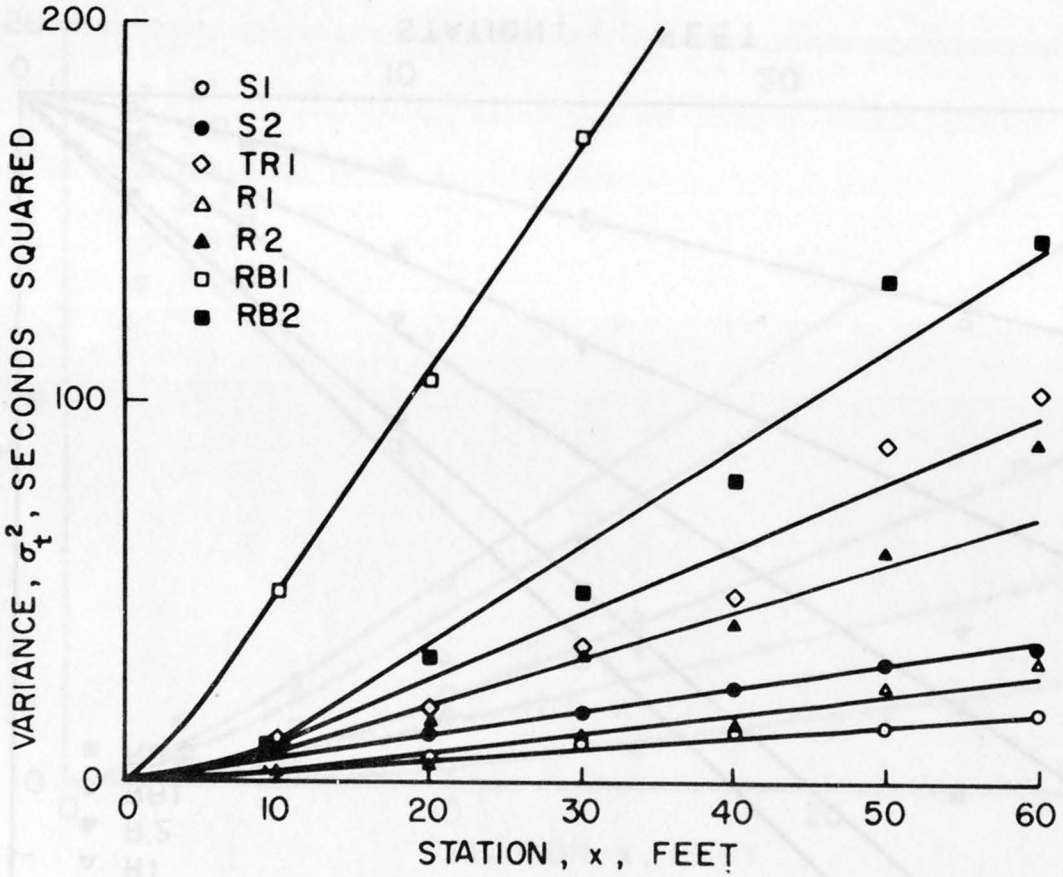

Figure 27. Dispersion variances from dye studies.

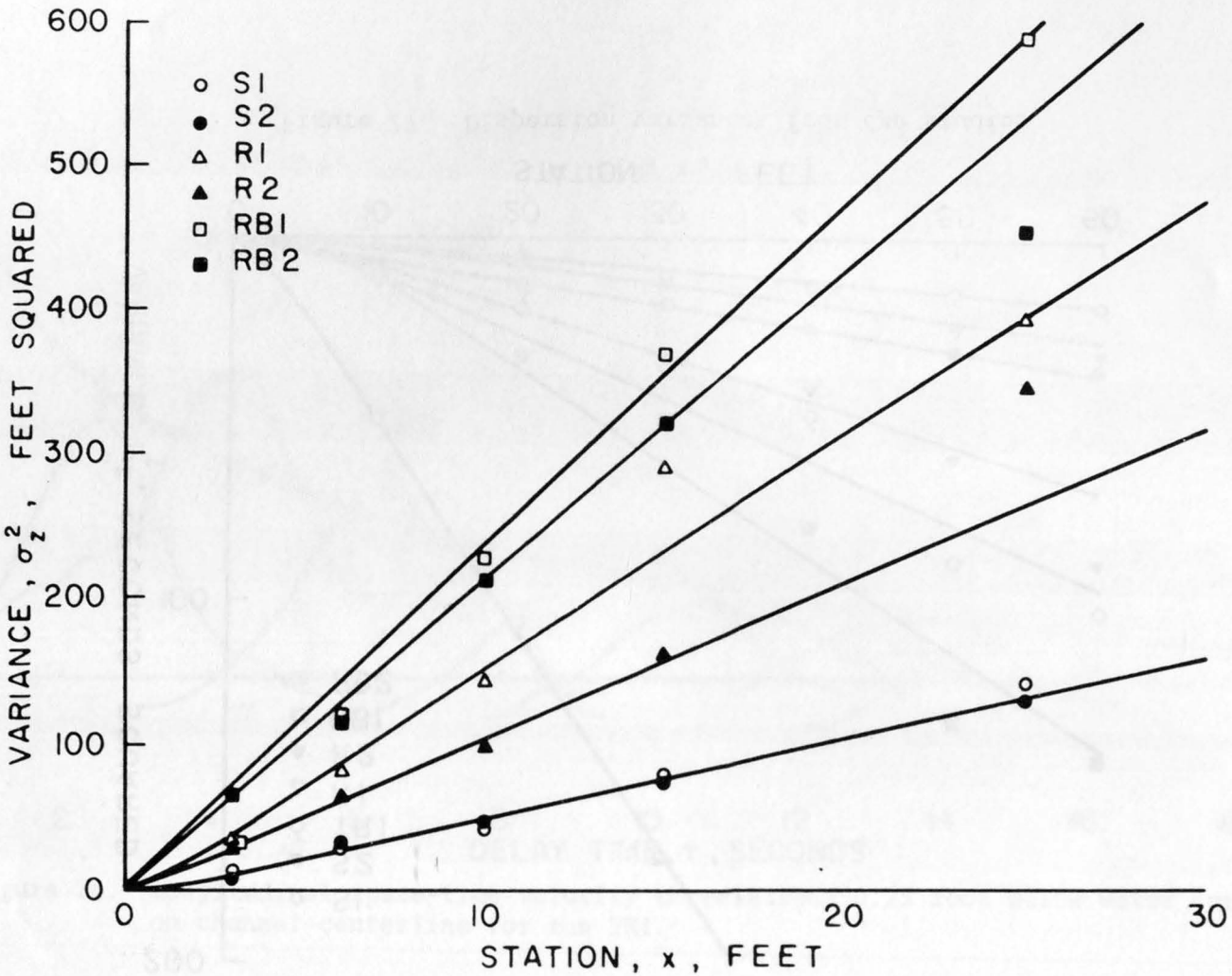

Figure 28. Lateral surface diffusion variances from particle studies.

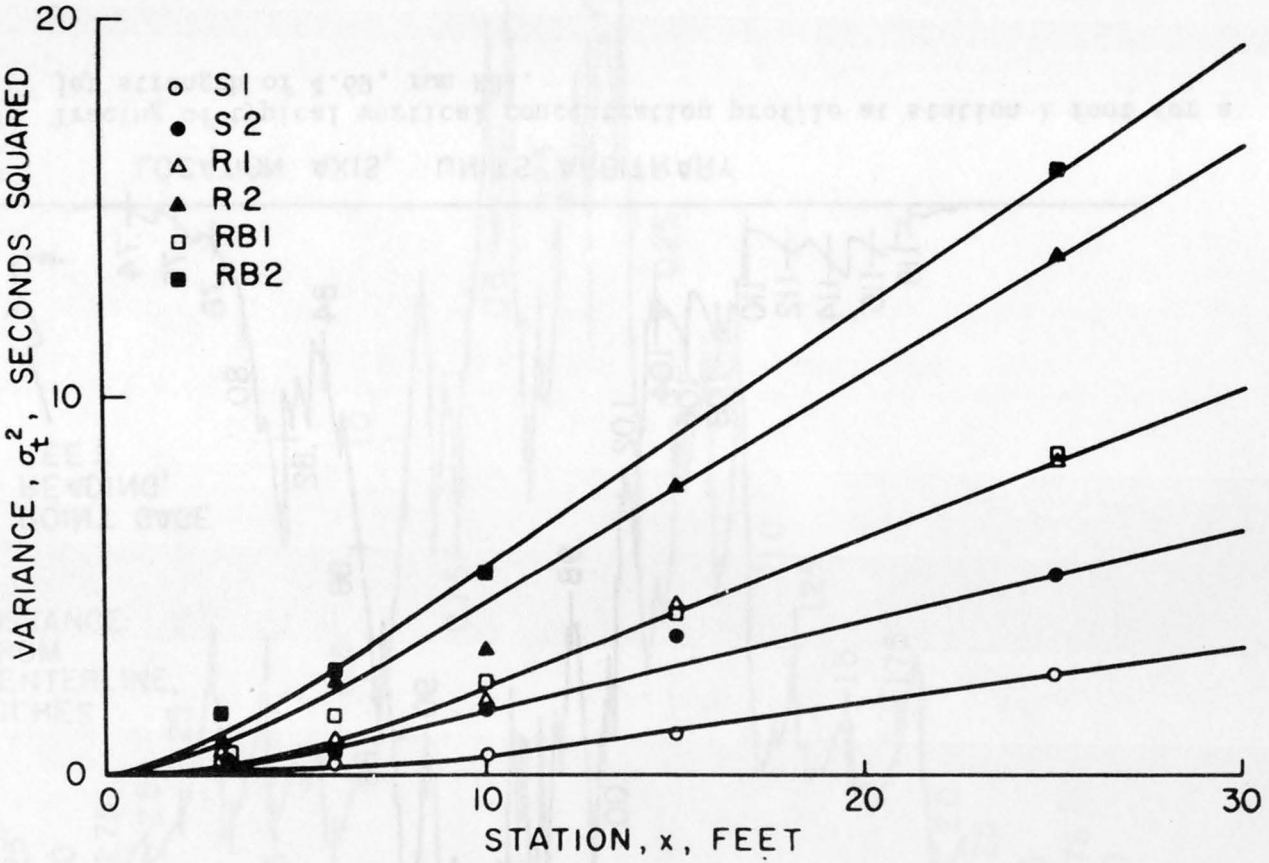

Figure 29. Longitudinal surface diffusion variances from particle studies.

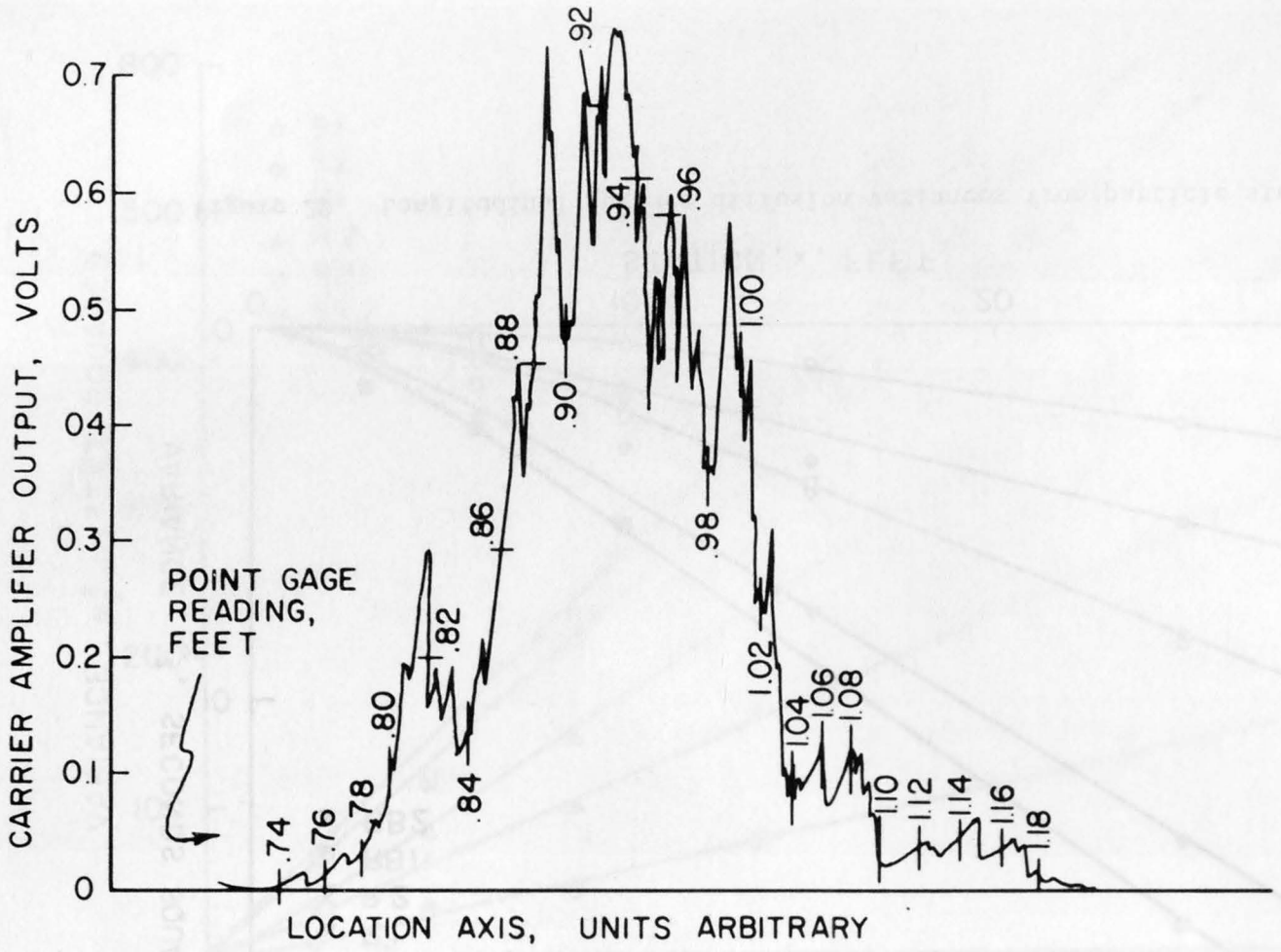

Figure 30. Tracing of typical vertical concentration profile at station 1 foot for a jet strength of 4.69, run RB1.

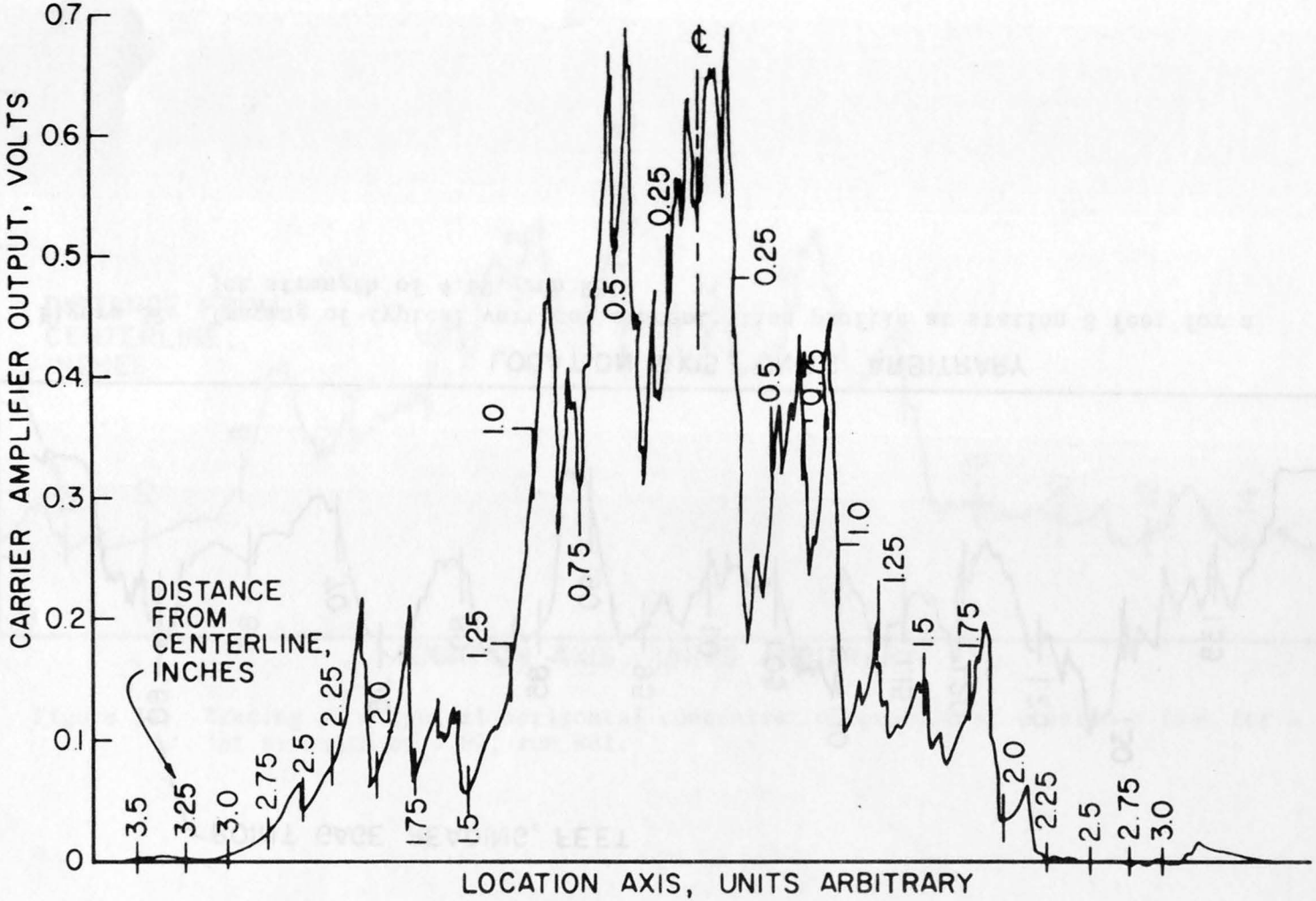

Figure 31. Tracing of typical horizontal concentration profile at station 1 foot for a jet strength of 4.69, run RB1.

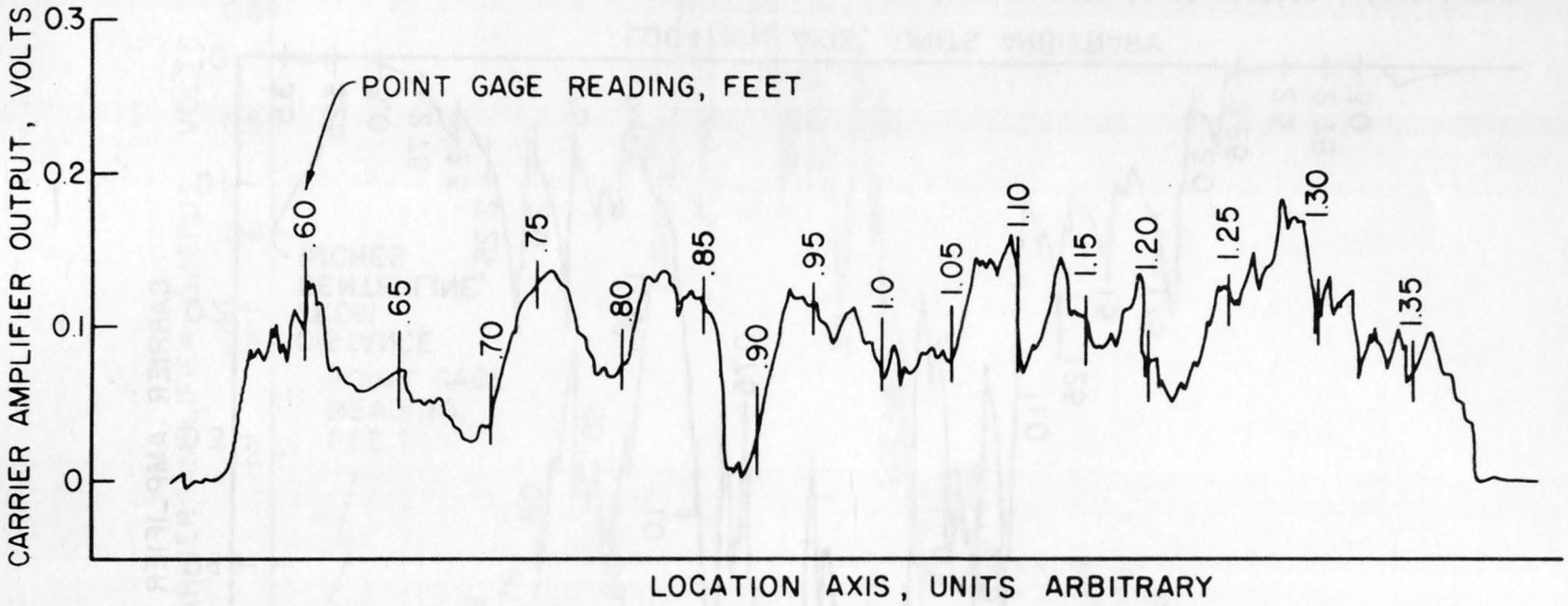

Figure 32. Tracing of typical vertical concentration profile at station 8 feet for a jet strength of 4.69, run RB1.

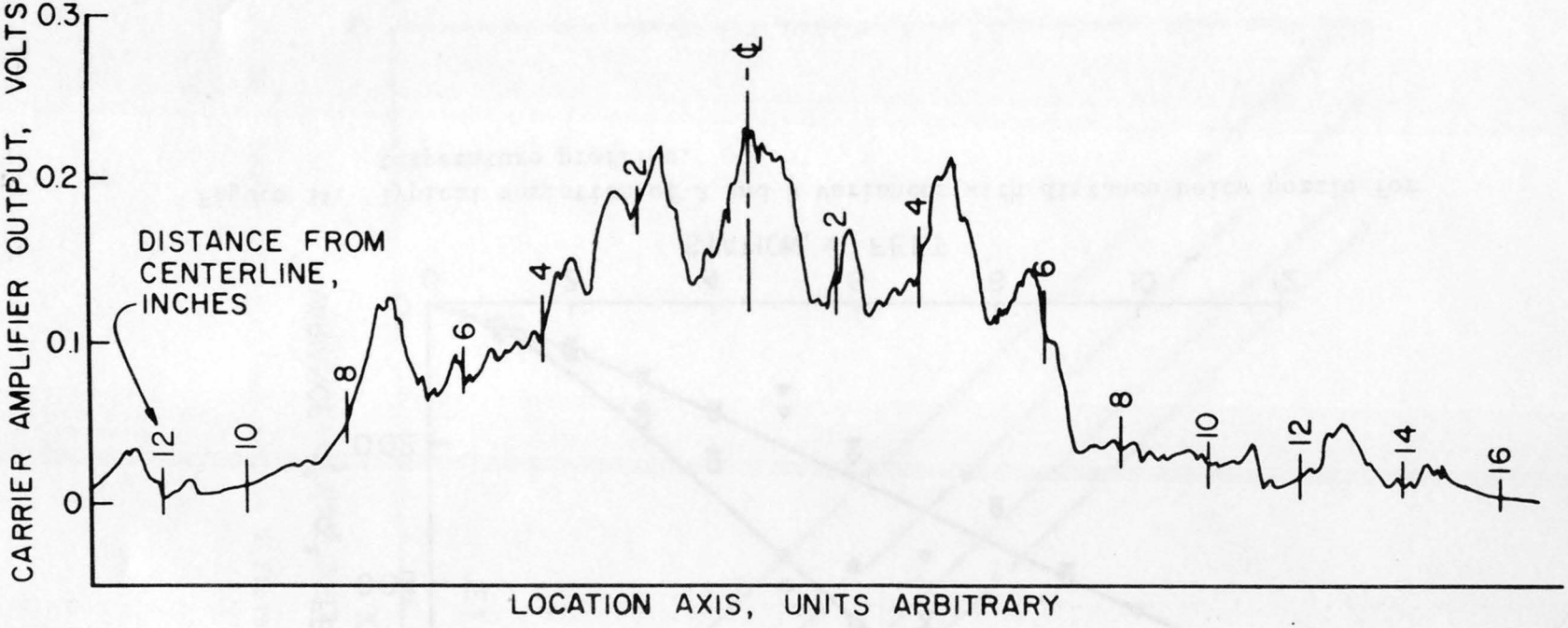

Figure 33. Tracing of a typical horizontal concentration profile at station 8 feet for a jet strength of 4.69, run RB1.

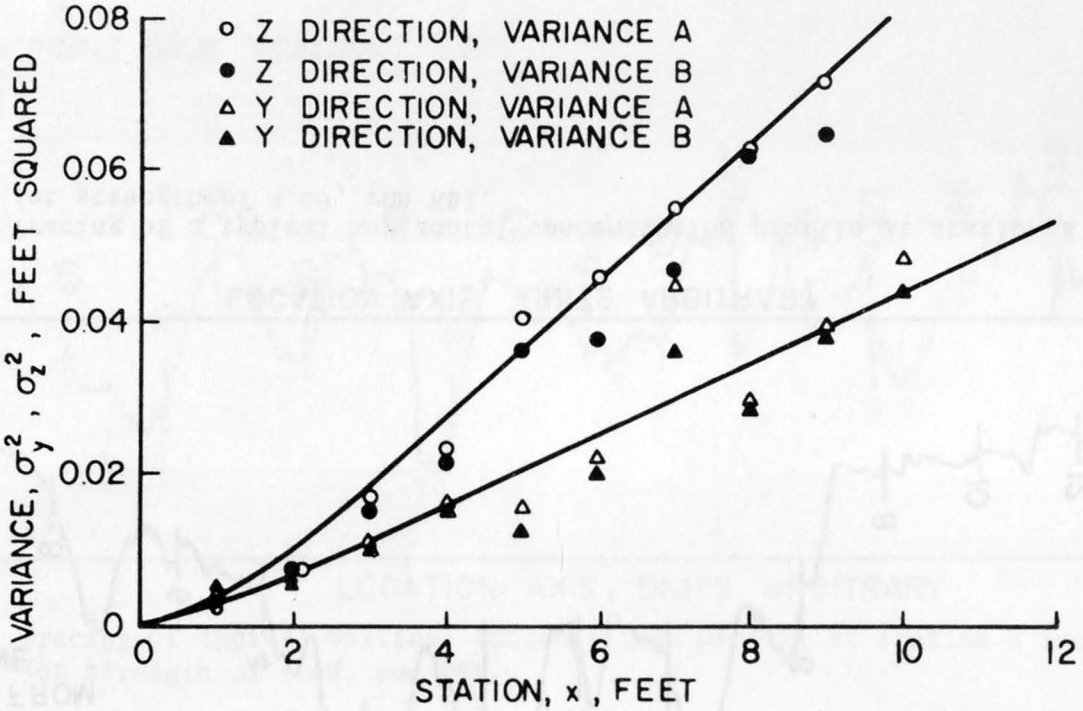

Figure 34. Typical variation of A and B variances with distance below nozzle for temperature profiles.

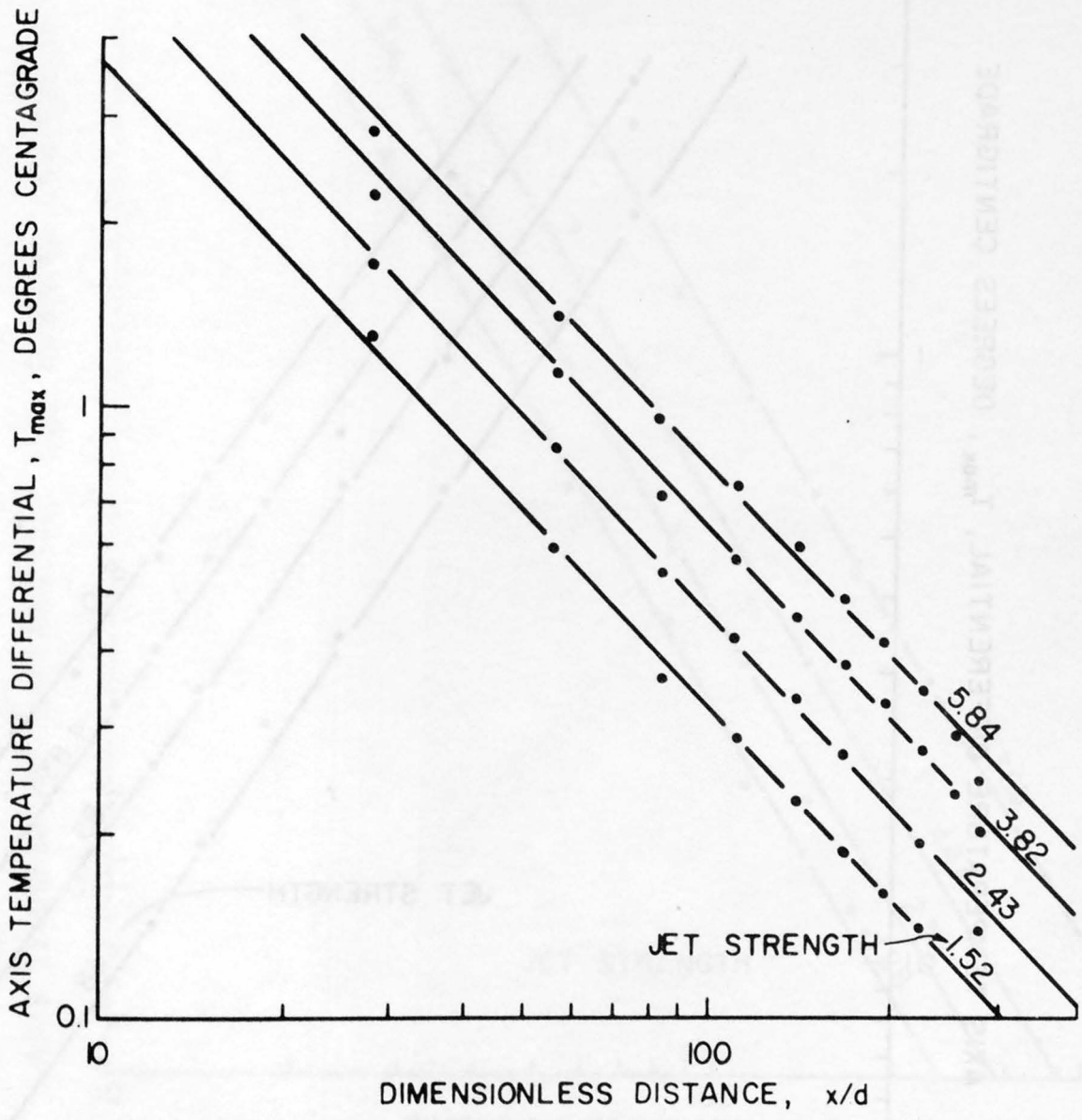

Figure 35. Decay of axis temperature differential of jets for run S1.

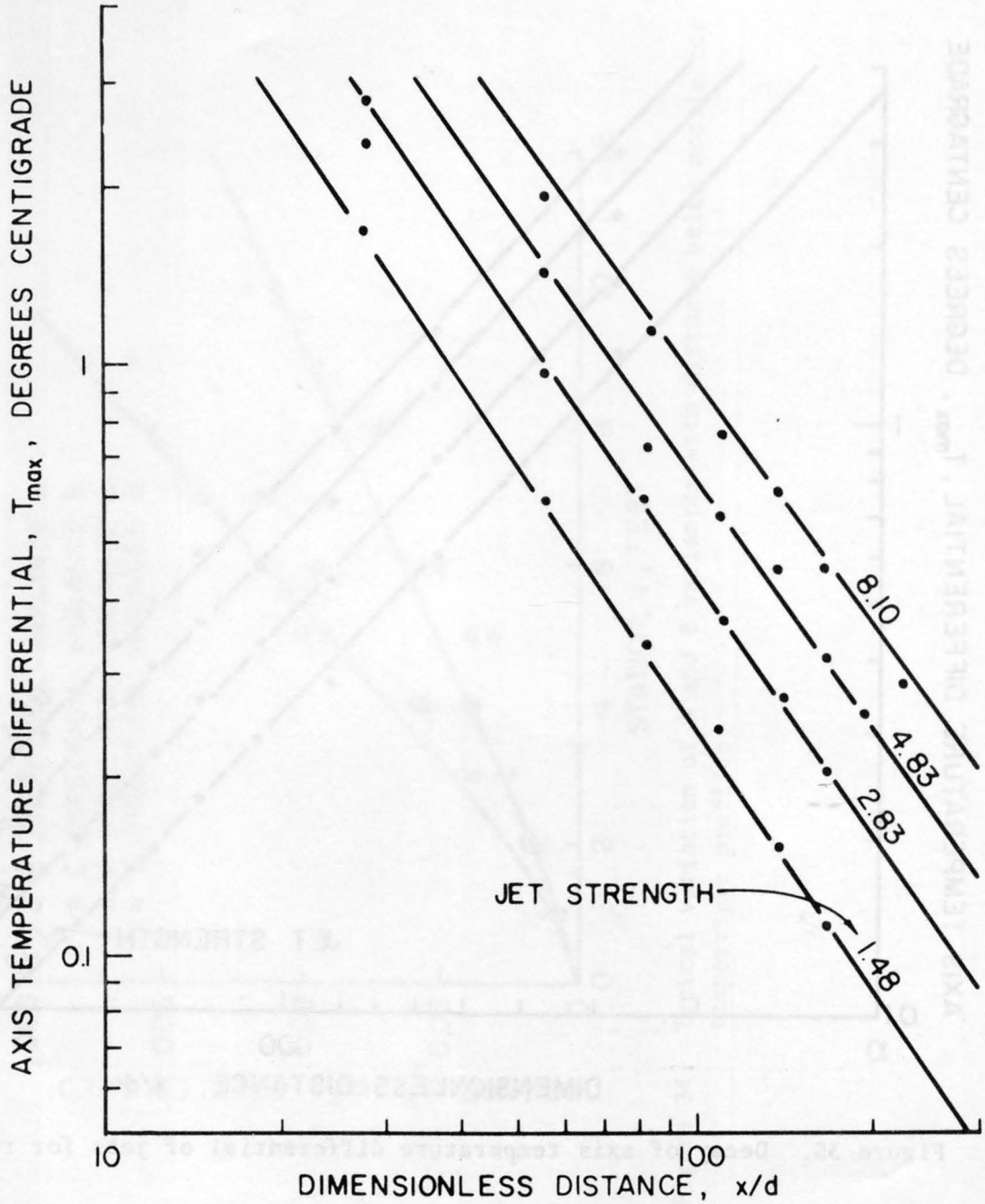

Figure 36. Decay of axis temperature differential of jets for run TR1.

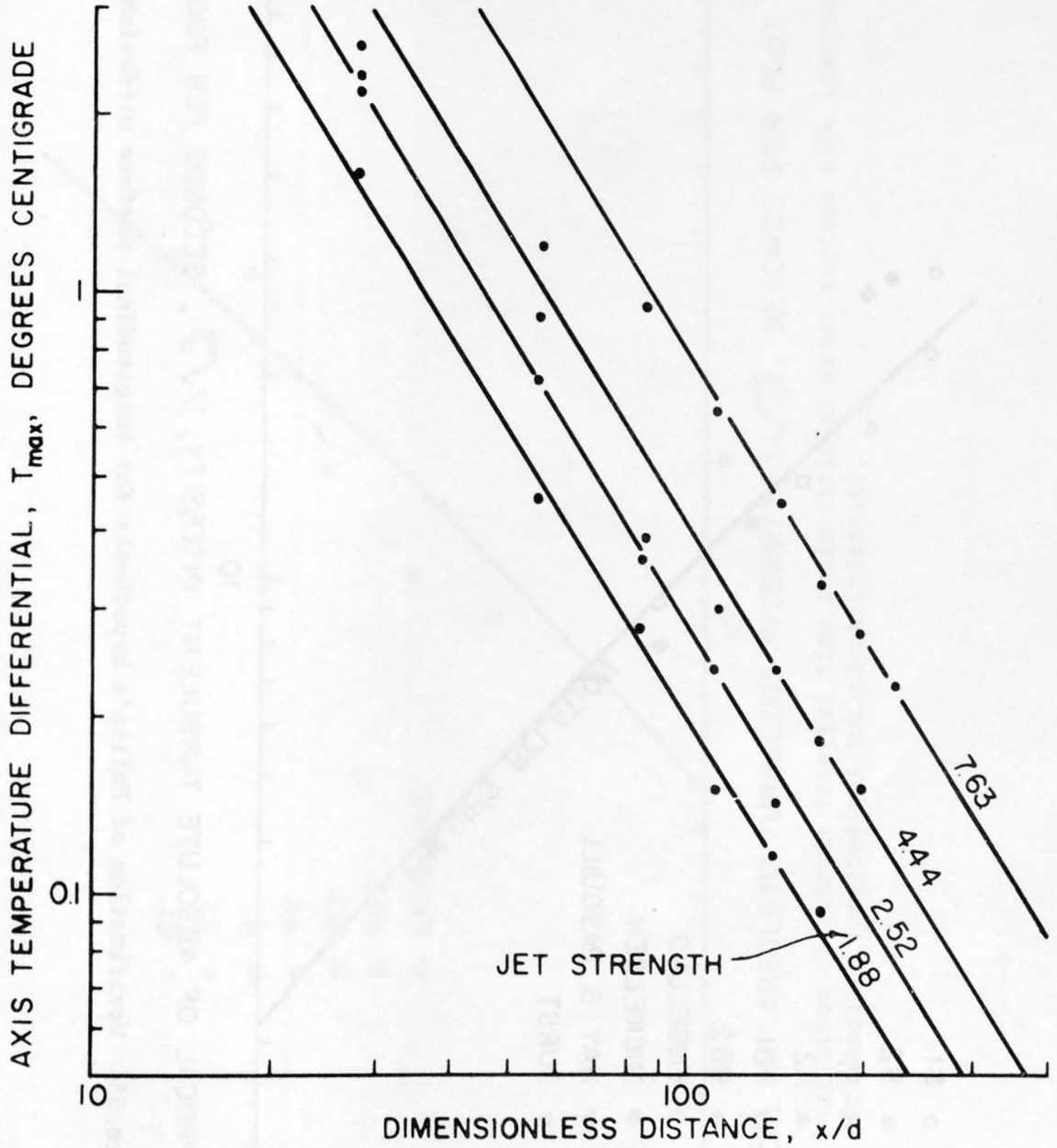

Figure 37. Decay of axis temperature differential of jets for run RB1.

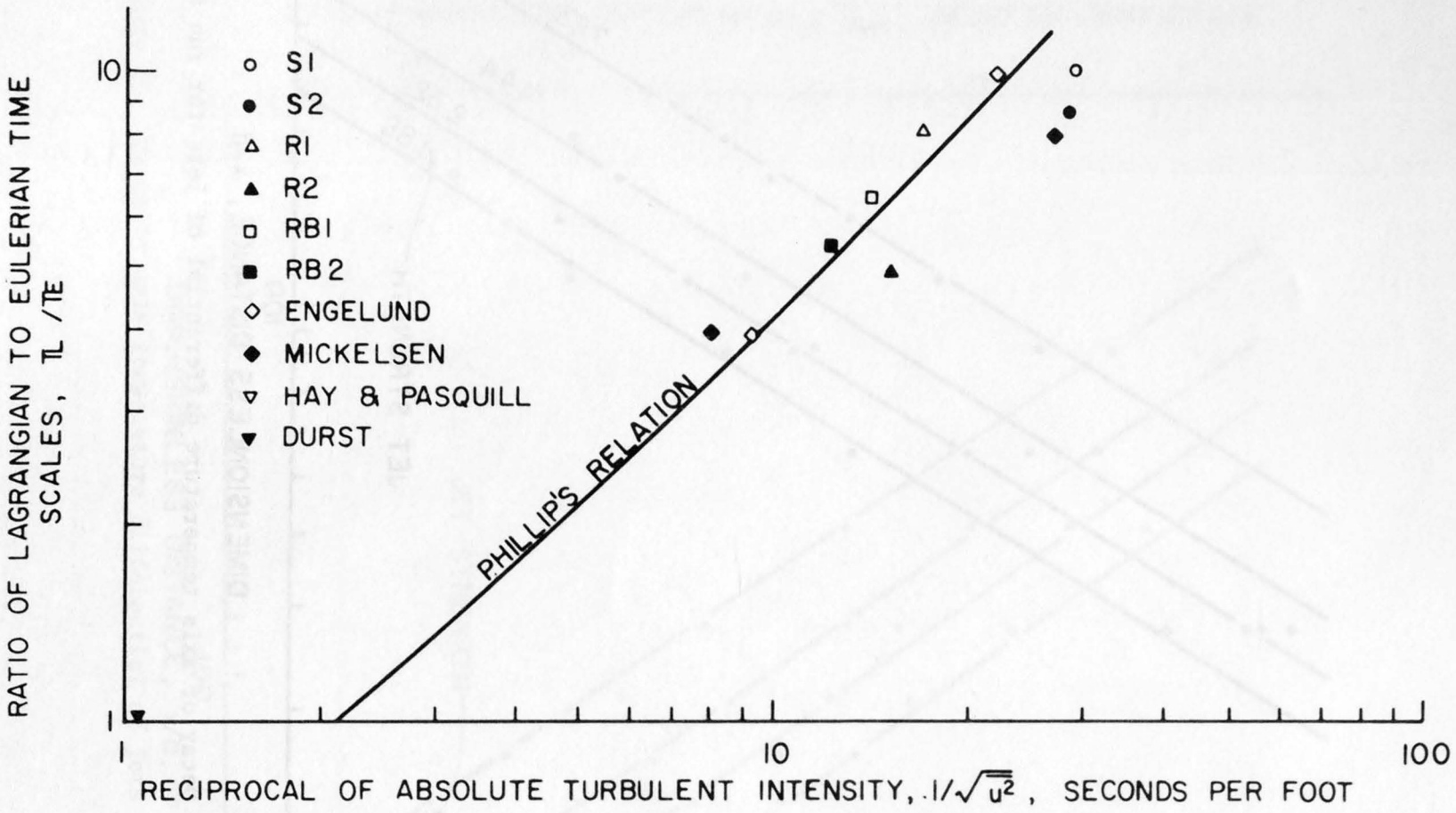

Figure 38. Verification of Philip's hypothesis for longitudinal surface diffusion.

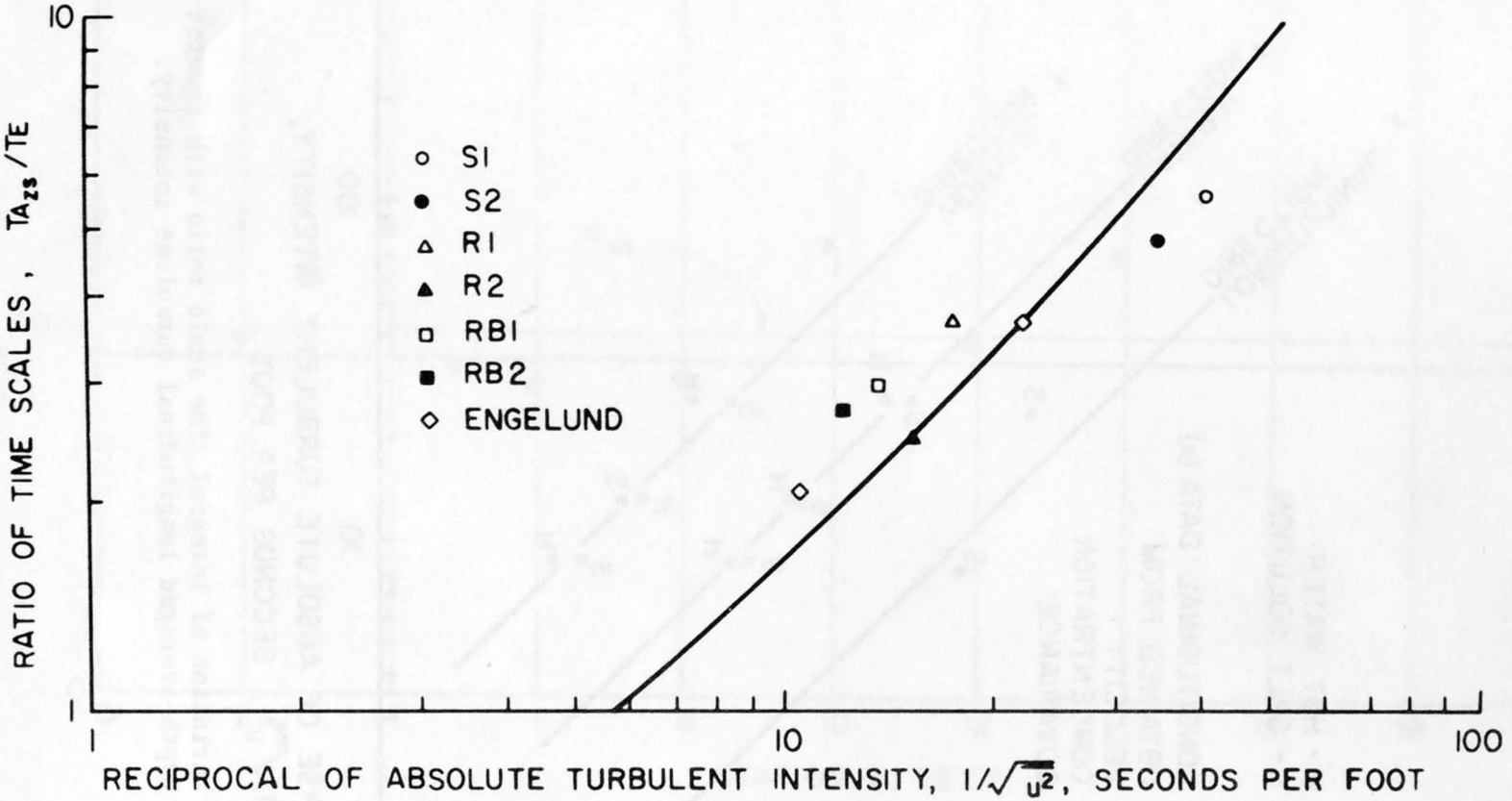

Figure 39. Variation of lateral integral time scale ratio at water surface with inverse of absolute longitudinal turbulent intensity.

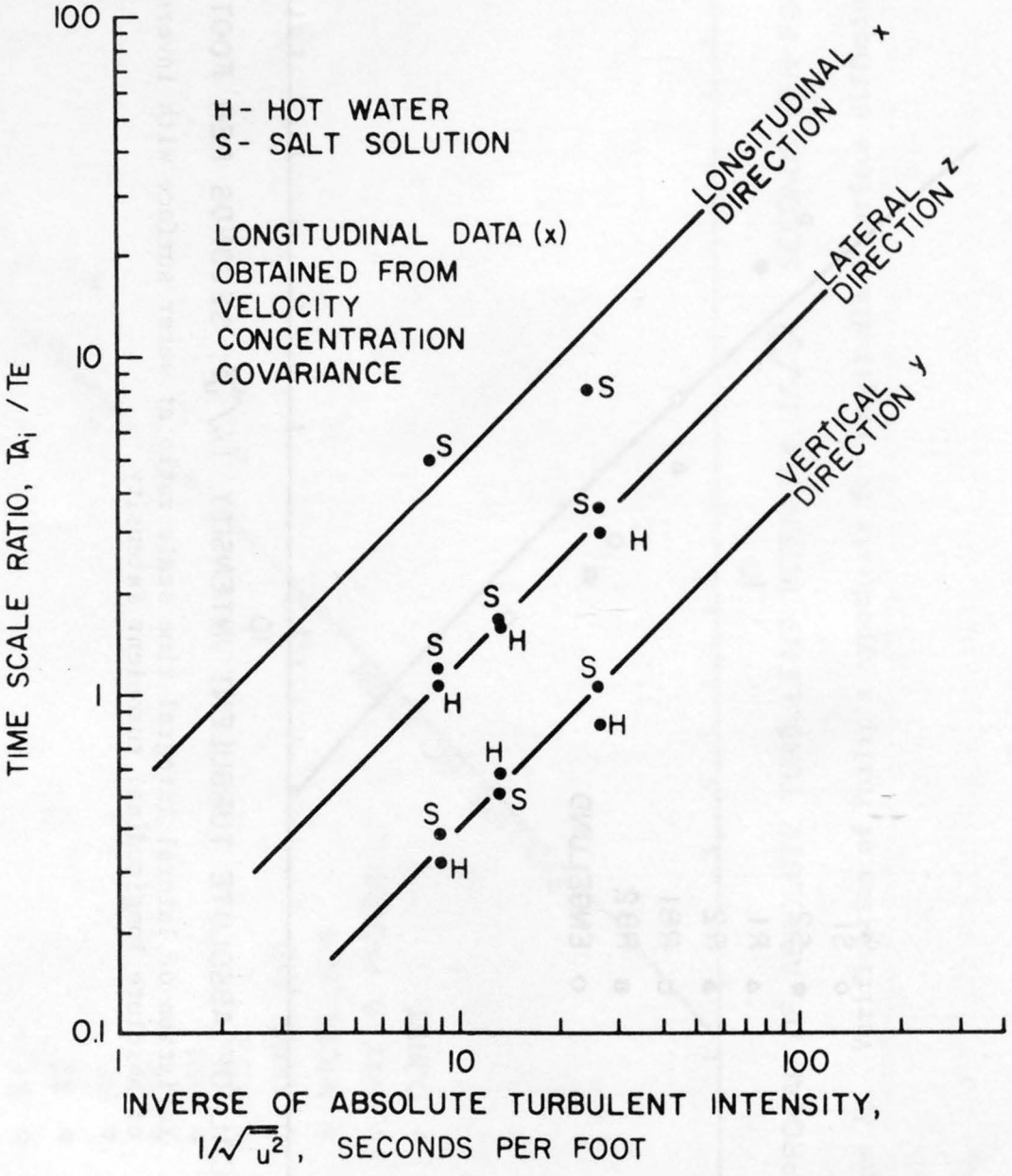

Figure 40. Variation of integral time scale ratio with inverse of depth-averaged longitudinal turbulent intensity.

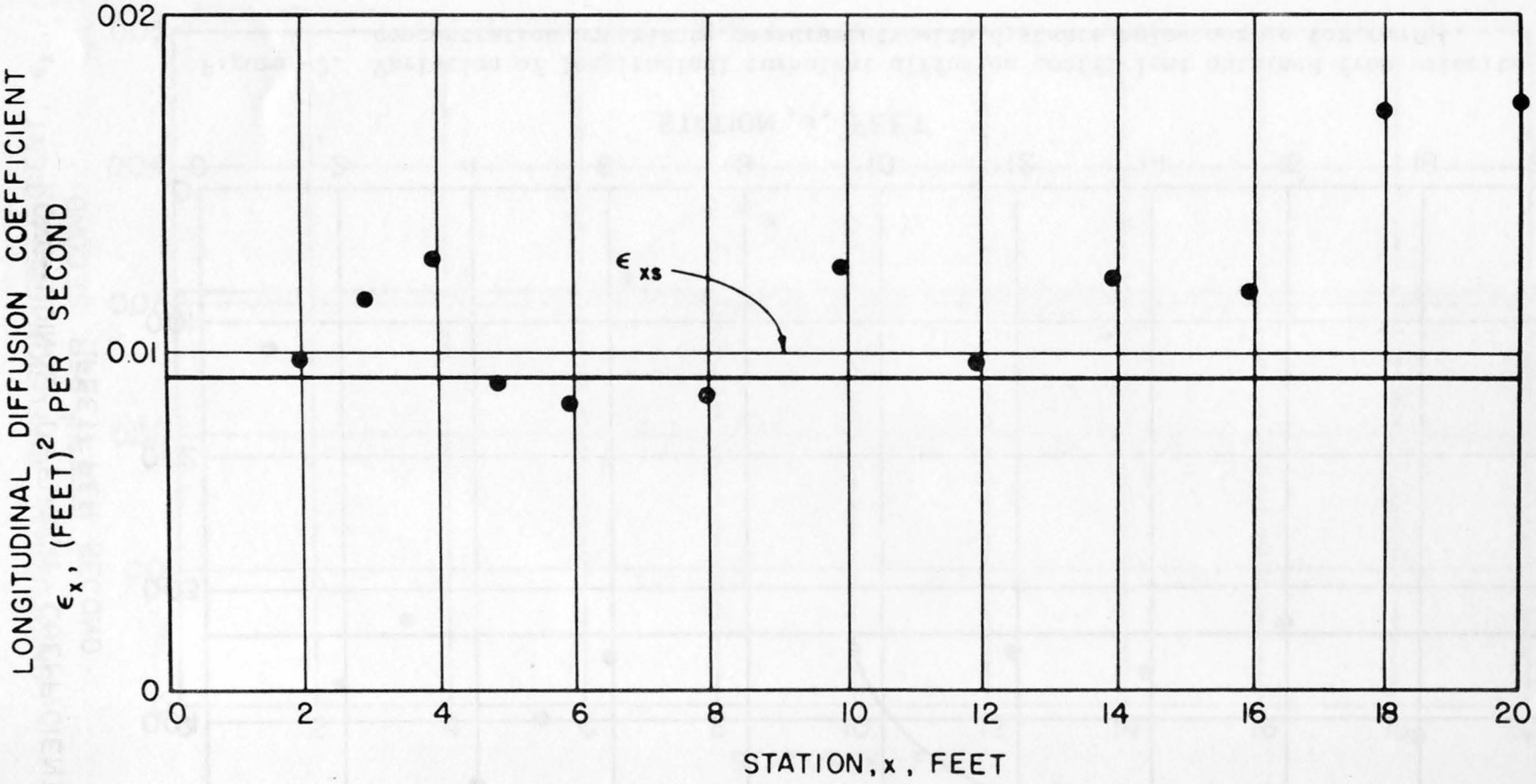

Figure 41. Variation of longitudinal turbulent diffusion coefficient obtained from velocity concentration covariance measurements with distance below nozzle for run S1.

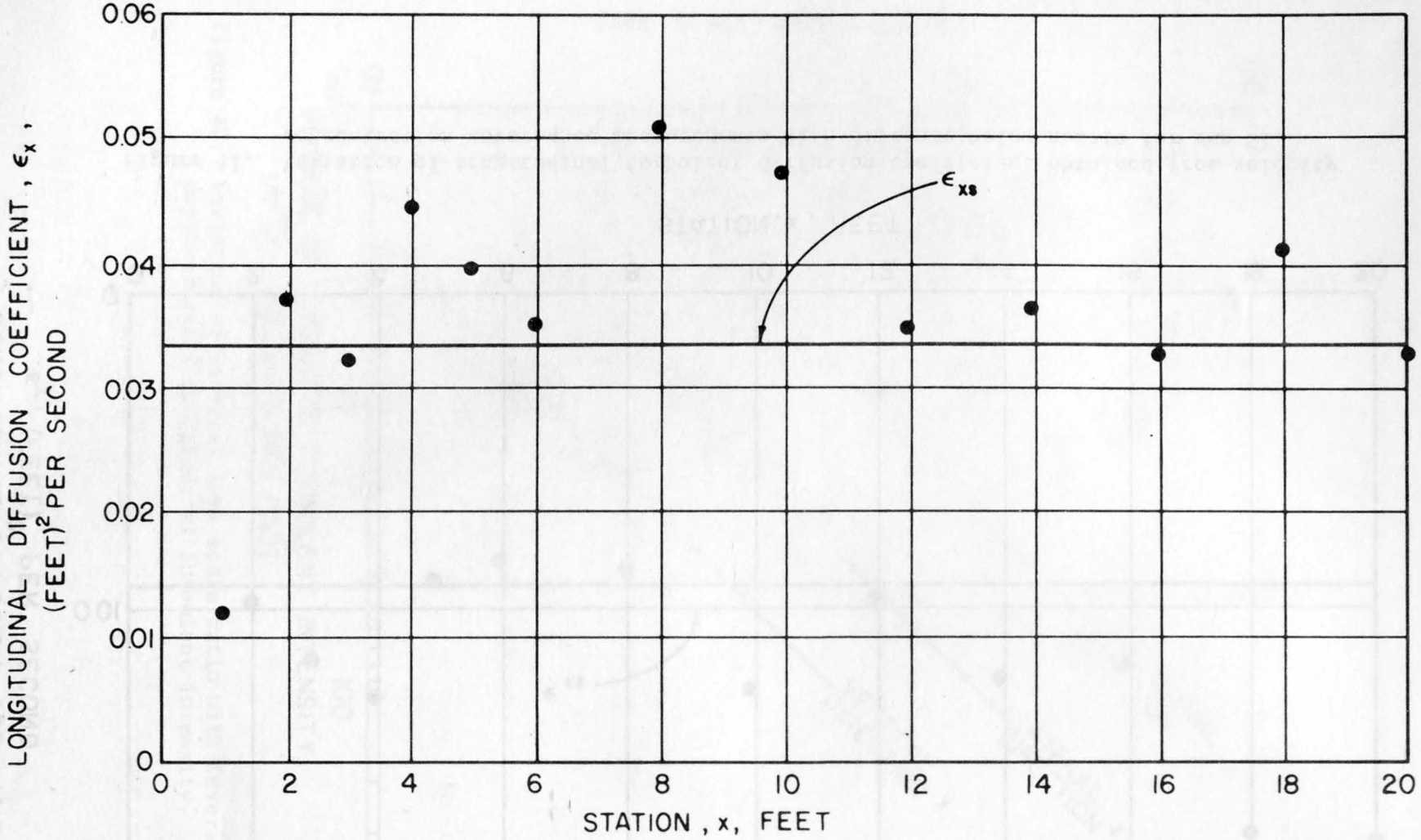

Figure 42. Variation of longitudinal turbulent diffusion coefficient obtained from velocity concentration covariance measurements with distance below nozzle for run R1.

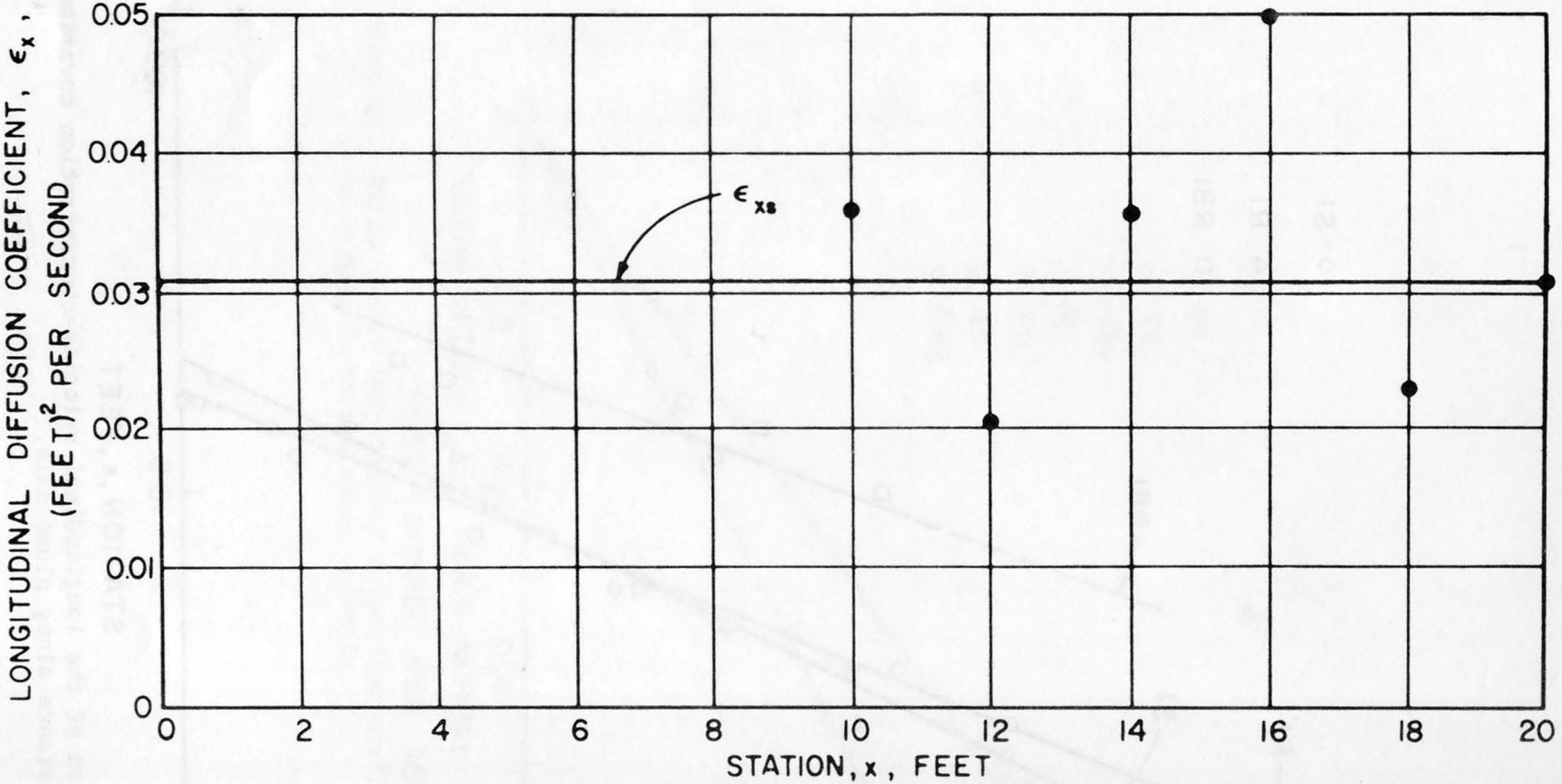

Figure 43. Variation of longitudinal turbulent diffusion coefficient obtained from velocity concentration covariance measurements with distance below nozzle for run RB1.

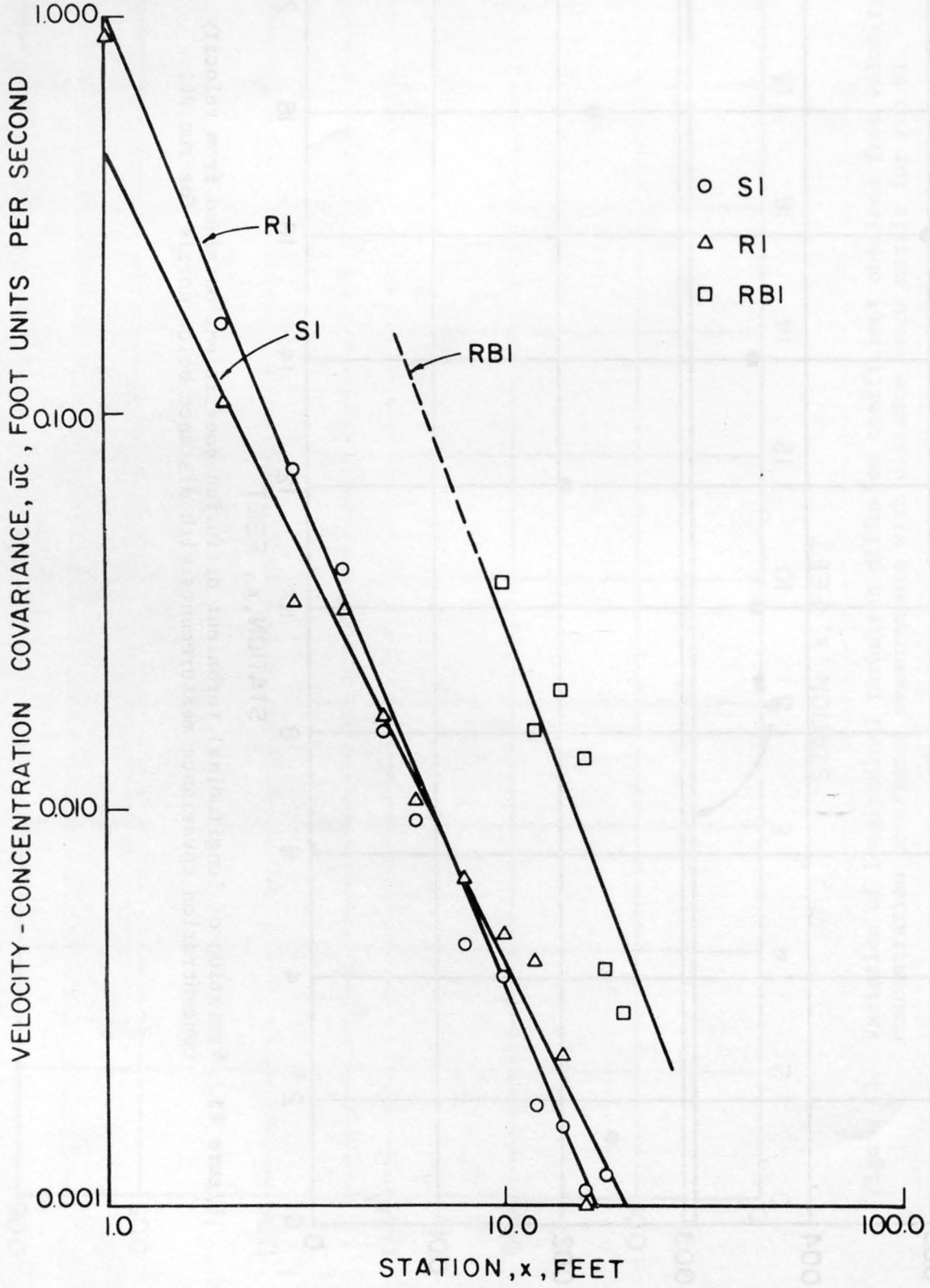

Figure 44. Variation of the longitudinal velocity-concentration covariance with distance along plume axis.

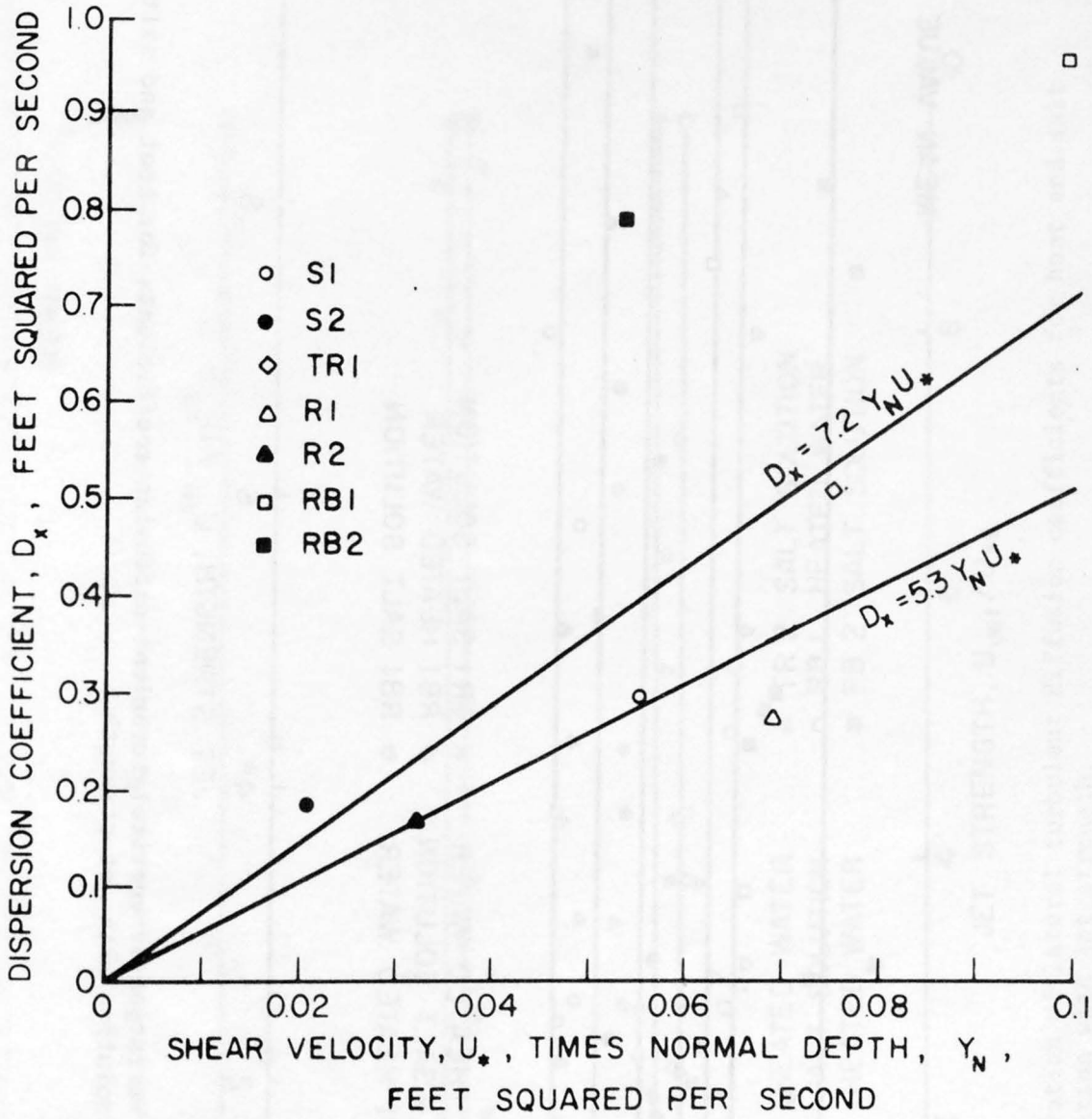

Figure 45. Variation of longitudinal dispersion coefficient with product of normal depth and shear velocity.

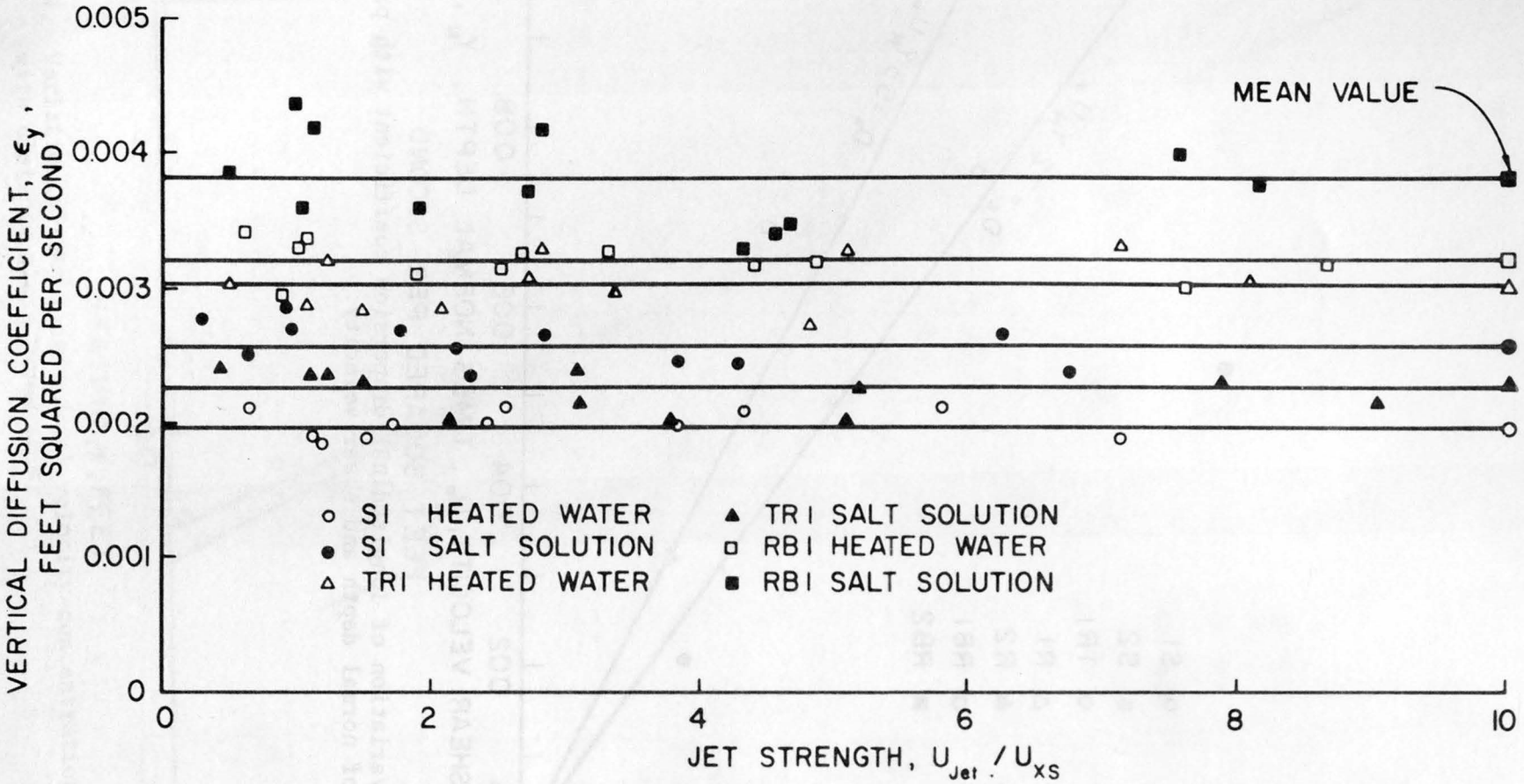

Figure 46. Variation of vertical turbulent diffusion coefficients for heat and salt solution with jet strength.

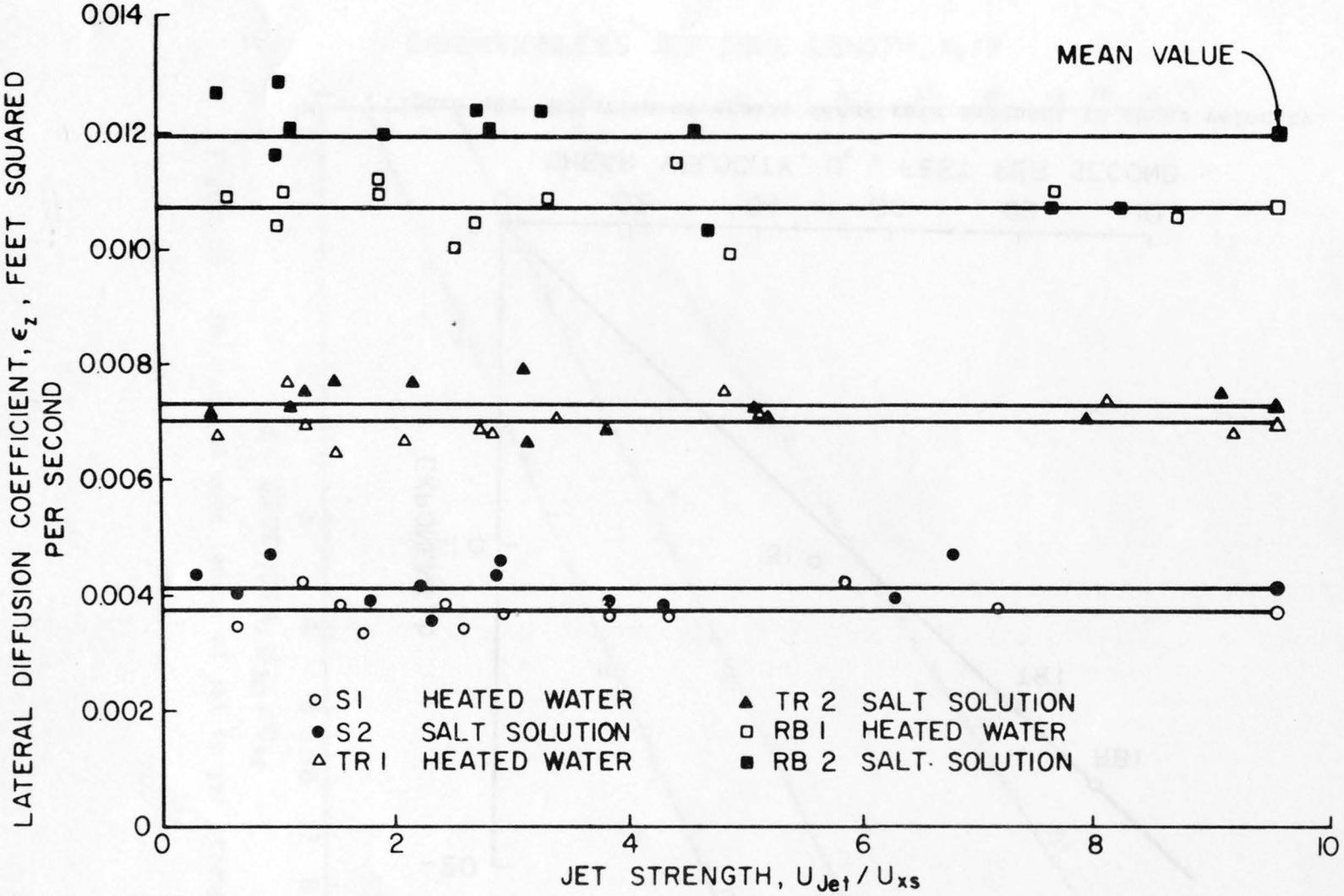

Figure 47. Variation of lateral turbulent diffusion coefficients for heat and salt solution with jet strength.

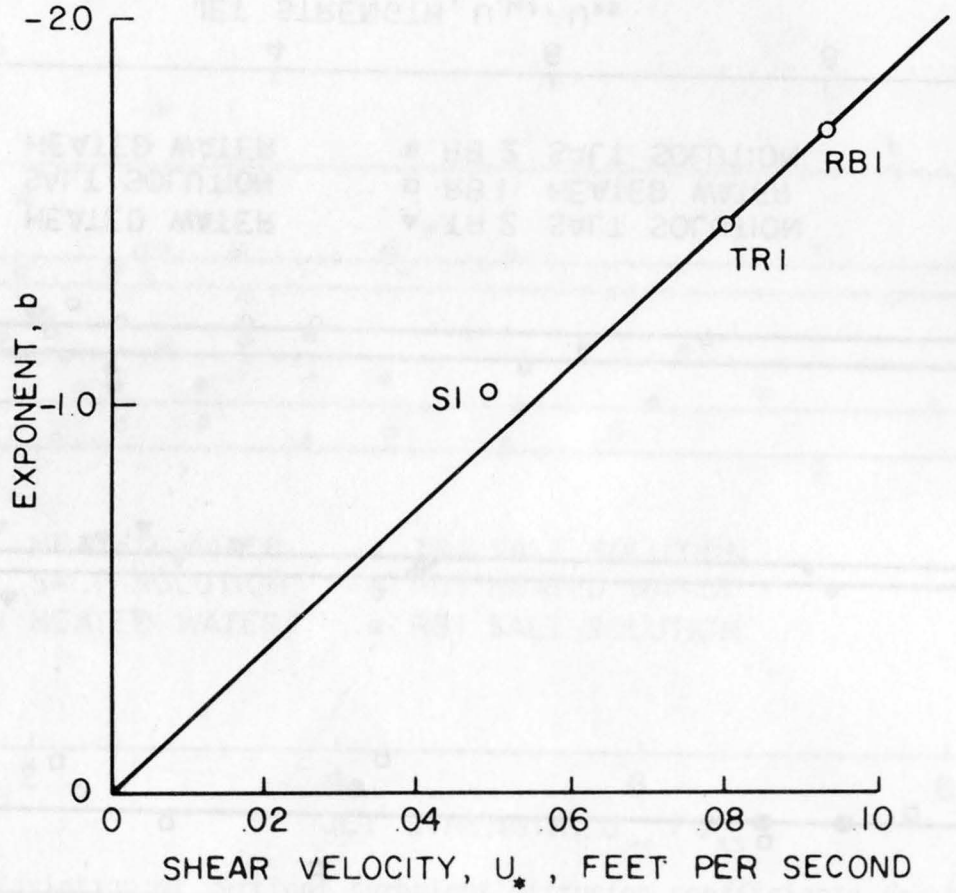

Figure 48. Relation of scalar decay rate exponent to shear velocity.

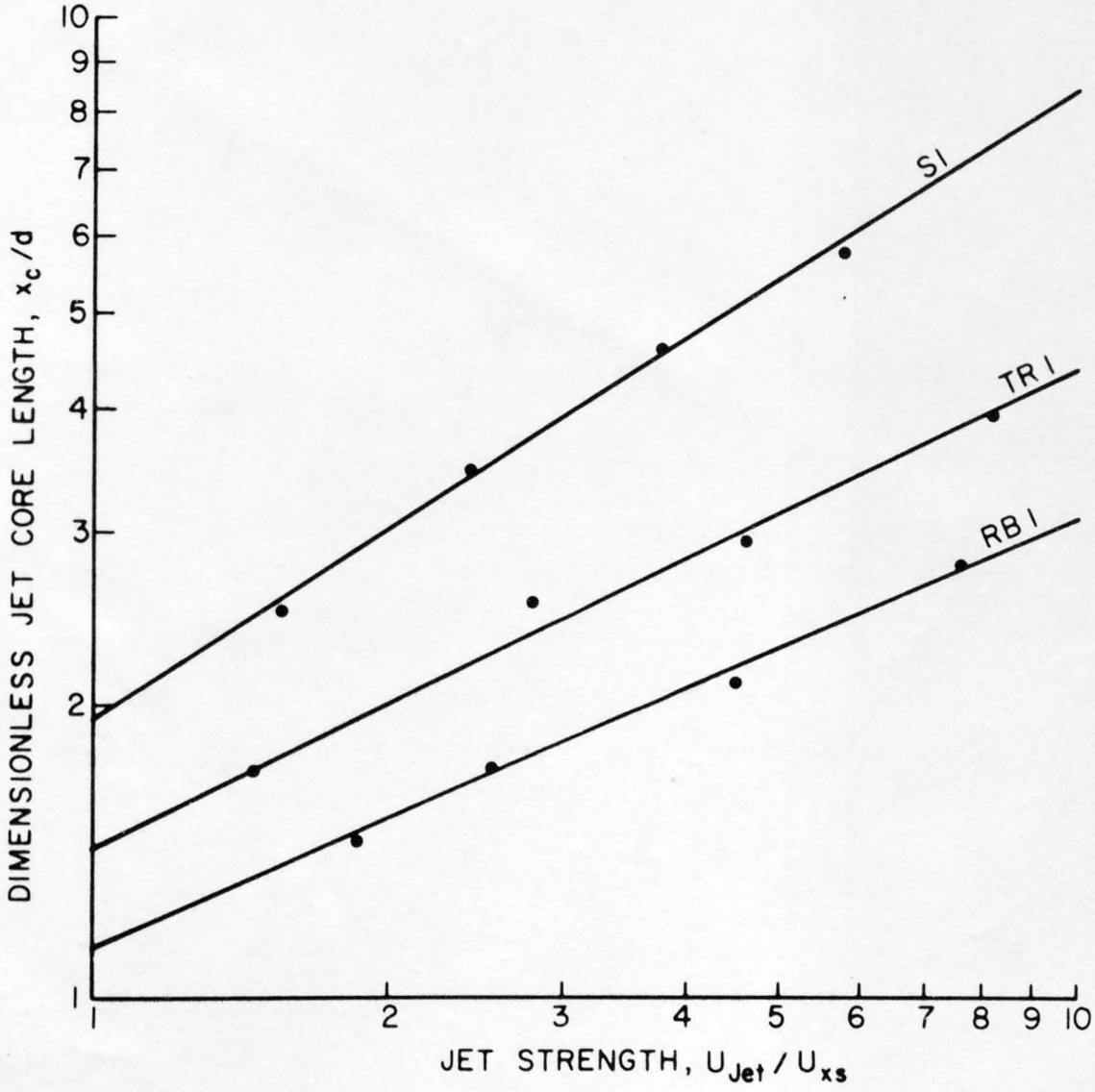

Figure 49. Relation of core length of jet to jet strength.